

**PONTIFICIA UNIVERSIDAD CATÓLICA DEL PERÚ**

**FACULTAD DE CIENCIAS E INGENIERÍA**



PONTIFICIA  
**UNIVERSIDAD  
CATÓLICA**  
DEL PERÚ

## **Masterarbeit**

**Für Herrn Martin Hennig**  
**Geboren am 24.02. 1988 in Erfurt**  
**Studiengang Maschinenbau**

## **THEMA**

**“Laser-assisted friction stir welding of magnesium and  
magnesium / aluminium dissimilar joints”**

**Verantw. Hochschullehrer**  
**Prof. Dr. Ing. Hábil. Jean Pierre Bergmann**

**Ausgabedatum: 01.12.2012**

**Abgabedatum: 03.06.2013**

**Ilmenau, den 19.03.2013**



Technische Universität Ilmenau  
Fakultät für Maschinenbau

# Masterarbeit

für Herrn Martin Hennig

---

geboren am 24.02.1988 in Erfurt

---

Studiengang Maschinenbau

---

## THEMA

„Laser-assisted friction stir welding of magnesium and magnesium/aluminium dissimilar joints“

verantw. Hochschullehrer: Prof. Dr.-Ing. habil. Jean Pierre Bergmann

---

Ausgabedatum: 01.12.2012

Abgabedatum: 03.06.2013

---

Ilmenau, den 19.03.2013

---



Univ.-Prof. Dr.-Ing. René Theska  
Vorsitzender des Prüfungsausschusses

## Statutory Declaration

I declare on oath that I completed this work on my own and that information which has been directly or indirectly taken from other sources has been noted as such. Neither this, nor a similar work, has been published or presented to an examination committee.

Ilmenau, June 03th, 2013

---

Martin Hennig



## Acknowledgment

I would like to take this opportunity to thank Prof. Dr.-Ing. habil. Jean Pierre Bergmann, Ph.D. Francisco Rumiche as well as M. Sc. René Schürer for giving me the chance to write the present master thesis.

Moreover, my thanks go also to all scientific and technical assistant who supported me.

Ilmenau, June 03th, 2013

Martin Hennig



## Abstract

The present master thesis is dealing with the influence of workpiece temperature on the process loads, generated during the FSW process. The investigation is focused on welding of the magnesium alloy AZ31. To affect the initial temperature of the joining members, two different methods are investigated. By using a laser, the material is heated and soften local direct in front of the welding tool. In contrast, a heating element, located beneath the workpieces, enable the heating of a larger area. The consequences of both methods are regarded and compared in the investigation. In addition, the comparison to the conventional welding process is made. Thereby, main aspects are the reached load levels as well as surface appearance and tensile properties. The successfully reduction of process forces is obtained for both procedures; however, the tensile properties got worse.

## Kurzdarstellung

Das Anliegen dieser Arbeit ist es, den Einfluss der Ausgangstemperatur der zu fügenden Teile auf die für den Rührreibprozess charakteristischen Belastungen zu erarbeiten. Fokus der Untersuchungen lag dabei auf dem Fügen der Magnesiumbasislegierung AZ31. Die Erhöhung der Grundtemperatur der Werkstoffe wurde dabei auf zwei unterschiedliche Weisen erzeugt. Zum einen das lokale Aufwärmen und Erweichen der Fügepartner, welches durch den Einsatz eines Lasers erreicht wurde, der direkt vor dem Schweißwerkzeug angebracht war. Die andere Methode beinhaltete das Einsetzen eines Heizelementes unter den Werkstoffen. Dadurch wurde eine gleichmäßige Erwärmung über die gesamte Fläche erreicht. Im Verlauf der Untersuchung wurden die Ergebnisse beider Methoden betrachtet und hinsichtlich der Prozesskräfte sowie Oberflächenbeschaffenheit und Festigkeitseigenschaften verglichen. Dazu wurden auch Schweißungen des konventionellen Rührreibschweißverfahrens herangezogen. Als Ergebnis konnte eine deutliche Verringerung der Prozesskräfte für beide Verfahren festgestellt werden. Allerdings war eine Verschlechterung der Festigkeitswerte zu beobachten.

**Content**

|  |            |
|--|------------|
| Abstract .....   | III        |
| List of figure .....   | V          |
| <b>1. Introduction .....</b>                                 | <b>1</b>   |
| <b>2. State of the art.....</b>                              | <b>2</b>   |
| <b>2.1. Friction Stir Welding: in general .....</b>          | <b>2</b>   |
| 2.1.1. Process.....  | 2          |
| 2.1.2. Deformation behavior.....                             | 5          |
| 2.1.3. Diffusion.....  | 8          |
| 2.1.4. Intermetallic Compound.....                           | 11         |
| 2.1.5. Influencing variables .....                           | 13         |
| <b>2.2. Materials.....</b>                                   | <b>17</b>  |
| 2.2.1. Magnesium.....  | 17         |
| 2.2.2. Aluminum.....   | 27         |
| <b>2.3. FSW: preheating systems.....</b>                     | <b>30</b>  |
| 2.3.1. Objective .....                                       | 30         |
| 2.3.2. LAFSW .....   | 30         |
| 2.3.3. Arc-enhanced FSW .....                                | 32         |
| 2.3.4. Induction heating system.....                         | 33         |
| 2.3.5. Electric heating elements.....                        | 34         |
| <b>2.4. FSW of magnesium/aluminum dissimilar joints.....</b> | <b>35</b>  |
| <b>3. Objective.....</b>                                     | <b>40</b>  |
| <b>4. Experimental approach.....</b>                         | <b>41</b>  |
| 4.1 General approach.....                                    | 41         |
| 4.2 Experimental setup .....                                 | 42         |
| 4.3 Welding tool .....                                       | 47         |
| 4.4 Material .....   | 48         |
| 4.5 Analyze evaluation of the welding results.....           | 51         |
| <b>5. Results.....</b>                                       | <b>55</b>  |
| 5.1. LAFSW .....   | 55         |
| 5.2 Preheating by heating element.....                       | 79         |
| <b>6. Summary and outlook.....</b>                           | <b>118</b> |
| Literature .....   | 120        |
| Appendix .....   | 128        |
| Appendix 1: overview of the laser power.....                 | 128        |

Appendix 2: technical drawing of tool 1 ..... 128

Appendix 2: technical drawing of tool 2 ..... 128



**List of figure**

|      |   |    |
|------|---|----|
| 1.1  | a) principle of the FSW process /Nor12/; b) schematic force progression during FSW  | 3  |
| 1.2  | schematic of a typical FSW cross-section (A) Parent Material; (B) Heat Affected Zone;(C) Thermal Mechanically Affected Zone, (D) Weld Nugget Sci07/ | 3  |
| 2.1  | schematic illustration of yield stress as function of a) true stress; b) strain rate; c) forming temperature /Doe07/                                | 5  |
| 2.2  | schematic illustration of stress-strain-diagram and flow curve from the tensile test /Lan08/  | 6  |
| 2.3  | flow curves received by tensile tests for different materials a) AZ31B; b) MN150; c) AW6016. /Kam00/, /Ost98/                                       | 7  |
| 2.4  | transposition processes in crystal lattice: a) direct phantom transposition; b) interstitial lattice; c) vacant lattice position. /Li12/            | 9  |
| 2.5  | diffusion paths. /Li12/   | 10 |
| 2.6  | for derivation of the resulting material flow J by diffusion processes /Sch10/  | 10 |
| 2.7  | phase diagram of al-mg-system /Mur82/   | 12 |
| 2.8  | intermetallic compounds thickness as function of diffusion time /Yam09/   | 13 |
| 2.9  | schematic illustration of the FSW-process /Ruh12/   | 14 |
| 2.10 | three incompressible flow fields of the FSW: a) rotation; b) translation and c) ring vortex /Sch04/   | 15 |
| 2.11 | material flow resulting from superimposed incompressible flow field /Sch04/   | 15 |
| 2.12 | comparison of mechanical properties of selected material classes related to the Respective material density /Müc05/                                 | 17 |
| 2.13 | a) basal plane in hexagonal close-packed crystal structure; b) principle of twinning /Kam00/  | 18 |
| 2.14 | reflection capacity of magnesium, aluminum and silver. The black beam marking the visible spectrum /Kam00/  | 19 |
| 2.15 | effect of axial force on macrographs of stir zone. /Raz11/  | 22 |
| 2.16 | maximum axial force and torque according to rotational and plunging speed /Zim10/   | 23 |
| 2.17 | different tool pin profiles /Pad09a/  | 24 |



|      |  |    |
|------|--|----|
| 2.18 | effect of tool pin profile on macrographs of stir zone. /Pad09a/.....  | 25 |
| 2.19 | a) effect of tool pin profile on hardness; b) effect of shoulder diameter on hardness; c) effect of tool material on hardness /Pad09a/.....  | 26 |
| 2.20 | adhesion of magnesium: a) threaded pin; alloy AZ91D, AM50 /Ska04/; b) taper cylindrical pin, alloy AZ31 .....  | 26 |
| 2.21 | face centered cubic lattice /Kam95/.....   | 27 |
| 2.22 | a) absorption as function of wavelength for various materials /Mor05/<br>b) absorption of aluminum as function of angle of incidence for a wavelength of 1,06 $\mu\text{m}$ /Bac00/.....   | 28 |
| 2.23 | the principle of LAFSW /Koh02/.....  | 31 |
| 2.24 | a simplified diagram of arc-enhanced FSW /Sch06/.....  | 32 |
| 2.25 | a FSW setup with induction heating /Wal06/.....  | 33 |
| 2.26 | comparison of process forces with and without preheating for 1018 steel /Wal06/.....   | 34 |
| 2.27 | a) normalized axial force for different welding speeds at different initial temperatures; b) normalized torque for different welding speeds at different initial temperatures. /Sin09/.....  | 35 |
| 2.28 | a) effect of material position on joint strength and heat input in butt joint FSW of AZ31 Mg and 6061 Al. The thermocouples are 3 mm away from the path of the tool axis and 0,25 mm above the bottom surface of the workpiece; b) process settings /Fir09/..... | 37 |
| 2.29 | a) interfacial layer observed in the AZ31/A5083 joint (offset = 0mm); b) chemical composition at points 1 to 6. /Yam09/.....   | 38 |
| 2.30 | Electron back-scattered image of aluminum-magnesium intermetallic at weld Interface (unetched sample) /Lea03/.....   | 38 |
| 2.31 | a) tensile strength comparison between various welding cases; b) comparison Vickers hardness for dissimilar FSW without Ni foil and hybrid welding with Ni Foil of Al/Mg alloy along the transverse section 2 mm below the top surface /Cha11/.....              | 39 |
| 4.1  | experimental setup welding system: a) axial force and torque measurement system (tool holder, sensor), b) laser, c) crossjet, d) clamping element, e) workpieces, f) arrestor, g) base plate.....  | 43 |
| 4.2  | schematic illustration of temperature measurement during welding with: a) temperature measuring points (BW; MW1; MW2; MW3; EW); b) workpiece; c) backing plate (three separate steel plates); d) heating element; e) arrestor; f) backing plate.....             | 44 |

|      |   |    |
|------|---|----|
| 4.3  | schematic illustration of measuring points for the performance test of the heating Elements.....  | 44 |
| 4.4  | measurement of temperature for heating element 1.....   | 45 |
| 4.5  | measurement of temperature for heating element 2.....   | 46 |
| 4.6  | schematic illustration of the simulation model.....   | 47 |
| 4.7  | tensile properties of the alloy AZ31 and AW6016 a) tensile strength;<br>b) fracture length.....   | 50 |
| 4.8  | fracture appearance a) AZ31 (extruded); b) AZ31 (rolled); c) AW6016.....  | 50 |
| 4.9  | calculated flow curves for the used alloys.....   | 51 |
| 4.10 | exemplary diagram of the measured force and torque.....   | 52 |
| 4.11 | schematic illustrations of the specimens for a) tensile test; b) microscopic Analyze.....   | 52 |
| 5.1  | schematic illustration of procedure for the investigation of laser power on extruded AZ31.....  | 55 |
| 5.2  | measuring points of temperature in the simulation model.....  | 57 |
| 5.3  | comparison of temperatures between simulation and experiment for different transverse speeds: a) 1400 mm/min and b) 20 mm/min.....  | 58 |
| 5.4  | surface appearance of FSW of extruded AZ31 for different welding speeds at constant rotational speed.....   | 61 |
| 5.5  | measured temperature for FSW of extruded AZ31 subject to different welding speeds and measuring points at constant rotational speed. BW-beginning of weld; MW-middle of weld; EW-end of weld..... | 62 |
| 5.6  | axial force and torque path for FSW of extruded AZ31 at N = 2000 rpm and f = 200 mm/min. (filtered curve).....  | 62 |
| 5.7  | axial force and torque path for FSW of extruded AZ31 at N = 2000 rpm and f = 1400 mm/min. (filtered curve).....   | 64 |
| 5.8  | measured forces and torques for FSW of extruded AZ31 subject to different Welding speeds at constant rotational speed. (plunging phase).....  | 65 |
| 5.9  | measured forces and torques for FSW of extruded AZ31 subject to different Welding speeds at constant rotational speed. (welding phase).....   | 65 |
| 5.10 | tensile strength for FSW of extruded AZ31 for different welding speeds at constant Rotational speed subject to: a) axial force; b) torque.....  | 66 |

|      |   |    |
|------|---|----|
| 5.11 | tensile properties for FSW of extruded AZ31 for different welding speeds at constant Rotational speed: a) fracture length as function of axial force; b) tensile strength as function of weld pitch.....                        | 67 |
| 5.12 | fracture appearance for FSW of extruded AZ31 for 20; 200 and 1400 mm/min At constant rotational speed.....  | 67 |
| 5.13 | micrograph for FSW of extruded AZ31 for 20 mm/min at constant rotational Speed.....   | 69 |
| 5.14 | micrograph for FSW of extruded AZ31 for 200 and 1400 mm/min at constant rotational speed.....   | 69 |
| 5.15 | hardness profile for FSW of extruded AZ31 for 20 and 200 mm/min at constant rotational speed.....   | 70 |
| 5.16 | surface appearance of LAFSW of extruded AZ31 for different welding speeds at constant rotational speed.....   | 72 |
| 5.17 | comparison of surface appearance of LAFSW and FSW of extruded AZ31 for different welding speeds at constant rotational speed.....   | 73 |
| 5.18 | comparison of loads for LAFSW and FSW of extruded AZ31 at constant rotational speed: a) axial force as function of welding speed; b) torque as function of welding speed. (plunging phase).....                                 | 74 |
| 5.19 | comparison of loads for LAFSW and FSW of extruded AZ31 at constant rotational speed: a) axial force as function of welding speed; b) torque as function of welding speed . (welding phase).....                                 | 74 |
| 5.20 | comparison of tensile strength for LAFSW and FSW of extruded AZ31 for different Welding speeds at constant rotational speed subject to: a) axial force; b) torque.....  | 75 |
| 5.21 | comparison of tensile properties for LAFSW and FSW of extruded AZ31 for different welding speeds at constant rotational speed: a) fracture length as function of axial force b) tensile strength as function of weld pitch..... | 76 |
| 5.22 | fracture appearance for LAFSW of extruded AZ31 for 20; 200 and 1400 mm/min at constant rotational speed.....  | 76 |
| 5.23 | micrographs for LAFSW of extruded AZ31 at constant rotational speed for a) 20 mm/min; b) 200 mm/min.....  | 77 |
| 5.24 | comparison of hardness profile for LAFSW and FSW of extruded AZ31 for 200 mm/min at constant rotational speed.....  | 78 |
| 5.25 | surface appearance of FSW of extruded AZ31 (bead on plate weld) for different welding speeds at constant rotational speed and a starting temperature of 28 °C.....  | 80 |

|      |   |    |
|------|---|----|
| 5.26 | surface appearance of FSW of extruded AZ31 (bead on plate weld) for different welding speeds at constant rotational speed and a starting temperature of 130 °C.....   | 81 |
| 5.27 | comparison of measured forces and torques for FSW of extruded AZ31 (bead on plate weld) at constant rotational speed: a) axial force as function of welding speed; b) torque as function of welding speed. (plunging phase).....                      | 81 |
| 5.28 | comparison of measured forces and torques for FSW of extruded AZ31 (bead on plate weld) at constant rotational speed: a) axial force as function of welding speed; b) torque as function of welding speed. (welding phase).....                       | 82 |
| 5.29 | surface appearance of FSW of extruded AZ31 for different welding speeds at constant rotational speed and initial temperature of 130 °C.....   | 84 |
| 5.30 | comparison of surface appearance of FSW of extruded AZ31 for different Welding speeds and initial temperatures at constant rotational speed.....  | 84 |
| 5.31 | comparison of occurring temperature during FSW of extruded AZ31 for Different initial temperatures at constant rotational speed for welding speed of: a) 20 mm/min and b) 1400 mm/min. BW- beginning of weld; MW- middle of weld EW- end of weld..... | 85 |
| 5.32 | comparison of measured forces and torques for FSW of extruded AZ31 at constant Rotational speed: a) axial force as function of welding speed; b) torque as function of welding speed. (plunging phase).....   | 86 |
| 5.33 | comparison of measured forces and torques for FSW of extruded AZ31 at constant Rotational speed: a) axial force as function of welding speed; b) torque as function of welding speed. (welding phase).....  | 87 |
| 5.34 | comparison of tensile strength for FSW of extruded AZ31 for different welding speeds and initial temperatures at constant rotational speed subject to: a) axial force; b) Torque.....   | 88 |
| 5.35 | comparison of tensile properties for FSW of extruded AZ31 for different welding Speeds and initial temperatures at constant rotational speed: a) fracture length as function of axial force; b) tensile strength as function of weld pitch.....       | 88 |
| 5.36 | fracture appearance for FSW of extruded AZ31 for 20; 200 and 1400 mm/min at constant rotational speed and an initial temperature of 130 °C.....   | 89 |
| 5.37 | micrograph for FSW of extruded AZ31 for 200 mm/min at constant rotational Speed and an initial temperature of 130 °C.....   | 90 |
| 5.38 | micrograph for FSW of extruded AZ31 for 1400 mm/min at constant rotational Speed and an initial temperature of 130 °C.....  | 90 |

|      |   |     |
|------|---|-----|
| 5.39 | comparison of hardness profile for FSW of extruded AZ31 at different initial Temperature for 200 mm/min at constant rotational speed.....   | 91  |
| 5.40 | surface appearance of FSW of rolled AZ31 for different welding speeds at constant Rotational speed and initial temperature of 27 °C.....  | 94  |
| 5.41 | surface appearance of FSW of rolled AZ31 for different welding speeds at constant Rotational speed and initial temperature of 225 °C.....   | 95  |
| 5.42 | comparison of surface appearance of FSW of rolled AZ31 for different initial temperature at constant rotational speed and welding speed.....  | 95  |
| 5.43 | comparison of occurrence temperature during FSW of rolled AZ31 for different initial temperature at constant rotational speed for welding speeds of a) 20 mm/min and b) 1400 mm/min. BW-beginning of weld; MW-middle of weld; EW-end of weld..... | 96  |
| 5.44 | comparison of measured forces and torques for FSW of rolled AZ31 at constant rotational speed: a) axial force as function of welding speed; b) torque as function of welding speed. (plunging phase).....   | 97  |
| 5.45 | comparison of measured forces and torques for FSW of rolled AZ31 at constant rotational speed: a) axial force as function of welding speed; b) torque as function of welding speed. (welding phase).....  | 97  |
| 5.46 | comparison of tensile strength for FSW of rolled AZ31 for different welding speeds and initial temperatures at constant rotational speed subject to: a) axial force; b) Torque.....   | 98  |
| 5.47 | comparison of tensile properties for FSW of rolled AZ31 for different welding speeds and initial temperatures at constant rotational speed: a) fracture length as function of axial force; b) tensile strength as function of weld pitch.....     | 99  |
| 5.48 | fracture appearance for FSW of rolled AZ31 for 20; 200 and 1400 mm/min at constant rotational speed.....  | 99  |
| 5.49 | micrographs for FSW of rolled AZ31 at constant rotational speed for a) 20 mm/min; b) 200 mm/min and c) 1400 mm/min.....   | 100 |
| 5.50 | micrographs for FSW of rolled AZ31 at constant rotational speed for 20 mm/min and a) 130 °C and b) 225 °C.....  | 101 |
| 5.51 | best surface appearance for FSW of extruded AZ31/AW6016 for different rotational speeds at constant welding speed of 20 mm/min.....   | 104 |
| 5.52 | surface appearance for FSW of extruded AZ31/AW6016 for different welding speeds at a constant rotational speed of 800 rpm.....  | 104 |

|      |  |     |
|------|--|-----|
| 5.53 | surface appearance for FSW of extruded AZ31/AW6016 for different welding speeds at a constant rotational speeds of 1000 rpm.....   | 105 |
| 5.54 | tensile strength for FSW of extruded AZ31/Aw6016 subject to welding speed and rotational speed.....  | 106 |
| 5.55 | fracture length for FSW of extruded AZ31/AW6016 subject to welding speed and rotational speed.....   | 107 |
| 5.56 | tensile strength for FSW of extruded AZ31/AW6016 subject to weld pitch and rotational speed.....   | 107 |
| 5.57 | surface appearance for FSW of extruded AZ31/AW6016 for different welding Speeds at a constant rotational speed of 900 rpm and 22 °C.....   | 110 |
| 5.58 | surface appearance for FSW of extruded AZ31/AW6016 for different welding speeds at a constant rotational speed of 900 rpm and 130 °C.....  | 111 |
| 5.59 | comparison of occurring temperature during FSW of extruded AZ31/AW6016 for Different initial temperatures at constant rotational speed for welding speeds of a) 40 mm/min and b) 100 mm/min. BW-beginning of weld; MW- middle of weld; EW-end of weld..... | 112 |
| 5.60 | comparison of measured forces and torques for FSW of extruded AZ31/AW6016 at constant rotational speed: a) axial force as function of welding speed; b) torques as function of welding speed. (plunging phase).....  | 112 |
| 5.61 | comparison of measured forces and torques for FSW of extruded AZ31/AW6016 at constant rotational speed: a) axial force as function of welding speed; c) torques as function of welding speed. (welding phase).....   | 113 |
| 5.62 | comparison of tensile strength for FSW of extruded AZ31/AW6016 for different Welding speeds and initial temperature at constant rotational speed subject to a) axial force; b) torque.....   | 114 |
| 5.63 | comparison of tensile properties for FSW of extruded AZ31/AW6016 for different welding speeds and initial temperatures at constant rotational speed: a)tensile strength as function of weld pitch; b) fracture length as function of axial force.....      | 114 |
| 5.64 | micrographs for FSW of extruded AZ31/AW6016 at constant rotational speed for 40 mm/min and a) 22 °C and b) 130 °C.....   | 115 |
| 5.65 | micrographs for FSW of extruded AZ31/AW6016 at constant rotational speeds for 300 mm/min and a) 22 °C and b) 130 °C).....  | 115 |
| 5.66 | comparison of hardness profile for FSW of extruded AZ31/AW6016 at different Welding speeds at constant rotational speed and initial temperature.....   | 116 |

5.67 comparison of hardness profile for FSW of extruded AZ31/AW6016 at different  
Temperature for 40 mm/min at constant rotational speed.....117



**List of tables**

|      |   |    |
|------|---|----|
| 2.1  | advantages and disadvantages of FSW /Mis07/, /Chao03/.....  | 4  |
| 2.2  | proportion constant $K_0$ and activation energy $Q$ for Al3Mg2 and Al12Mg17.<br>/Yam09/.....                    | 13 |
| 2.3  | main FSW process variables /Loh10/,/IWB10/,/Zim10/.....   | 13 |
| 2.4  | physical properties of pure magnesium /Gup11/.....  | 17 |
| 2.5  | Absorption coefficient and specific electrical resistance for different materials<br>/Mor05/.....               | 19 |
| 2.6  | overview of process parameters of several investigations on FSW of<br>magnesium alloys.....                     | 21 |
| 2.7  | properties of pure aluminum /Kam95/.....  | 27 |
| 2.8  | designation of aluminum alloys /Ost98/.....   | 29 |
| 2.9  | Temperature dependency of AL AA6061-T6 yield strength /Cra06/.....  | 30 |
| 2.10 | overview of studies about FSW of dissimilar aluminum/magnesium joints.....                                      | 36 |
| 4.1  | Hermle UWF 1000 technical specifications /Her86/.....   | 42 |
| 4.2  | used welding tools.....   | 48 |
| 4.3  | chemical composition of the alloys AZ31 and AW6016 in wt-%<br>/Kam00/,/Nor04/.....                              | 49 |
| 4.4  | physical properties of the alloys AZ31 and AW6016 /Kam00/,/Nor10/.....  | 49 |
| 4.5  | process steps of wet grinding and polishing.....  | 53 |
| 5.1  | determination of values for electrical current for different welding speeds.....                                | 56 |
| 5.2  | settings for simulation of laser interaction on magnesium.....  | 57 |
| 5.3  | experimental settings for FSW of extruded AZ3.....  | 60 |
| 5.4  | experimental settings for LAFSW of extruded AZ31.....   | 71 |
| 5.5  | experimental settings for FSW of extruded AZ31 with heating element in bead<br>on plate weld configuration..... | 79 |
| 5.6  | experimental settings for FSW of extruded AZ31 with heating element in butt<br>weld configuration.....          | 83 |



|     |   |     |
|-----|---|-----|
| 5.7 | experimental settings for FSW of rolled AZ31 with heating element in butt weld configuration..... | 93  |
| 5.8 | experimental settings for FSW of extruded AZ31/Aw6016.....  | 103 |
| 5.9 | experimental settings for FSW of extruded AZ31/AW6016 with heating element...                     | 109 |



**Abbreviations and symbols**

|       |   |                                      |
|-------|---|--------------------------------------|
| AS    | - | Advancing Side                       |
| FSW   | - | Friction Stir Welding                |
| HAZ   | - | Heat Affected Zone                   |
| HV    | - | Vickers Hardness                     |
| IMC   | - | Intermetallic Compounds              |
| LAFSW | - | Laser Assisted Friction Stir Welding |
| RS    | - | Retreating Side                      |
| TMAZ  | - | Thermal Mechanical Affected Zone     |
| UTS   | - | Ultimate Tensile Strength            |

| Symbol     | Explanation                            | Unit              |
|------------|--|-------------------|
| $k_f$      | Yield stress                           | N/mm <sup>2</sup> |
| $R_m$      | Tensile strength                       | N/mm <sup>2</sup> |
| $\sigma$   | Stress                                 | N/mm <sup>2</sup> |
| F          | Acting Force                           | N                 |
| $A_0$      | Cross-section                          | mm <sup>2</sup>   |
| A          | Current cross-section                  | mm <sup>2</sup>   |
| $\varphi$  | True strain                            |                   |
| $\sigma_0$ | Initial stress of dislocation movement | N/mm <sup>2</sup> |
| N          | Rotational speed                       | rpm               |
| f          | Welding speed                          | mm/min            |
| $\alpha$   | Tool tilt angle                        | °                 |
| $D_p$      | Plunge depth                           | mm                |
| $A_{ab}$   | Coefficient of absorption              |                   |
| $\lambda$  | Wave length                            | μm                |
| $P_{real}$ | Real laser power                       | W                 |

## 1. Introduction

The requirement of lightweight construction in different industrial fields increases steadily. Especially the automotive industry represents a mainspring for it in order to reduce emission and fuel consumption. Therefore, the light metal aluminum ( $2,7 \text{ g/cm}^3$ ) was successfully used for structural applications in the last years. Increasing requirements necessitated lighter materials whereby magnesium came into focus. A density of  $1,74 \text{ g/cm}^3$  and high specific mechanical properties enable to replace components made of aluminum by magnesium. Nowadays it is already used in terms of castings, e.g. as back door and crankcase. /Kam95/

Another beneficial aspect is represented by joining of dissimilar materials like aluminum and magnesium. Due to different physical properties like melting point and the formation of intermetallic compounds, the joining of aluminum and magnesium is inapplicable by fusion welding processes. Whereas a solid-state welding process, called Friction Stir Welding, is considered as a promising procedure for this approach. High reproducible quality and a smaller heat affected zone in comparison to fusion welding are beneficial advantages of this process./Raz11/ Indeed, the cost effectiveness is less in comparison to other procedures based on low welding speeds. In case of FSW, the joining is made by plastic deformation and mixing of the materials, whereby the process strongly depends on the yield stress. To initial plastic deformation, this stress has to be overcome. For that purpose, high forces are necessary. The yield stress exhibit a high dependency on temperature. A remarkable reduction of yield stress is possible by increasing the forming temperature as well as the initial temperature of the workpiece. /Doe07/ This effect is very useful for FSW and provides a valuable approach for the improvement of the process. Considerations to raise the initial temperature of workpieces leads to the development of different advanced FSW processes like the Laser Assisted Friction Stir Welding (LAFSW). The workpieces are locally heated by laser, which decrease the level of required force to deform the material. Lower process forces enable higher welding speeds whereby the efficiency of FSW can be improved. The effect of initial temperature of workpieces on process loads will be investigated in the present work.

## 2. State of the art

### 2.1. Friction Stir Welding: in general

#### 2.1.1. Process

In December 1991 a new solid-state joining process, called Friction Stir Welding (FSW), was invented and patented by Wayne Thomas at TWI (The Welding Institute) in the United Kingdom. This relatively new process enables joining so called non-weldable materials like highly alloyed 2XXX and 7XXX series, which are very difficult to weld by fusion processes due to cracking susceptibility and porosity. Nowadays the use of FSW is extended to join other materials like magnesium, copper, steel, titanium and plastics. Even joining of different materials is possible /Rod09/

In comparison to fusion welding, FSW is a relatively simple process shown in figure 1.1 (a). A nonconsumable rotating tool consisting of shoulder and pin plunges into the workpieces to be welded. Afterwards, the tool makes a transversal motion along the joint. A more specialized consideration enables figure 1.1 (b). A typically force progression during FSW is shown. In general, the process can be divided in four parts (figure 1.1 b) I to IV). In the first step (I), the rotating tool moves downward for the workpiece and plunges in. Since it is a solid state joining process, a high axial force (some kN) is required, which is represented by the peak value. Subsequent the tool dwells for some seconds in a position, whereby heat is generated by the friction between tool and workpiece. Consequently, the material is plasticized and starts to flow, which results in a decreasing force (II). Step three (III) is the actual welding process. As mentioned, the tool moves along the joint with a constant speed. Thereby a constant force level (figure 1.1 b) III) is produced. During the movement, the material is transported around the pin and shoulder from the advancing side (welding speed is in direction of rotational speed) to the retreating side (welding speed is not in direction of rotational speed). In part four, the process force decreases due to the upward motion of the tool (IV).

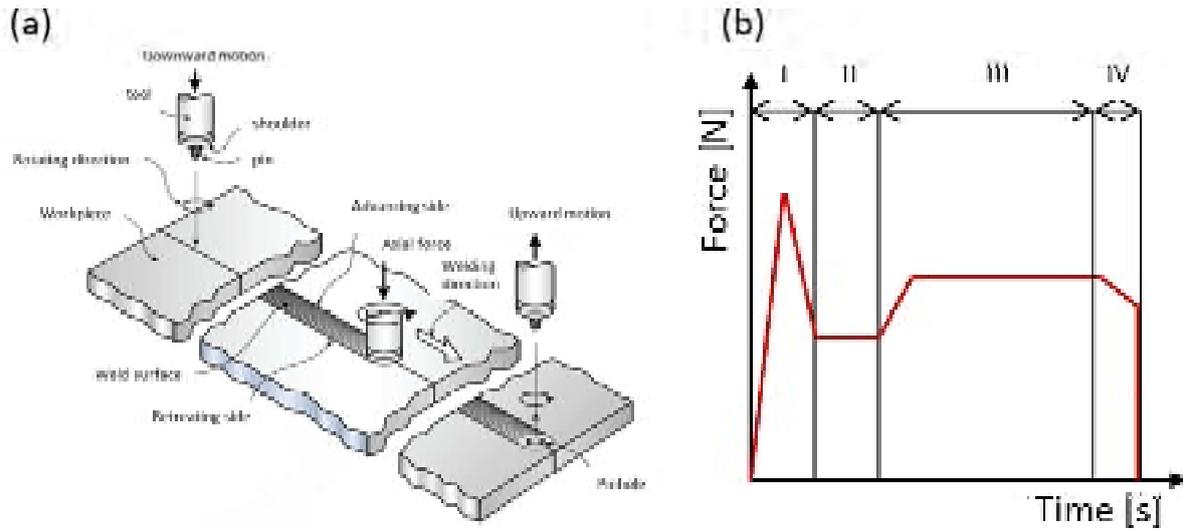


Figure 1.1: a) principle of the FSW process /Nor12/ b) schematic force progression during FSW.

The relative movement between workpiece and tool results in heat input and deformation of the material, whereby four characteristic microstructural regions are created as shown in figure 1.2. The area of recrystallization, called weld nugget, suffers the greatest deformation caused by the tool pin. Its shape is asymmetrical due to the differing flows of material between the advancing side and retreating side. The region surrounding the weld nugget contains grains of the base material plastically deformed by the tool. It is called thermal mechanically affected zone (TMAZ). Besides the TMAZ is located the heat affected zone (HAZ) which is characterized by material influenced by thermal load, but without plastic deformation. The parent material or unaffected zone is not affected by the heat or deformation. /Sci07/

Both advantages and disadvantages of FSW are given in table 2.1.

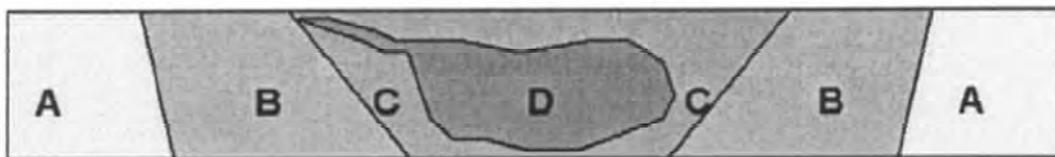


Figure 1.2: schematic of a typical FSW cross-section (A) Parent Material; (B) Heat Affected Zone; (C) Thermal Mechanically Affected Zone; (D) Weld Nugget. /Sci07/

Table 2.1: advantages and disadvantages of FSW /Mis07/, /Cha03/

| Advantages                              | disadvantages                        |
|---|--------------------------------------|
| Solid-state process (no melting)        | High process forces                  |
| High heat efficiency                    | High requirements on clamping system |
| No filler material                      | Low welding speed                    |
| No inert gas atmosphere                 | Pinhole at the end of the weld       |
| High reproducible quality               |                                      |
| No smoke generation                     |                                      |
| No requirement of high purity materials |                                      |
| Possibility of dissimilar joints        |                                      |



### 2.1.2. Deformation behavior

The deformability behavior of material is an important aspect in the forming technology but also in the FSW process. As already mentioned a rotational tool is plunged into the joining members. Due to the rotation sufficient heat is generated for plastic deforming and mixing the material. From this, a dependency of yield stress  $k_f$  can be assumed. According to /Doe07/, the yield stress is defined as the stress which introduces and abides plastic deformation of material. This applies with regard to the uniaxial stress state.

Influencing parameters are given in figure 2.1. The diagrams show a strongly dependency of the yield stress on temperature. An increase of the forming temperature results in significant reduction of the stress. Thereby the required forces to deform the material decrease, too. In case of low temperature the yield stress raise by increasing true strain. In contrast, the true strain rarely affects yield stress at high temperature. This is based on the regeneration of new grains (recrystallization) at higher temperature. Thereby the generation of dislocations is prevented. /Doe07/

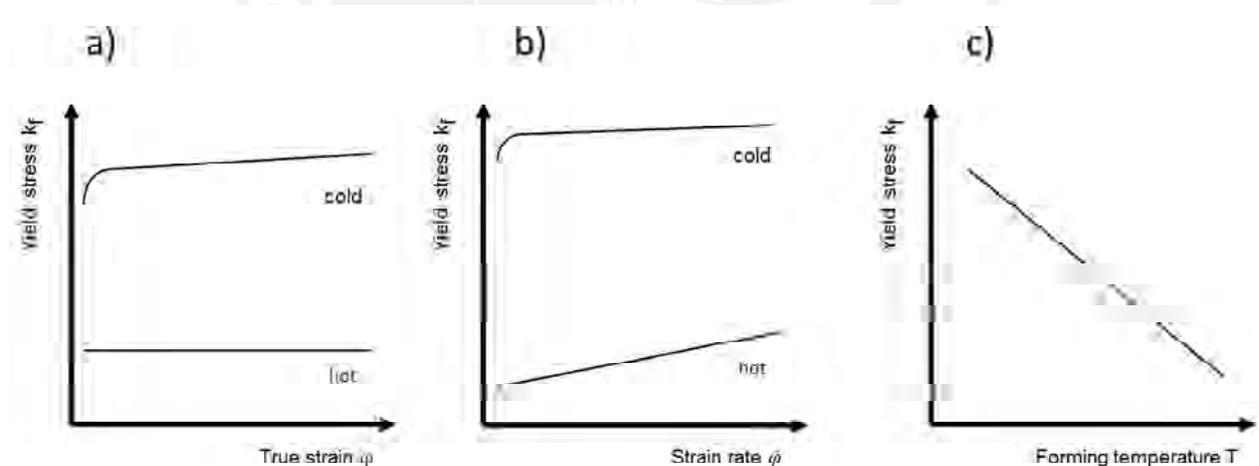


Figure 2.1: schematic illustration of yield stress as function of a) true stress; b) strain rate; c) forming temperature /Doe07/

The determination of the yield stress can be carried out by different methods like compression or tensile test. In the following part, determination of yield stress by tensile test is regarded.

The procedure of tensile test supplies the stress-strain-diagram which enables to establish a statement about elastic and plastic material behavior. A schematic illustration with characteristic values is given in figure 2.2. At the beginning of the test, the specimen is elongated elas-

tically up to proof stress  $R_{p0,2}$ . In case of unload at this point, the sample would possess a plastically deformation of 0,2 %.

The maximum load is characterized by the tensile strength  $R_m$ . Up to this point, the elongation is carried out without necking. Afterwards, the cross-section decrease until fracture. /Doe07/

The yield stress as function of the true strain is called flow curve. It describes the plastic flow behavior of materials from the end of elastic deformation up to fracture. /Doe07/

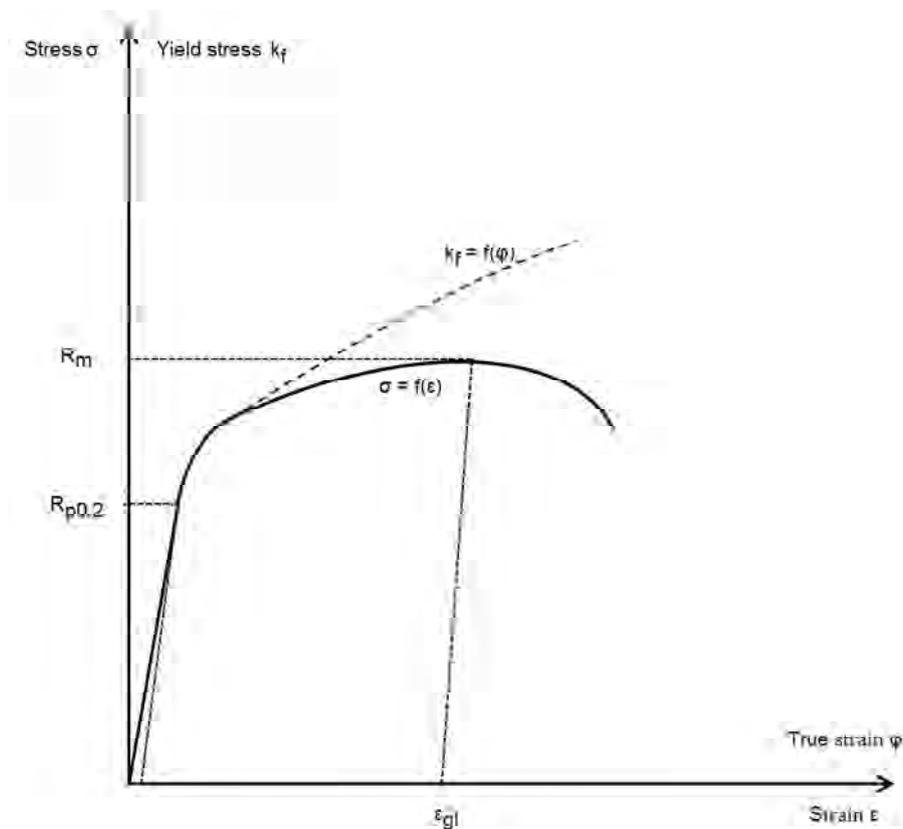


Figure 2.2: schematic illustration of stress-strain-diagram and flow curve from the tensile test. /Lan08/

The diagrams showed in figure 2.3 are received by tensile tests. Presented are yield stresses as function of true strain and temperature for different alloys. Obviously, the level of yield stress is different for each alloy. For the magnesium alloys it can be seen that more stress is required to initial plastic deformation for AZ31B a) than for MN150 b). The difference is based on the alloying elements. AZ31 mainly contains aluminum and zinc which improve tensile properties and hardness. In contrast MN150 is alloyed by manganese. This element leads to advanced corrosion behavior. /Kam00/



The effect of decreasing yield stress by raising temperature is clearly observable for all alloys. At higher temperatures and increasing true strain, the curves are obviously smoother than for low temperatures.

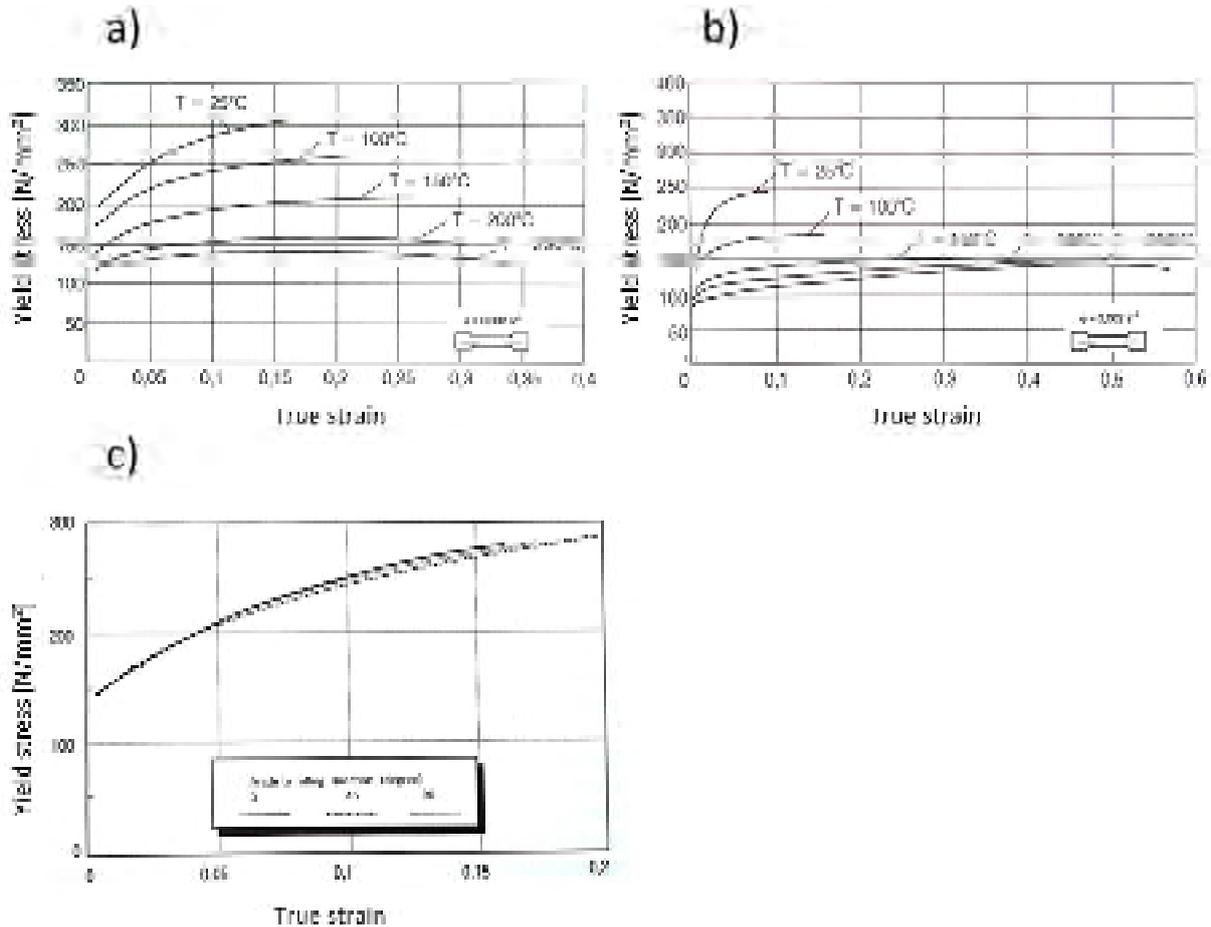


Figure 2.3: Flow curves received by tensile tests for different materials a) AZ31B; b) MN150; c) AW6016./Kam00/, /Ost98/

The calculation of the stress  $\sigma$  [N/mm<sup>2</sup>] and the elongation  $\varepsilon$  is carried out as follows:

$$\sigma = \frac{F}{A_0} \tag{2-1}$$

$$\varepsilon = \int_{l_0}^l \left(\frac{1}{l_0}\right) dl = \frac{l-l_0}{l_0} = \frac{\Delta l}{l_0} \tag{2-2}$$

By means of (2-2) can be seen that the stress  $\sigma$  is the relation of acting force F [N] and the initial cross-section  $A_0$  [mm<sup>2</sup>]. The elongation  $\varepsilon$  determined by the length change  $\Delta l$  [mm] related to the initial length  $l_0$  [mm]. /Lan08/, /Doe07/

In contrast to the stress  $\sigma$ , the yield stress  $k_f$  is calculated with respect to the current cross-section  $A$  [mm<sup>2</sup>] as shown in (2-3). Because of this, yield stress is also called true stress in literature.

$$k_f = \frac{F}{A} \quad (2-3)$$

(2-4) represents the calculation of the true strain  $\varphi$ . /Doe07/

$$\varphi = \int_{l_0}^l \left(\frac{1}{l}\right) dl = \ln l - \ln l_0 = \ln \frac{l}{l_0} \quad (2-4)$$

By using (2-2) a relation between the yield stress  $k_f$  and the stress  $\sigma$  can be done as shown in (2-5). /La08/

$$k_f = \sigma(\varepsilon + 1) \quad (2-5)$$

An important factor concerning yield stress is the grain size of the material. A decreasing grain size results in a lower yield stress. That means, grain refinement can be used to improve the plastic deformability of materials. The relation of grain diameter  $d$  and yield stress  $k_f$  is described by the Hall-Petch- relation:

$$k_f = \sigma_0 + k \frac{1}{\sqrt{d}} \quad (2-6)$$

Moreover the equation contains the initial stress of the dislocation movement  $\sigma_0$  and the resistance of grain boundary  $k$ . Besides, the effect can be applied to the tensile strength respective micro hardness. By decreasing grain diameter, the micro hardness respective tensile strength rise. /Raz11/

### 2.1.3. Diffusion

The thermal activated process of migration of atoms and molecules, so called diffusion, is a well-known effect in solids. Reason for diffusion is an existing concentration gradient. Atoms aim to balance this gradient by moving from areas with high concentration to those with low concentration. /Sch10/ Diffusion in solids supports the FSW process of dissimilar joints by reinforcement the bonding between the joint members.

A statistic disordered and directionless movement occurs in homogenous workpieces and is called self-diffusion. In addition a directed particle stream results in inhomogeneous materials in case of a concentration gradient. /Sch10/

Diffusion in solids is not affected by external forces, but strongly by temperature. /Sch03/ By elevate temperature, the amount of diffusion processes increase. /Li12/ Above a temperature of 0 K, the atoms begin to oscillate around their idle state in the crystal lattice. By introduction of heat the kinetic energy of the atoms increase until a certain level, which is called activation energy (needed energy to start the diffusion process). As result the particles are able to switch their position. /Gob06/ This movement takes place in three different kinds as shown in figure 2.4.

Most improbable is the mass-shifting by direct transposition (figure 2.4 a) due to the required high activation energy  $Q$ . In contrary the needed energy level in case of vacancy diffusion (figure 2.4 c) is much less therefore it is the most prevalent form. The higher the temperature, the larger the number of vacancies becomes. Figure 2.4 b shows another common form of diffusion: the interstitial lattice mechanism. The degree of efficiency rises with diminution of the foreign atoms diameter. /Sch10/

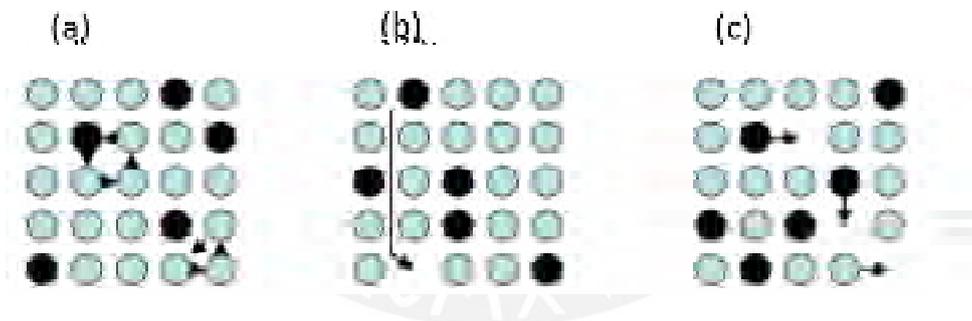


Figure 2.4: transposition processes in crystal lattice: a) direct transposition b) interstitial lattice c) vacant lattice position. /Li12/

Additional to the three mentioned mechanisms there are three ways for diffusion. The schematic illustration in Figure 2.5 clarify that diffusion can be effected on the material surface, along the grain boundaries or in the grains. Decreasing required activation energy lead to a higher rate of movements of the atoms and consequently to easier diffusion processes. This circumstance affects especially the diffusion on the material surface because of the available vacancies. In the area of the grain boundaries exist a lot of lattice defects, thus the needed energy is reduced. In comparison the movability of particles in the grains is much lower. /Sch10/

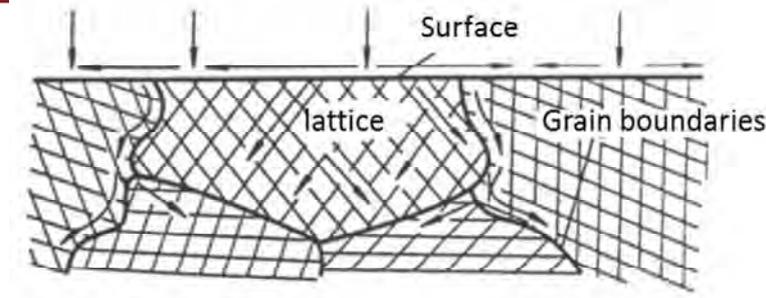


Figure 2.5: diffusion paths. /Li12/

A quantitative description of the diffusion in inhomogeneous materials in case of steady-state is given by the first Fick's law:

$$J = \frac{dm_n}{dt} = -D \cdot \frac{dc_n}{dx} \cdot S \quad (2-7)$$

$J$  represents the number of particles  $n$  per time unit which flow ( $\frac{dm_n}{dt}$ ) through a surface  $S$  (perpendicular to diffusion direction) with  $m$  = mass of the diffusing atoms,  $t$  = time,  $c$  = concentration of the diffusing atoms,  $x$  = diffusion direction (distance) and  $D$  = coefficient of diffusion. According to (2-7) material-flow is a function of a concentration gradient ( $\frac{dc_n}{dx}$ ). The concentration of atoms is shown in figure 2.6 as a function of the distance. /Sch10/

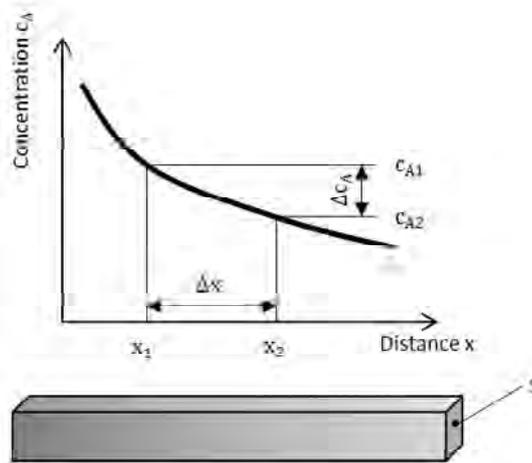


Figure 2.6: for derivation of the resulting material-flow  $J$  by diffusion processes. /Sch10/

According to/Sch10/ the diffusion coefficient is crucial for the diffusion process. This strongly temperature-dependent parameter is described by the Arrhenius equation:

$$D = D_0 \cdot \exp\left(-\frac{Q_A}{RT}\right) \quad (2-8)$$

Moreover,  $D$  depends on  $D_0$  = diffusion constant,  $Q_A$  = activation energy and  $R$  = gas constant (=8,314 J/K·mol). The diffusion constant describes the proper motion (frequency of oscillation) of the particles.

Provided that a constant concentration gradient exists, the mean diffusion way  $x$  can be derived by (2-7):

$$x^2 = Dt \quad \text{or} \quad x = \sqrt{Dt} \quad (2-9)$$

In case of dynamic (no constant concentration gradient) processes the second Fick's law is suitable:

$$\frac{\partial c}{\partial t} = D \cdot \frac{\partial^2 c}{\partial x^2} \quad (2-10)$$

In consideration of specific basic condition there exist solutions for equation (2-10).

#### 2.1.4. Intermetallic Compound

Intermetallic compounds are chemical bonds which consist of two dissimilar components (at least one part is a metal). Characteristic of these compounds is the lattice structure, because it is neither the base constituent structure nor the structure of the other component. /Uym07/ In accordance to /Wei10/ this case occurs if the amount of alloying element exceeds the absorption capacity (solubility) of the base element. The solubility of magnesium in aluminum and vice versa is illustrated in the binary phase diagram for the aluminum/magnesium-system (figure 2.7). The maximal solubility of magnesium in aluminum amount to 18,9% at 450°C. At 437°C aluminum is soluble in magnesium up to 11,8%. Both temperatures represent the eutectic points at a concentration of 38% at magnesium (450°C) and 69% at magnesium (437°C). Above these temperatures the intermetallic compounds arise from the solidification of the melt. By contrast the formation of the phases occurs below the eutectic temperatures by interdiffusion. Moreover figure 6 gives an overview about the intermetallic phases of aluminum and magnesium. Besides the  $\beta$ -phase (approximate stoichiometry of  $\text{Al}_3\text{Mg}_2$ ) there is the  $\gamma$ -phase (approximate stoichiometry of  $\text{Al}_{12}\text{Mg}_{17}$ ). /Sep12/

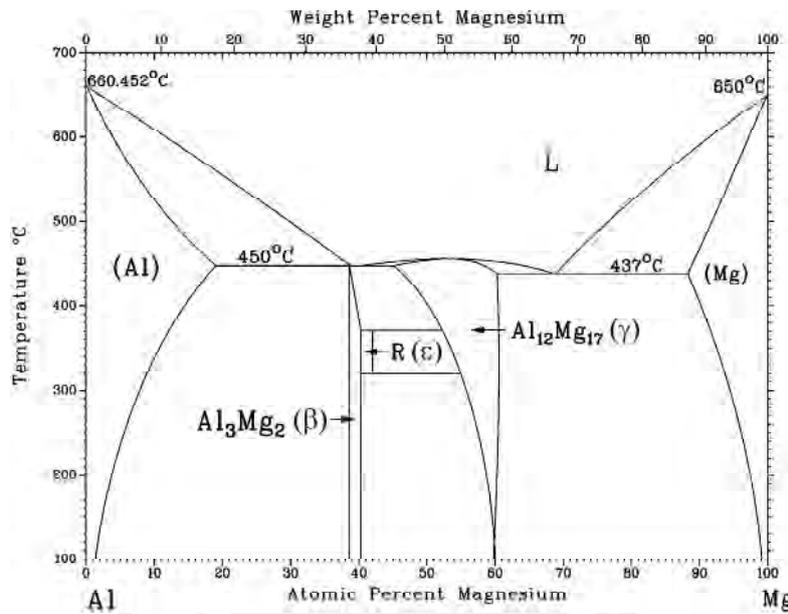


Figure 2.7: Phase diagram of Al-Mg-system. /Mur82/

Intermetallic compounds are very brittle substances /Uym07/ wherefore their influence, especially of Al<sub>12</sub>Mg<sub>17</sub> and Al<sub>3</sub>Mg<sub>2</sub> on tensile properties is investigated in numerous studies. In regard to fusion welding of aluminum and magnesium the formation of the intermetallic compounds is problematic because they leading to a degradation of mechanical properties/Cho11/. Pursuant to /Yam09/ the knowledge about the influence of intermetallic phases on FSWed aluminum/magnesium-joints is rarely due to problems in observing layers of less than 1μm with an optical microscope.

Caused by the relation between formation and growth of intermetallic compounds and react diffusion the layer thickness  $d$  should increase with diffusion time  $t$ . This circumstance enables the description of the thickness by the Arrhenius equation:

$$d^2 = K \cdot t \tag{2-11}$$

where

$$K = K_0 \cdot e^{\frac{-Q}{R \cdot T}} \tag{2-12}$$

With  $K_0$ = proportion constant,  $Q$  =activation energy,  $R$  =gas constant and  $T$  =absolute temperature.

Table 2.2: proportion constant  $K_0$  and activation energy  $Q$  for  $Al_3Mg_2$  and  $Al_{12}Mg_{17}$ . /Yam09/

|                    | $Al_3Mg_2$           | $Al_{12}Mg_{17}$ |
|--------------------|----------------------|------------------|
| $K_0$ [ $cm^2/s$ ] | $1,5 \times 10^{-4}$ | 22               |
| $Q$ [kJ/mol]       | 55,3                 | 125,7            |

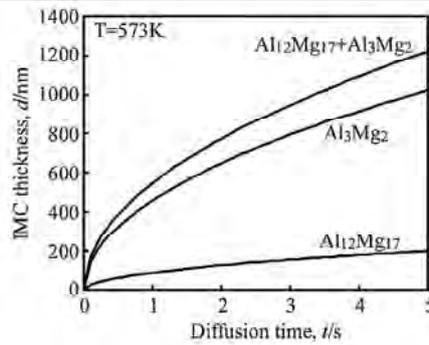


Figure 2.8: intermetallic compounds thickness as function of diffusion time /Yam09/

Table 2.2 gives the results for the proportion constant and the activation energy calculated by/Yam09/. The temperature at the interfacial region during the FSW process was measured with 573K. This enables the calculation of the intermetallic compounds thickness at different diffusion times as shown in figure 2.8. By means of figure 2.8 it is obviously that  $Al_3Mg_2$  grows faster than  $Al_{12}Mg_{17}$ .

### 2.1.5. Influencing variables

Although FSW seems to be a relatively simple process, there are a lot of variables which affect the welding result. As shown in Table 2.3 the main parameters include tool design, machine and other variables. These influence the joint result through heat generation, material flow, defect formation, process forces, temperature distribution and grain size. /Loh10/

Table 2.3: main FSW process variables/Loh10/, /IWB10/, /Zim10/

| Tool design variables      | Machine variables     | Other variables         |
|----------------------------|-----------------------|-------------------------|
| Shoulder and pin materials | Welding speed         | Anvil material          |
| Shoulder diameter          | Rotational speed      | Anvil size              |
| Pin diameter               | Plunge force or depth | Workpiece size          |
| Pin length                 | Tool tilt angle       | Workpiece properties    |
| Thread pitch               | Plunging speed        | Clamping technology     |
| Feature geometry           |                       | Type of joint           |
|                            |                       | Deformation of facility |

Fundamental for the welding process are the properties of the material to be welded. Besides aluminum it is possible to joint other materials like magnesium, titanium, copper, steel, lead and plastics by FSW. Moreover, the regarded process enables to weld dissimilar joints like aluminum and magnesium. /Loh10/

Pursuant to/Mis05/, the rotational speed  $N$  and the welding speed  $f$  are significant for FSW. The tool rotation occurs in clockwise or counterclockwise direction and is responsible for stirring and mixing the material around the pin. /Kum12/ Furthermore, it influences the axial force and the heat input into the welding zone. /Kum12/ Increasing the rotational speed cause higher friction heating and thereby, higher temperature in the material. /Mis05/ About 95 % of this generated frictional heat flows into the workpiece. This means a heat loss of 5 % into the tool. /Cha03/ The movement of the tool along the joint line is fulfilled by the welding speed. /Mis05/ In addition to axial force and heat input, it is a significant parameter for the longitudinal force. /Kum12/

A tool tilt angle  $\alpha$  (figure 2.9) is helpful in regarding to hold the plasticized material under the tool shoulder. Usually, it is between  $2^\circ$  and  $5^\circ$  towards the trailing direction./Mis05/

High joint qualities and sound welds also depend on plunge depth  $D_p$ . It describes the depth with which the trailing shoulder edge is located in the material.

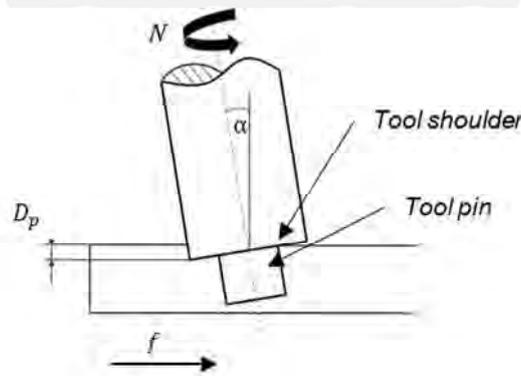


Figure 2.9: schematic illustration of the FSW-process /Ruh12/

As mentioned in 2.1.1 the FSW process generates high forces, therefore the requirements on the clamping technology are high. The fixture system has to ensure that the workpiece is located in a fixed position during the process. Especially the plunging phase causes high axial forces which could disperse the workpieces. Investigations have shown that the maximum loads during plunging phase can be reduced by higher rotational speed and lower plunging speed. /Zim10/



In accordance with /Mis05/ the most important factor of process development is the tool geometry. Because of its influence on the material flow and the heat-distribution, the tool can provide for high quality welds.

Essentially three functions are achieved by the FSW-tool. Both pin and shoulder (figure 2.9) are responsible for the heat input into the workpiece./Mis07/ Different investigations/Käl05/, /Wil06/, /Kum12/ show that the shoulder diameters influence on heat input is higher than the pin diameters. /Käl05/, /Wil06/ indicates an area of influence between 2% and 50% for the tool pin.

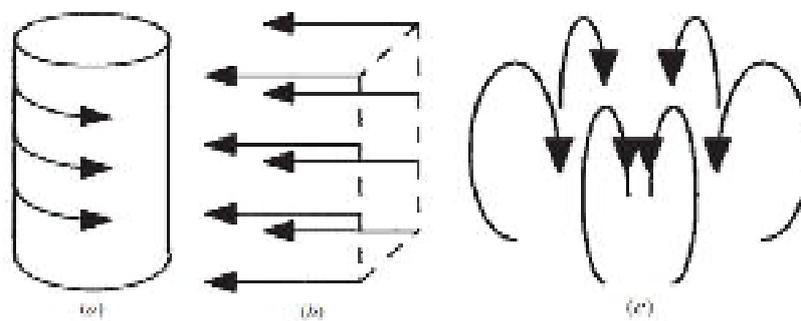


Figure 2.10: Three incompressible flow fields of FSW: a) rotation, b) translation and c) ring vortex.

/Sch04/

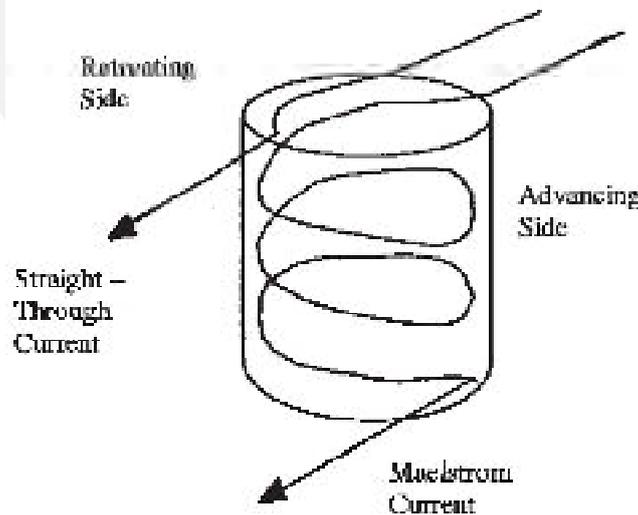


Figure 2.11: material flow resulting from superimposed incompressible flow fields. /Sch04/

Another purpose of the tool is the movement of the plasticized material around the pin. As described in /Loh10/ the breakup of the faying surfaces of the joint materials and the mixing among themselves is achieved by the pin. Near by the material flow (figure 2.11) consists of three parts (rotation, translation and ring vortex) as shown in figure 2.10. /Sch04/ In /Ath09/ is

described that an asymmetric flow field occurred which leads to differing velocity and pressure fields. Several researches indicate that the flow behavior of the material is similar to the extrusion process which means high strain and strain rates are generated./Col199/, /Nan08/ A strain of 3.5 with a strain rate of up to 85 s<sup>-1</sup> are reported by/Che09/.

The third primary function of the FSW tool is the containment of the plasticized material in the welding zone, which is accomplished by the tool shoulder. /Mis07/

Welding and rotational speed, tool design as well as plunging depth are very important parameters for the FSW process. They strongly affect the level of the occurring force and torque and finally the heat input. By increasing the rotational speed, a reduction of loads is observable. In contrary, higher forces and torques occurred in case of raising welding speed and plunge depth as soon as shoulder diameter. /Jan13/Concerning forces, the deformation of facility have to be regarded. An occurrence of elastic deformation of the machine due to high axial forces can lead to a reduction of the plunge phase during welding. In consequence, defects at the weld bottom can occur because of lack of penetration. /IWB10/

An important factor in the FSW process is represented by the weld pitch. /Abb06/ It is the ratio of welding speed and rotational speed and describe the amount of heat that is introduced in the welding process. In case of a high weld pitch, the weld is assumed to be “cold weld”. The high weld pitch means a low rotational speed and a high welding speed. As a result, the duration of contact between tool and material is short, whereby the generated heat level is low. In contrast, a low ratio results in a “hot weld”. Due to the low welding speed, the heat generated by friction is high. Thereby the material’s yield stress decrease and the plastic deformation is easier. According to /Ke04/, a low weld pitch is an indicator for sound welds. In case of a high ratio, defects appear in the weld caused by inadequate material flow. This is produced by insufficient heat generation. Typical defects are the wormhole, surface lack of fill and the lack of penetration. All of them results in inferior tensile properties. In contrast, defect can also be formed by “hot welds”. The following defects can occur due to excessive heat input: welding burr, surface galling and root flow.

**2.2. Materials**

**2.2.1. Magnesium**

**Characteristics of pure magnesium**

Magnesium is the eighth most abundant element in the earth’s crust. Because of its responsiveness it does not exist in an elemental form, but magnesium compounds are available all over the world. According to (MGu11) magnesite ( $MgCO_3$ ), dolomite ( $MgCO_3 \cdot CaCO_3$ ), carnallite ( $KCl \cdot MgCl_2 \cdot 6H_2O$ ) and seawater are the most common compounds. With a density of about  $1,74 \text{ g/cm}^3$  is magnesium the lightest industrial used metal and one-third lighter than aluminum ( $2,7 \text{ g/cm}^3$ ) and three-fourth lighter than steel ( $7,2 \text{ g/cm}^3$ ). Based on excellent properties like low density and high specific mechanical properties (Figure 2.12), magnesium materials have a huge potential in lightweight tasks. Table 2.4 shows the most significant physical properties of pure magnesium. /Gup11/

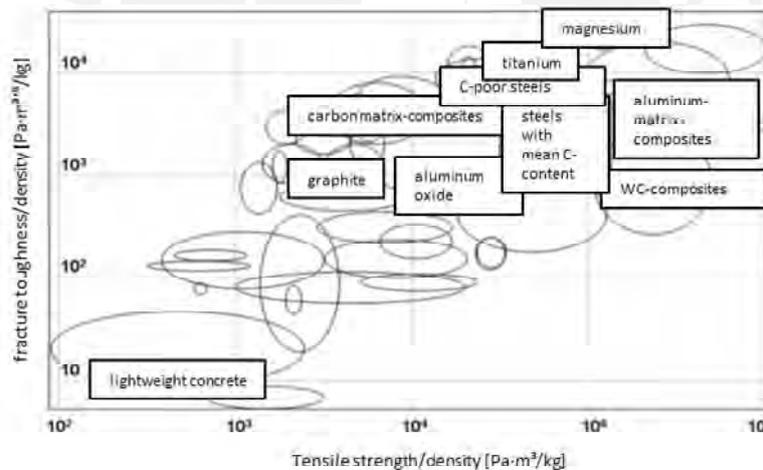


Figure 2.12: comparison of mechanical properties of selected material classes related to the respective material density /Müc05/

Table 2.4: physical properties of pure magnesium. /Gup11/

|  |                              |
|--|------------------------------|
| <b>Crystal structure</b>                     | Hexagonal close-packed (HCP) |
| <b>Density (at 20°C)</b>                     | 1,738 g/cm³                  |
| <b>Elasticity modulus</b>                    | 45 GPa                       |
| <b>Melting point</b>                         | (650 ± 1) °C                 |
| <b>Boiling point</b>                         | 1090 °C                      |
| <b>Thermal conductivity (at 27 °C)</b>       | 156 W/(mK)                   |
| <b>Specific heat capacity (at 20 °C)</b>     | 1,025 kJ/(kgK)               |
| <b>Latent heat of fusion</b>                 | 360 -377 kJ/kg               |
| <b>Latent heat of vaporization</b>           | 5150 -5400 kJ/kg             |
| <b>Latent heat of sublimation (at 25 °C)</b> | 6113 -6238 kJ/kg             |
| <b>Electrical conductivity</b>               | 22,6 m/Ωmm²                  |
| <b>standard electrode potential</b>          | -2,375 V                     |

A standard electrode potential of  $-2,375$  V shows the base character of magnesium whereby the responsiveness is justified. The affinity of magnesium to non-metals (e.g. oxygen) results in the generation of a grey oxide film in contact with air. Thereby the material is protected against corrosion at low temperatures. /Mor05/

A negative property of magnesium is the burning with a bright white light slightly above the melting point ( $650$  °C). Due to a relative high thermal conductivity ( $156$  W/(mK)), this characteristic is uncritical in concern to a compact form. In contrast, swarf is easily flammable because of a large specific surface. /Kam00/

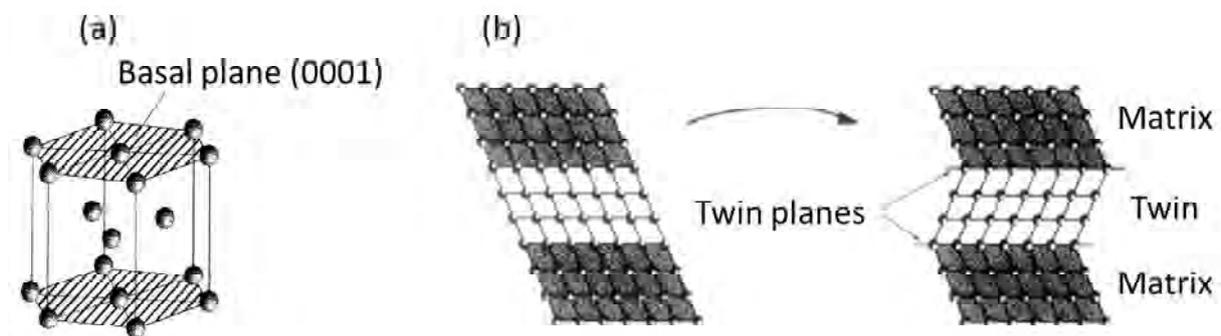


Figure 2.13: a) basal plane in hexagonal close-packed crystal structure b) principle of twinning /Kam00/

The deformability of pure magnesium at room temperature is very poor. This circumstance is caused by the hexagonal close-packed crystal structure (Figure 2.13 a)) since sliding occurs mainly in the basal plane. Additionally, the generation of twin planes (figure 2.13 b)) in the pyramid plane supports the deformation at room temperature. These planes are mirror symmetrical to the initial position (Matrix) excited by shear strain. Above a temperature of about  $225^{\circ}\text{C}$ , the atoms possess a higher movability whereby additional pyramidal slide-planes are activated. In conclusion the deformability increases erratically. /Kam00/

The deformability is especially important in the deformation technology, whereas applications like laser material processing require good optical properties. These are strongly dependent on the surface condition, which represents the place for interactions between material and radiation.

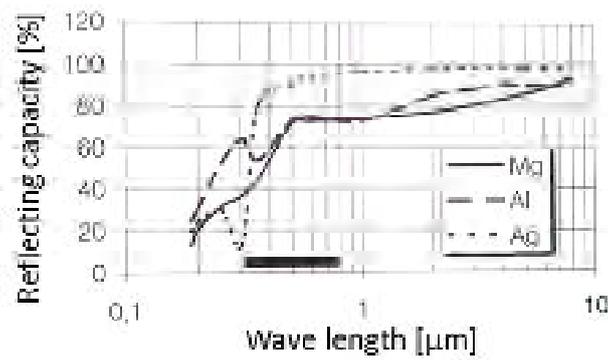


Figure 2.14: reflection capacity of magnesium, aluminum and silver. The black beam marking the visible spectrum /Kam00/

The reflecting capacity of magnesium in dependence of wave length is shown in figure 2.14. In comparison to aluminum the graph indicates a similar high level. In reverse, high reflection means a low absorption capacity. /Kam00/ In accordance to/Pie07/, the absorption is affected by many factors. Besides surface roughness, wavelength, angle of incident laser beam and temperature are important. Thus, a precise prediction is almost impossible.

Pursuant to/Mor05/, there does not exist a value for the absorption coefficient  $A_{ab}$  of magnesium. Indeed it could be calculated with the specific electrical resistance  $\Omega$  and the wave length  $\lambda$ :

$$A_{ab} \approx 0,0365 \cdot \Omega^{0,5} / \lambda^{0,5} \tag{2-14}$$

For validating the equation, the absorption coefficient was also calculated for aluminum and iron and compared with proved data. The differences were insignificant. Calculated results and values for electrical resistance are given in table 2.5. The calculation is only applicable for blank metal surfaces. /Mor05/

Table 2.5: Absorption coefficient and specific electrical resistance for different materials /Mor05/

|                  | $\Omega$ [ $\mu\Omega$ cm] | $A_{ab}$ for $\lambda=1,06 \mu\text{m}$ | $A_{ab}$ for $\lambda=10,6 \mu\text{m}$ |
|------------------|----------------------------|---|---|
| <b>Magnesium</b> | 4,5                        | 0,08                                    | 0,02                                    |
| <b>Aluminum</b>  | 2,65                       | 0,06                                    | 0,02                                    |
| <b>Iron</b>      | 9,5                        | 0,11                                    | 0,04                                    |

In contrast to the calculated values (table 2.5), an investigation of the absorption coefficient of the magnesium alloy WE43 and the aluminum alloy 1050 during Nd:YAG- laser ( $\lambda=1,06 \mu\text{m}$ )

interaction provides higher absorption values. Absorption of about 90 % is reached for WE43 at 2500 W laser power. At 3250 W, the aluminum alloy 1050 possesses a maximum absorption of about 70 %. /Pie07/

## Magnesium alloys

As mentioned before, magnesium possesses a lot of industrial useful properties. By addition of alloying elements characteristics like mechanical properties, corrosion resistance and castability can be enhanced. The effect is mainly based on precipitation hardening, solid solution hardening and fine grain hardening. /Gup11/ In the following section is described the effect of the most common alloying elements aluminum, zinc and manganese. /Nos03/

Alloying with aluminum (to about 10 wt%) and zinc (to about 6,5 wt%) has a positive effect on castability, hardness as well as strength. Negative is the increase of microporosity. Furthermore, zinc affects the weldability in a negative way and facilitates the generation of hot cracks. /Nos03/ Usually both elements are used together to reach a high strength level without a reduction in ductility. A beneficial effect on corrosion resistance provides the addition of manganese (to about 1,5 wt%) /Gup11/

The denotation for magnesium alloys is carried out by different norms in several nations, for instance DIN EN 1753 and DIN EN 1754 are applied in Europe. However, the common industrial designation is referred to the American Society for Testing and Materials (ASTM B 275), which is also used in this work. The designation consists of three parts. In the first part, the two main alloying elements, besides magnesium, are stated by letters (e.g. A for aluminum and Z for zinc) in order of decreasing percentage. The amount of both elements (in wt%) is given in the second part by two whole numbers. In case of AZ31, aluminum is contained with about 3 wt% and zinc with about 1 wt%. Part three represents different developmental stages in terms of letters, e.g. X indicates an experimental alloy.

## FSW of magnesium

Primarily developed for joining aluminum, the relevance for the FSW process of magnesium increased in the last years to force light weight design. In contrary to fusion welding of magnesium alloys FSW enables the joining without producing defects like porosity and hot cracks. Moreover the use of magnesium in the industry, e.g. automobile industry, results in a weight reduction due to their low density and finally to decrease fuel consumption. /Raz11/

Table 2.6: overview of process parameters of several investigations on FSW of magnesium alloys

| Alloy               | N<br>[rpm] | f<br>[mm/min] | UTS base<br>[MPa] | UTS joint<br>[MPa]     | source   |
|---------------------|------------|---------------|-------------------|------------------------|----------|
| AZ31B<br>6mm thick  | 1600       | 40            | 215               | 208<br>(97% of base)   | /Pad10a/ |
| AZ61A<br>6mm thick  | 1200       | 90            | 271               | 224<br>(82,6% of base) | /Raz11/  |
| AZ31<br>6,4mm thick | 2000       | 160-224       | 288, 292          | 201<br>(70% of base)   | /Joh03/  |
| AZ91D<br>6mm thick  | 500        | 160           | 203               | 183<br>(91% of base)   | /Joh03/  |
| AM50<br>6mm thick   | 250        | 224           | 215               | 180<br>(84% of base)   | /Joh03/  |
| AZ31B<br>6mm thick  | 1600       | 40,2          | 215               | 208<br>(97% of base)   | /Pad10/  |
| AZ31B<br>6mm thick  | 1600       | 40,2          | 215               | 208<br>(97% of base)   | /Pad09a/ |
| AZ91D<br>3mm thick  | 1100       | 120           | 229               | 199<br>(87% of base)   | /Ska04/  |
| AM50A<br>3mm thick  | 1200       | 180           | 225               | 157<br>(70% of base)   | /Ska04/  |

Despite of the high capability of FSW of magnesium, the number of relevant researches is less in comparison to aluminum. A plurality of these is concerned to the AZ31 alloy. Moreover, the joining of AZ61, AZ91, AM60 and AM50 by FSW were also studied. /Raz11/ In /Ska04/ was presented that the process window for FSW of magnesium is much smaller than for aluminum. It was justified by the influence of small changes in the parameters on the results.

Other investigations generated similar outcomes as shown in table 2.6. The best results, in regarding to the ultimate tensile strength, were obtained by /Pad09a/, /Ska04/ and /Pad10/. Un-

der almost identical conditions for welding the magnesium alloy AZ31B; all three studies present a tensile strength of 208 MPa which equates to 97% of the base-material. The elongation in /Pad09a/ and /Pad10/ is greatly reduced by about 50%. Whereas, a reduction of approximately 20% is reported in/Ska04/.

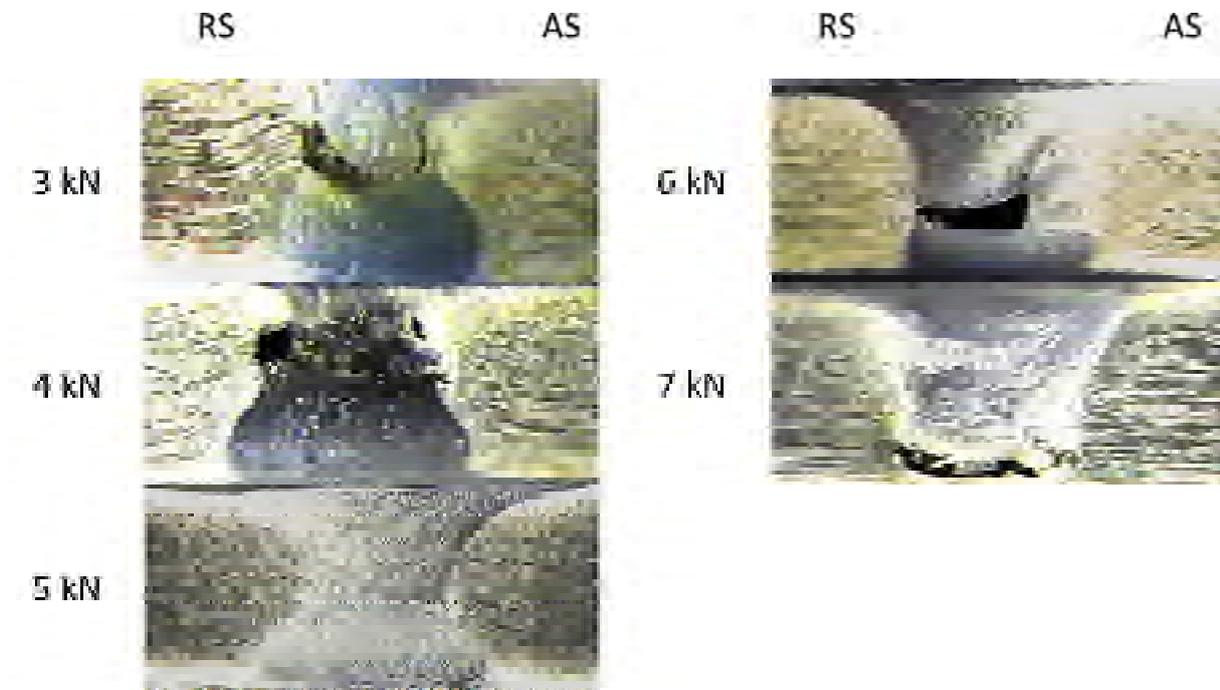


Figure 2.15: effect of axial force on macrographs of stir zone. /Raz11/

The occurring loads during FSW are identified as important indicator for weld quality. To form defect free welds, a certain level of axial force is required. /Pad10/ According to/Raz11/, the “formation of defect free FSW welds is a function of optimum axial force” due to the effect on heat input. The investigation contains FSW of 6 mm thick AZ61A for five different axial forces (3; 4; 5; 6 and 7 kN) at constant welding speed of 90 mm/min and tool rotational speed of 1200 rpm. As shown in figure2.15, the only defect free weld is obtained by welding at 5 kN axial force. The author indicates the formation of finer grains and optimum material flow as reason. Caused by an adequate heat input, dynamic recrystallization occurs whereby the finer grains are formed.

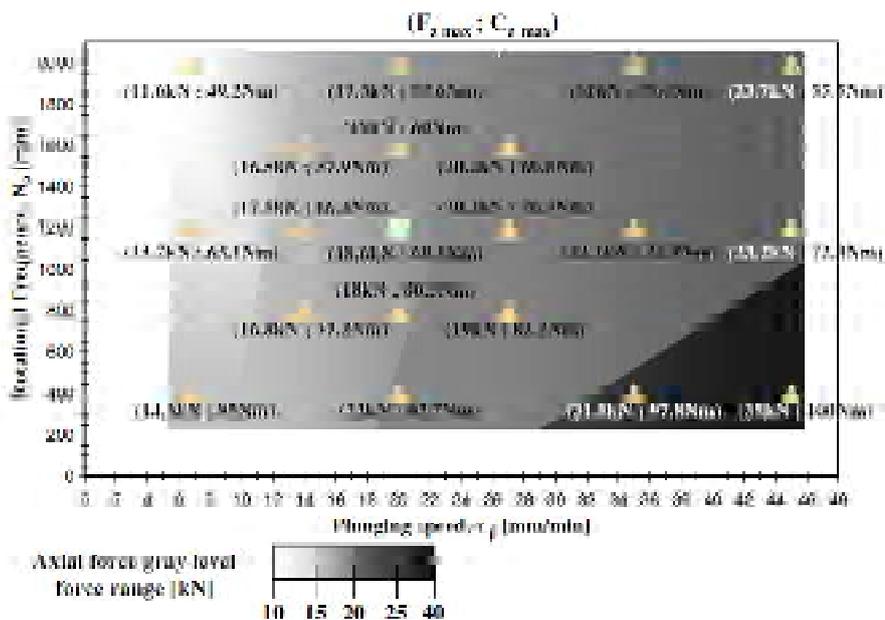
Under the condition of 3 and 4 kN, defects appear at middle of weld. The forces are too low to generate sufficient heat for the optimum mixing of the material. In contrast, high forces (6 and 7 kN) generate excess heat input which results in the transportation of stirred material from the lower to the upper surface. The consequences are tunnel defects at the weld bottom. /Raz11/ In other researches, the formation of welding burr in consequence of excess heat in-



put is described. The plasticized material is released to the upper surface and subsequently pushed out of the weld where the material consolidates in the form of welding burr. This results in a diminished weld cross section which has a negative effect on the tensile properties. /Völ09/

The process forces during FSW can be influenced by welding and rotational speed as soon as plunge depth. /Jan13/ For FSW of aluminum alloy 6061, it was found that an increase in welding speed and plunge depth results in higher axial force. In contrary, raising the rotational speed causes lower forces. Furthermore, the same observations are made for the process torque except regarding to plunge depth. /Jan13/

Only a few studies, concerning to process loads during FSW, consider the occurring torque as well. The influence of plunge and rotational speed on the maximum generated force and torque during FSW of the aluminum alloy 6082-T651 are investigated in/Zim10/. Although the research is not concerning to FSW of magnesium, the results are important. As shown in figure 2.16, the loads during plunge phase are studied for a widely range of rotational and plunge speed. It is obviously that high rotational and low plunging speed results in a minimum of loads. By increasing the tool rotational speed the frictional heat rising and the resistance to deformation decrease. This results in less process loads. Because of higher plunging speeds, the generated heat is very small whereby high torque and forces are generated. /Zim10/



According to/Pad09a/, the most important factor in the welding process is the tool including pin profile, shoulder diameter and material.

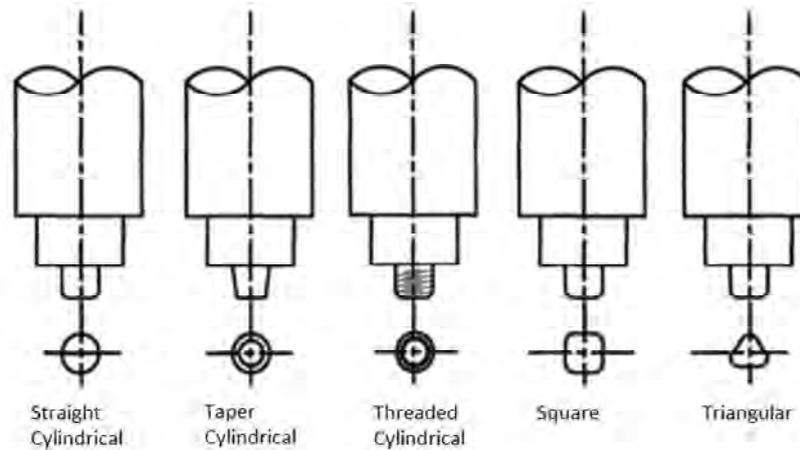


Figure 2.17: different tool pin profiles. /Pad09a/

The welding tool geometry has a high influence on the welding process and become investigated in/Pad09a/. The effect of five different tool pin profiles (figure 2.17), five different tool materials (mild steel (MS), stainless steel (SS), armour steel (AS), high carbon steel (HCS), high speed steel (HSS)) and three different shoulder diameters (15 mm, 18mm, 21 mm) on tensile strength, macrostructure and microhardness and –structure were investigated. The highest tensile strength (table 8) was reached by a tool made of high carbon steel wit threaded pin profile and a shoulder diameter of 18 mm. Due to the thread pin the heat generation is supported, thus the material flow around the pin is improved. This circumstance results in higher welding speeds and a void free weld (figure 2.18). The outcomes exhibit that pins without thread lead to defects like tunnel in the welding zone as shown in figure 2.18. In case of triangular profiles the frictional area is too small to produce sufficient heat at the bottom. As a result of the absent vertical motion of material in the stirring zone, straight and taper cylindrical profiles cause tunnel at the bottom. /Pad09a/

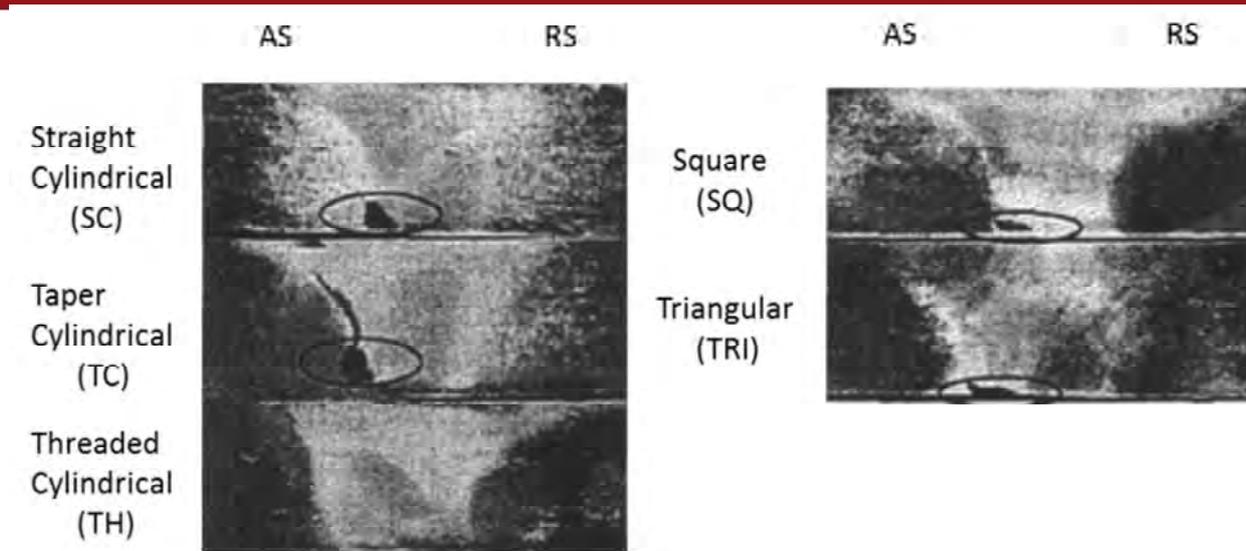


Figure 2.18: Effect of tool pin profile on macrographs of stir zone. /Pad09a/

The researches contemplated so far concerning to magnesium sheet with a thickness of 6mm. Best results was occurred by using a threaded pin because of improved material flow by an additional vertical velocity. In/Lea08/, it is reported that tools without thread provide good results for thin plates. Due to the lower thickness, the required heat input is remarkable smaller in comparison to thick sheets. For this reason, the material is sufficient heated and mixed by the tool shoulder.

A crucial factor for the mechanical properties is the grain size. An increase of the grain size leads to lower ductility, lower hardness and lower tensile strength. /Sch10/The same effect was observed in/Pad09a/. It was reported that the failure (during tensile test) occurs in the area of coarser grains. These coarser grains are formed by insufficient plastic flow and in case of excessive heat input. Dynamic recrystallization occurs due to the heat input during FSW witch normally results in finer grains. In case of very high temperatures grain-growth arises. /Pad10/

A sufficient heat input generated by friction between material and tool leads to a finer grain size in the nugget zone which raises the hardness. As presented in figure 2.19 the highest hardness-values are reached by a threaded pin made of HCS with a shoulder diameter of 18 mm on the retreating side. /Pad09a/In/Pad10/, it is reported that the straining is higher on the advancing side. Thereby, the grains are coarser and the hardness decrease.

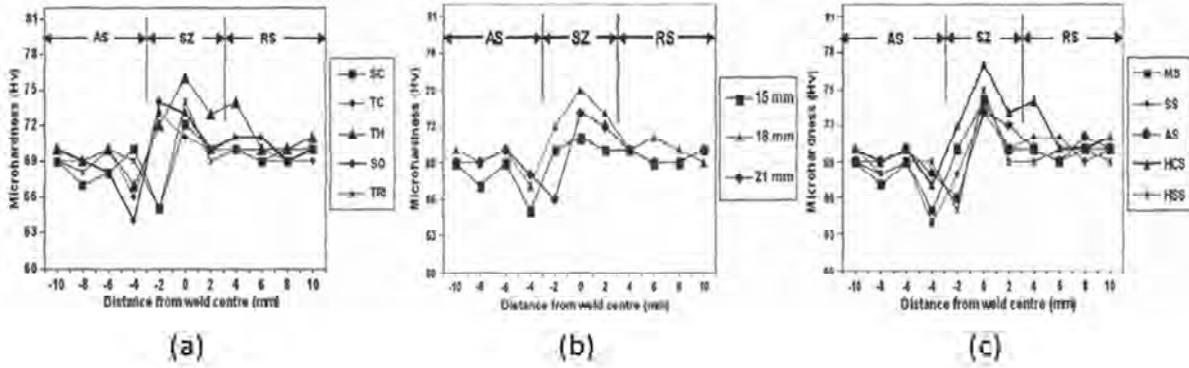


Figure 2.19: a) effect of tool pin profile on hardness; b) effect of shoulder diameter on hardness; c) effect of tool material on hardness /Pad09a/

The choice of the material plays a big role due to the relation between friction and hardness. A higher hardness means a higher friction and finally a higher heat input in the workpiece. /Pad09a/

As reported in/Mis07/, there is an ideal ratio of the shoulder diameter to the pin diameter. But the ratios between 2,5 to 1 and 3 to 1 only apply for FSW concerning to aluminum sheets with a thickness of 6mm. With a ratio of 3 (shoulder diameter = 18 mm, pin diameter = 6 mm) for the best result, the statement in /Mis07/ can be transferred to friction stir welded magnesium alloys. /Pad09a/

A negative result in joining magnesium alloys by FSW is recorded by /Ska04/ and/Joh03/. As shown in figure 2.20 a), magnesium tends to adhere to the tool. Furthermore in /Ska04/ was reported that the tool occasional stuck into the material. Both effects could be affirmed in the present study (figure 2.20 b)). Moreover, it could be discovered that the adhesion leads to a rough welding surface.



Figure 2.20: adhesion of magnesium: a) threaded pin; alloy AZ91D, AM50 /Ska04/ b) taper cylindrical pin; alloy AZ31

### 2.2.2. Aluminum

#### Characteristics of pure aluminum

The second most common metal used in industry is the light metal aluminum. Due to useful properties, e.g. low density, it is applied in fields like transport sector, mechanical engineering and building industry. Aluminum in pure form is not found in the nature due to its base character. The production is carried in a two-step process (1. Bayer-process 2. Electrolysis). /Kam95/

In table 2.7 are summarized important physical properties of pure aluminum. It crystallizes in face centered cubic (fcc) lattice (figure 2.21) whereby an excellent deformability is available. The good heat dissipation of aluminum, represented by high thermal conductivity, enables a low thermal load for the workpiece. In spite of its base character, which is shown by a standard electrode potential of  $-1,67$  V, the corrosion resistant is remarkable. The reason is that pure aluminum forms a dense oxide layer on air. /Ost98/

Table 2.7: properties of pure aluminum /Kam95/

| Crystal structure                     | Face centered cubic (FCC) |
|---------------------------------------|---------------------------|
| Density (at 20°C)                     | 2,7 g/cm <sup>3</sup>     |
| Elasticity modulus                    | 66,6 GPa                  |
| Melting point                         | 660,2 °C                  |
| Boiling point                         | 2500 °C                   |
| Thermal conductivity (at 27 °C)       | 235 W/(mK)                |
| Specific heat capacity (at 20 °C)     | 0,89 kJ/(kgK)             |
| Latent heat of fusion                 | 390 kJ/kg                 |
| Latent heat of vaporization           | 11400 kJ/kg               |
| Latent heat of sublimation (at 25 °C) | 31000 kJ/kg               |
| Electrical conductivity               | 37,67 m/Ωmm <sup>2</sup>  |
| standard electrode potential          | -1,67 V                   |

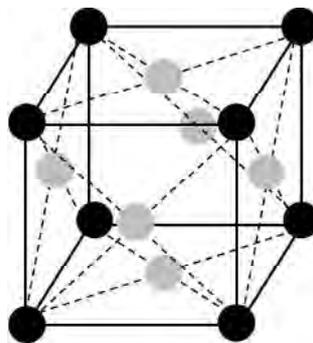


Figure 2.21: face centered cubic lattice /Kam95/

A high reflecting capacity for light and heat enable the use of aluminum as reflector and protection against heat rays. From this it follows that the absorption capacity is poor as shown in figure 2.22 a)./Kam95/ It is obviously that the absorption depends on wavelength (figure 2.22 a)) as well as temperature and angle of incidence (figure 2.22 b)). For a wavelength of about  $0,81 \mu\text{m}$  aluminum possesses a maximum value for absorption. In case of a Nd:YAG-Laser ( $\lambda=1,06 \mu\text{m}$ ) the absorptive part is very poor. /Mor05/ By increasing temperature and angle of incidence (figure 2.22 b)) the value can be increased. /Bac00/

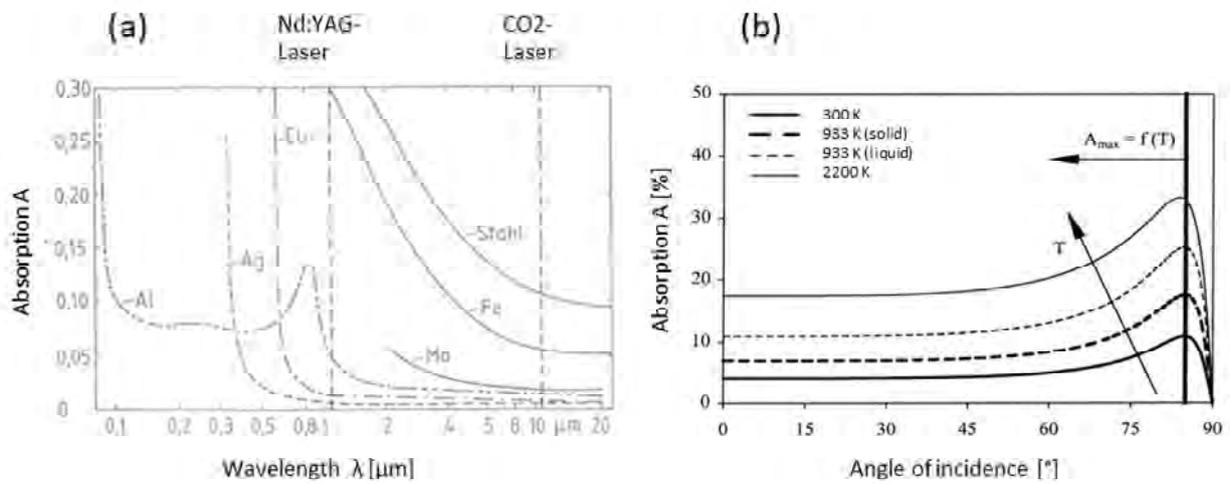


Figure 2.22: a) absorption as function of wavelength for various materials /Mor05/ b) absorption of aluminum as function of angle of incidence for a wavelength of  $1,06 \mu\text{m}$  /Bac00/

## Aluminum alloys

Basically the denotation of aluminum alloys is carried out by two variations: the numerical designation system and the system with chemical symbols. In the following the first kind of classification will be explained.

Initially, the alloys are distinguished in accordance to their application. Wrought alloys are used for the production of rolled products as well as extrusion products. The denotation is written down in DIN EN 573. In contrast cast alloys are applied for fabricate of cast iron because of better mold filling properties. The denotation of wrought alloys and cast alloys is carried out by DIN EN 573 and DIN EN 1780 as well as 1706, respectively. /Ost98/

Parts of the designation are given in table 2.8:

Table 2.8: designation of aluminum alloys /Ost98/

| Example wrought alloy | Example cast alloy | Part of designation  |
|-----------------------|--------------------|--|
| EN AW-6082            | EN AC-42100        |  |
| EN                    | EN                 | Prefix EN, followed by space   |
| A                     | A                  | Letter A for aluminum  |
| W                     | C                  | Letter for form of manufacture (W- wrought alloy; C- cast alloy)                                     |
| -                     | -                  | Hyphen   |
| 6082                  | 42100              | Four letters for wrought alloys, five letters for cast alloy for description of composite-boundaries |



## 2.3. FSW: preheating systems

### 2.3.1. Objective

How described in 2.1.2, FSW has a lot of advantages, but also disadvantages. Major problems are tool wear, the requirement of high clamping pressure and the forces to move the tool translational and rotatory. Caused by these conditions, there are a couple of researches regarding to reducing forces, torques and tool wear by using an additional heating source. Basic idea is the dependency of material's strength to temperature. Table 2.9 shows exemplary for Al alloy AA6061-T6 the decreasing character of yield strength with increasing temperature. If the initial material temperature increase, wear can be reduced due to less required heat input by the tool, which means lower frictional loads. /Sin09/

Table 2.9: Temperature dependency of Al AA6061-T6 yield strength /Cra06/

| Temperature [K] | Yield Strength [MPa] |
|-----------------|----------------------|
| 311             | 241                  |
| 339             | 238                  |
| 366             | 232                  |
| 394             | 223                  |
| 422             | 189                  |
| 450             | 138                  |
| 477             | 92                   |
| 533             | 34                   |
| 589             | 19                   |
| 644             | 12                   |

One common system is the Laser Assisted Friction Stir Welding (LAFSW). Moreover there are studies in Arc-enhanced FSW, induction heating systems and electric heating elements. /Sin09/

### 2.3.2. LAFSW

The LAFSW-process is a topic, which is discussed in several investigations like/Mes04/, /Daf09/, /USD06/, /Pat04/,/Sin09/ ,/Cha11/. Since it is called Laser assisted, the FSW is the main process, while laser heating has a supportive function.

The principle of this, in 2002 developed, procedure is simple, as shown in Figure 2.23: a laser system (commonly an Nd: YAG laser) is fixed just in front of the FSW-tool. Due to the laser the material is locally preheated and softened, whereby less clamping force is needed likewise



the forces for moving the tool forward. Furthermore, the softening also has a positive effect on tool wear and breakage. /Koh02/

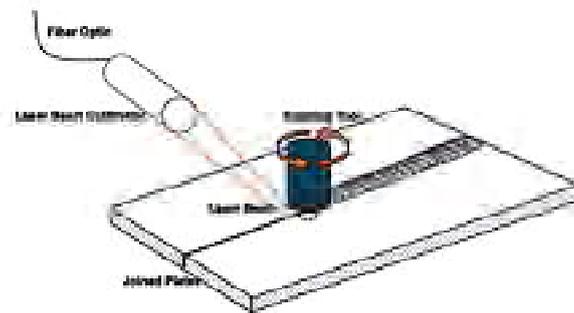


Figure 2.23: the principle of LAFSW. /Koh02/

/Pat04/, A United States patent describes an LASFW method, especially for thick workpieces. In addition to reduce process forces this technique affords short welding times and an excellent joint quality. Moreover, the reliability increases and in the long term costs in production could be saved because of fewer loads for the welding machines.

Besides laser power also material properties are important for LAFSW, like melting temperature and absorption behavior (absorption coefficient). Especially the last point plays a significant role because it defines the interaction between laser beam and material which is responsible for the input of the laser energy into workpiece. /Bac00/

Actually there are not many investigations with results concerning to reduce process loads. In /Sin09/

The LAFSW of carbon steel (SS400) was studied in/Fuj08/. The 3,2 mm thick plates were welded in an argon atmosphere by a WC based tool. With a constant rotational speed of 400 rpm, the conventional FSW process was compared to LAFSW. The welding speed was varied between 100 and 800 mm/min for LAFSW and between 50 and 700 mm/min for FSW. A 2,0kW Nd:YAG laser served as preheating source and was mounted in front of the tool with an angle of 45 degrees. Sound welds were received between 50 and 300 mm/min for the conventional process. Above 400 mm/min small defects occurred. Moreover, conventional welding up to 500 mm/min was impossible because of high loads on the tool which resulted in fracture. In contrast, preheating reduced the formation of defects, whereby sound welds were achieved up to 700 mm/min. Significant differences in tensile strength and hardness could not be observed between both processes. Average values of about 440 MPA (overall welding speeds) approximate the base materials tensile strength. According to the author, the results show the benefit of an additional heating system in regard to enlarger the process window. /Fuj08/

### 2.3.3. Arc-enhanced FSW

Figure 2.24 shows another similar preheating system claimed by/Sch06/. In contrast to LASFSW this method uses a TIG arc-welding torch to soften the workpiece for less loads and tool wear and higher welding speed. Furthermore, the described procedure enables the conventional FSW process to join harder materials and dissimilar metals. /Sch06/

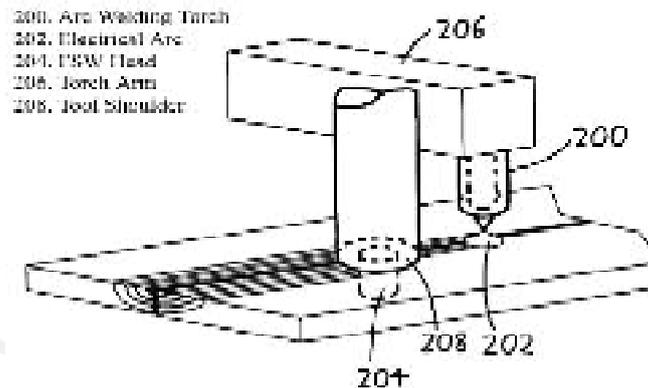


Figure 2.24: a simplified diagram of arc-enhanced FSW /Sch06/

Influencing factors are the arc current and voltage as well as arc polarity and oscillation. The arc polarity offers the possibility to weld steel as well as aluminum. In case of gas tungsten arc welding (GTAW) the commonly way to join steel are the DC electronegative (DCEN) welds. Typically the joints are narrow and deep with oxide films on their weld surface. Another option is the DC electropositive (DCEP) weld. Unlike DCEN, the joints are wide and shallow without oxide films. /Sch06/ With these settings it is impossible to weld aluminum because of its oxide film on the surface, which has a much higher melting temperature (2050 °C) than the basic material (550 °C -660 °C). /Kew11/

For this reason AC welds are generally used in GTAW aluminum. The positive half wave removes the oxide film (cleaning effect) because of the negative polarized aluminum. The following negative half wave generates the necessary power to weld the basic material and increases the fusion penetration. /Fro13/ Due to this experience, it is recommended to use DCEN for arc-enhanced FSW of steel and AC for welding aluminum. Arc oscillation is very helpful to spread heating over a larger area on the workpiece to plasticize it without melting. For example the arc can oscillate perpendicular to the joint while moving along it. /Sch06/ Information about practical researches is not given in/Sch06/.

### 2.3.4. Induction heating system

In regard to join cast iron by using FSW the tool wear became a major problem. Therefore in /Wal06/ was investigated a FSW process supported by induction heating to reduce process loads unlike other systems. As seen in Figure 2.25 an induction coil is mounted in front of the FSW tool to heat the material.



Figure 2.25: a FSW setup with induction heating /Wal06/

The investigation has shown that a reduction in forces is feasible by preheating with an induction system. Figure 2.26 shows the effect on a difficult-to-weld material (1018 steel). Caused by fewer loads, the tool wear decreased and a better material flow in the weld arose. /Wal06/ A disadvantage of this induction assisted FSW is the need of magnetic welding materials. Moreover, an inhomogeneous temperature distribution exists within the workpiece. /Sin09/

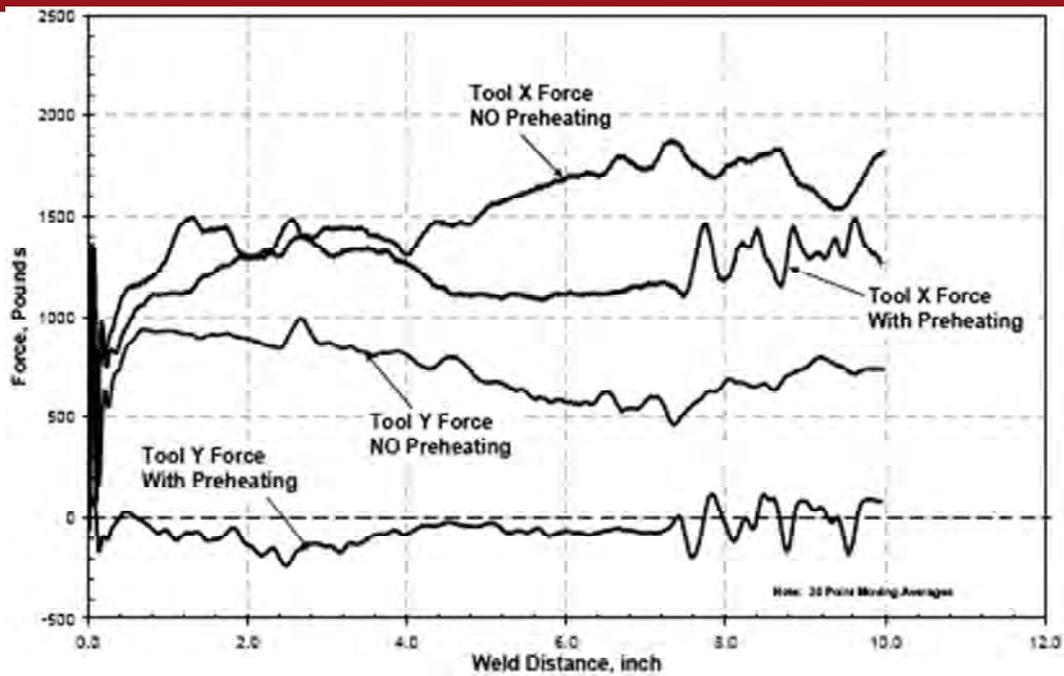


Figure 2.26: comparison of process forces with and without preheating for 1018 steel. /Wal06/

### 2.3.5. Electric heating elements

The effect of higher initial material temperatures caused by electric heating elements was investigated by/Sin09/. Plates (76,2x228,6x6,35 mm) made of AA6061-T6 aluminum alloy were welded with a triangular shaped Trivex tool, developed by TWI /Wil06/. As preheating system were used two different heating elements. One wide fiberglass heavy insulated heating strip with a power of about 313 W (possible temperature: 100°C). The other one were a ceramic heating strip which generates 1600 W (possible temperature: 300°C). Investigated were four different welding speeds (127; 203,2; 279,4; 355,6 mm/min) each with eight different initial temperatures (22; 50; 75; 100; 150; 200; 250; 300 °C). The results are given in figure 2.27 in terms of the normalized (to room temperature) axial force (figure 2.27 a)) and torque (figure 2.27 b)) in dependency of the initial temperature for all welding speeds. It can be seen that with increasing temperature the axial force decrease overall welding speeds. In case of low speeds (127; 203,2 mm/min) a local minimum is reached at 200°C. With increasing welding speed, this minimum moves to lower temperatures. Moreover, it is obviously that the effect on reducing forces is higher in case of lower welding speeds (force reduction about 43%) than with high speeds (force reduction about 21%). Regarding to torques, the graphs show

almost linear behavior. By increasing the initial temperature the torque decreased. Indeed the graph also shows a beginning convergence at higher temperatures. /Sin09/

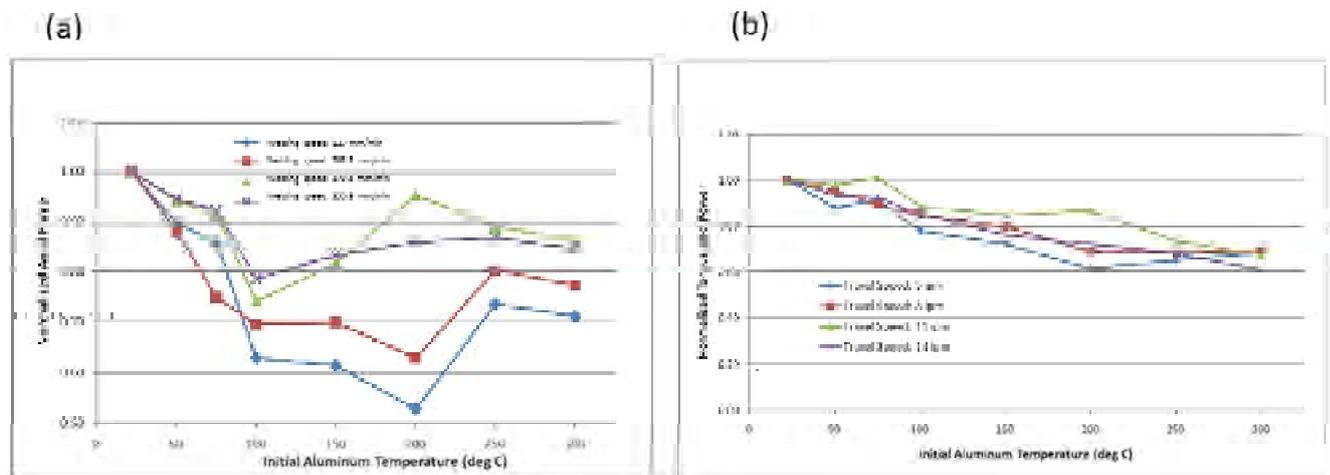


Figure 2.27: a) normalized axial force for different welding speeds at different initial temperatures; b) normalized torque for different welding speeds at different initial temperatures. /Sin09/

#### 2.4. FSW of magnesium/aluminum dissimilar joints

Joining dissimilar materials is an important topic in times of weight reduction in automotive, aerospace and ship industries to reduce environment pollution. In regard to industrial applications, the requirement of various properties cannot be achieved by one material. Therefore, the need of joining dissimilar materials is crucial. A promising combination is represented by aluminum and magnesium. /Cao10/ Due to the low weight and high strength, aluminum is widely used in industrial applications. With a low density and high specific strength, magnesium also has a beneficial purpose. /Yan10/ To receive sound joints of aluminum-magnesium-combination by using conventional fusion welding processes is improbable due to the generation of inter-metallic compounds. These brittle phases cause cracking and lower mechanical properties. Thanks to the solid-state and a lower welding temperature, the FSW process represents an alternative for dissimilar material combinations. /Cao10/ The literature offers numerous researches which report of sound welds in case of friction stir welded dissimilar aluminum alloys, aluminum/steel, aluminum/copper and aluminum/magnesium. /Yan10/

Table 2.10: overview of studies about FSW of dissimilar aluminum/magnesium joints

| Material   | Position Mg | Position Al | N [rpm] / f [mm/min] | UTS base [MPa] | UTS [MPa]         | joint | source  |
|--|-------------|-------------|----------------------|----------------|-------------------|-------|---------|
| 6061-AZ31B<br>1,6mm thick<br>Butt joint            | AS          | RS          | 1400 / 38            | -              | -                 |       | (VFi09) |
| AA2024-T3-AZ31B-H24<br>4,95 mm thick<br>Butt joint | RS          | AS          | -/-                  | 300 (Mg)       | 105 (35% of base) |       | (XCa10) |
| 5052-AZ31<br>6mm thick<br>Butt joint               | RS          | AS          | 600/40               | -              | -                 |       | (YYo10) |
| AA6040-AZ31<br>1,5mm thick<br>Butt joint           | AS          | RS          | 1400/225 (3,75 mm/s) | -              | -                 |       | (AKo09) |
| A5052P-AZ31B (2mm)<br>Butt joint                   | RS          | AS          | 1000-1400/300        | 200 (Al)       | 132 (66% of base) |       | (YJK08) |

In table 2.10 are listed some investigations concerning to FSW of dissimilar aluminum/magnesium joints. It can be concluded that the range of settings for rotational speed (600-1400 rpm) and transverse speed (19-300 mm/min) are very limited.

Due to different properties (e.g. thermal conductivity, thermal expansion) the influence of process parameters on mechanical properties is wide and therefore an essential part of scientific studies. A crucial factor is the position (advancing or retreating side) of the materials in regard to the welding tool. Remarkable differences exist in the temperature distribution. During the welding process the materials flows against the welding direction. On the Advancing side the material is pushed forward and the tool rotation occurs counter to the material-flow direction. In contrary, the material is pushed backward on retreating side because the tool rotation and the material-flow have the same direction. This results in higher shearing and heat input at advancing side. In combination with the used materials, this fact can be helpful to influence the heat input. In case of welding 6xxx aluminum alloy to AZ or AM magnesium alloy, heating occurs more in the aluminum. /Kos09/ That means positioning of aluminum on the advancing side causes more heat stress in comparison to placing it on the retreating side. This influence is obviously in figure 2.28 a). The explanation for the experiment numbers are given in figure 2.28 b). As expected, if aluminum is located on the advancing side (B-11, B-3) the temperature is higher than on the retreating side. As mentioned in aluminum occur more heat than in magnesium, wherefore the reached temperature on retreating side in case of B-5 and B-7 is higher, but the average temperature is lower in comparison to B-11 and B-3. This circumstance has a significant effect on the tensile strength: With decreasing heat input increases the joint strength. /Fir09/The author notes the need of a certain heat input-level to

generate sound welds. In opposite to the presented results, other studies (/Cao10/) give an account of sound welds with the location of aluminum and magnesium on the advancing side and retreating side, respectively.

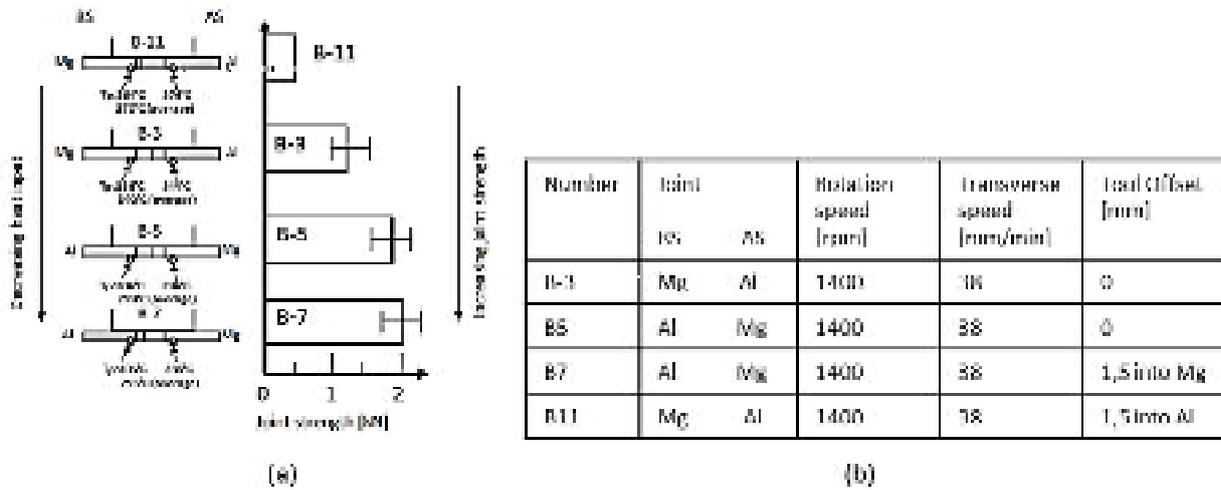


Figure 2.28: a) effect of material position on joint strength and heat input in butt joint FSW of AZ31 Mg and 6061 Al.

the thermocouples are 3 mm away from the path of the tool axis and 0.25 mm above the bottom surface of the workpiece b) process settings /Fir09/

Another influencing parameter is the tool offset. According to /Fir09/ an increasing offset to magnesium (advancing side) improve the tensile properties (figure 2.28 a)). This effect is reached by decreasing the aluminum-tool contact area wherefore less heat is generated. Conversely an offset to aluminum results in higher thermal stress and consequently in worse tensile strength, which is also reported by /Cao10/ and/Yam09/. In /Yam09/ is assumed that the reason for higher heat generation in aluminum is the higher friction coefficient between the aluminum alloy and welding tool. As consequence defects occur easier because of the higher amount of welding burr. /Yam09/

The influence of heat on tensile strength is based on the behavior of friction stir welded aluminum/magnesium. As described before, welding of aluminum and magnesium forms intermetallic compounds ( $Al_3Mg_2$ ,  $Al_{12}Mg_{17}$ ) at certain temperatures (450°C, 437°C). Above these temperatures, the transition in the liquid phase occurs. This formation is called constitutional liquation /Sat04/ and rise with increasing heat input. /The formation is located along the grain boundaries and the aluminum/magnesium interface (figure 2.29 a)). Due to the following cooling, the liquid films reform in  $Al_3Mg_2$ ,  $Al_{12}Mg_{17}$ . The presence of intermetallic compounds weak the material and in consequence, cracks along the interface are caused as shown in figure 2.30. The author identified the intermetallic compound as  $Al_{12}Mg_{17}$  with a thickness

of about 2,5 μm. Moreover, it is reported that the intermetallic phase is generated by the above described process. Regions of broken and distributed intermetallic compounds in the weld would be indicators for a solid state transformation. /Lea03/

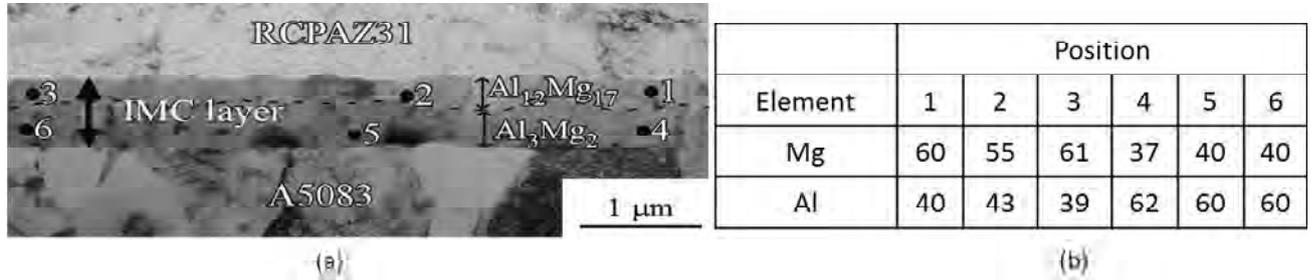


Figure 2.29: a) interfacial layer observed in the AZ31/A5083 joint (offset =0 mm). b) chemical compositions at points 1 to 6 (at%). /Yam09/

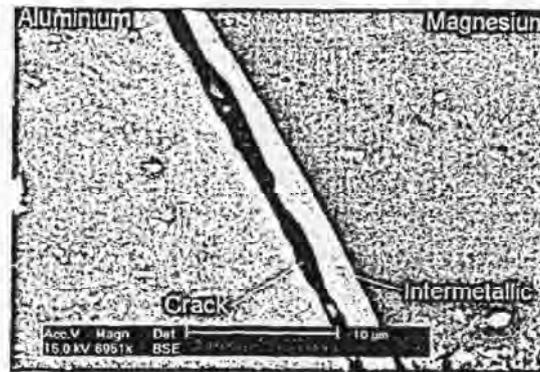


Figure 2.30: Electron back-scattered image of aluminum-magnesium intermetallic at weld interface (unetched sample) /Lea03/

Because of the crucial influence of intermetallic phases, in /Yam09/ is suggested to welding below the eutectic temperature (437°) to avoid the generation of intermetallic compounds. Another possibility is to use an filler material between aluminum and magnesium/Lea03/, which is investigated in /Cha11/. By using a tool made of SKD-51 steel with a concave shoulder (diameter: 18mm) and a taper cylindrical probe (diameter at bottom 3,6 mm) AA6061-T6 and AZ31 were joint by FSW in different settings. At first step the plates were welded by conventional FSW. Afterwards, the process was added by a nickel foil between the faying surfaces of the aluminum and magnesium alloys. These conditions were studied in the last case with additional heating by a 2kW pulsed Nd:YAG laser. All experiments were made at a constant rotational speed of 800 rpm and a transverse speed of 35 mm/min. The results in concern to tensile strength are shown in figure 2.31 a). The lowest tensile strength is obtained by case one. Due to the formation of Al<sub>12</sub>Mg<sub>17</sub>, the maximum strength is about 38% (95 MPa) of the base material (magnesium). The use of a nickel foil between the faying surfaces results



in a lower formation of the brittle intermetallic compounds, whereby the tensile strength increase up to about 45% (115 MPa) of the magnesium base metal. With a maximum tensile strength of about 66% (169 MPa) of the base material strength, the laser assisted process causes the best result. Furthermore, the fracture occurred along the HAZ and TMAZ. In contrast, the position of fracture for the other settings was in the stir zone. /Cha11/

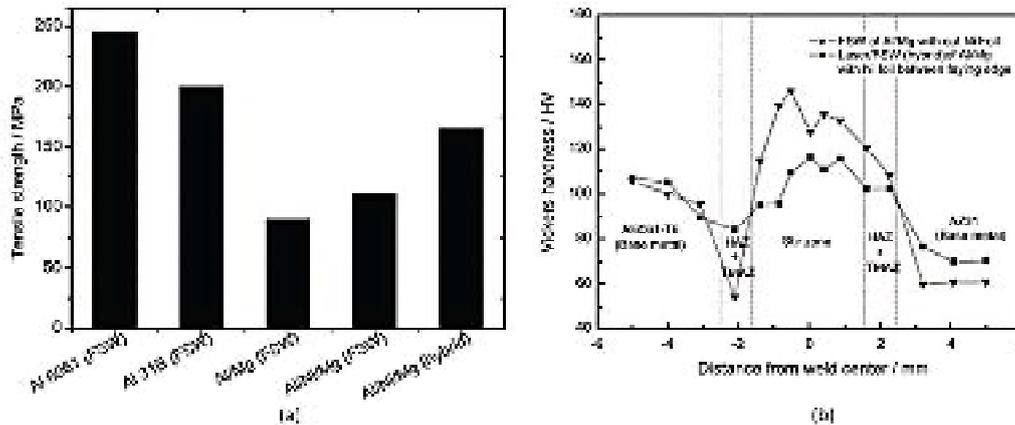


Figure 2.31: a) tensile strength comparison between various welding cases; b) comparison Vickers hardness for dissimilar FSW without Ni foil and hybrid welding with Ni foil of Al/Mg alloy along the transverse section 2 mm below the top surface /Cha11/

In figure 2.313 b) is given a comparison of hardness distribution for case 1 (dissimilar FSW of aluminum/magnesium) and case 3 (Dissimilar hybrid-laser-FSW of aluminum/magnesium with nickel foil between the faying surfaces). The formation of the brittle phase  $Al_{12}Mg_{17}$  resulted in a much higher hardness-value (within the stir zone) in comparison to the base material. Relative low differences in hardness were caused by using laser and nickel foil. Caused by heating with laser, nickel distributed well at the interface during the process. Consequently, the formation of  $Al_{12}Mg_{17}$  is reduced. /Cha11/

### 3. Objective

The objective of the present study is to investigate the improvement of FSW. Due to the characteristic of joining in the solid phase, the process possesses some benefits like welding of dissimilar materials. However, the high process loads and relative low welding speeds bound a widely industrial use. This welding process strongly depends on the yield stress of the respective materials. From literature, it is known that the yield stress can be positively influenced by process temperature. Based on this fact, the dependency of occurring process forces on different initial temperatures of the joining members should be investigated. It is expected that the resistance of materials against plastic deformation decrease with increasing temperature. As a result, the level of generated process loads should remarkably decline. Thereby, welding at higher travel speeds without rising forces should be possible.

The focus of this master thesis is the improvement of FSW of similar magnesium alloy AZ31 joints. Besides, a consideration of the effect of higher temperature on FSW of dissimilar magnesium AZ31/aluminum AW6016 joints is carried out.

The preheating of the materials is realized in two different ways. At first a laser is used to preheat the material locally just in front of the welding tool. As a result, the heat input is bounded at a certain area.

The alternative is the use of a heating element to increase the initial temperature of workpieces. Thereby, a larger area is affected by the heat.

In addition to the effect on process loads, a comparison of the results -obtained by the presented procedures- should be considered.

## 4. Experimental approach

The following chapter gives an overview of the experimental approach. It includes the general approach, experimental setup as well as materials and results evaluation.

### 4.1 General approach

#### 1) LAFSW

This part contains different investigations concerning laser use during FSW of the extruded magnesium alloy AZ31.

At first, the sole influence of laser beam on the magnesium alloy should be considered for different welding speeds. The object is to find settings for the maximum laser power before the material begins to melt or burn. Moreover, the occurring maximum temperatures are measured and serve as evaluation of a simulation model. This model will produce information about the temperatures in the material, which are important for the FSW process in concern to the relation between starting temperature of material and process loads.

The identified settings for laser are used in the combined LAFSW process with the aim to analyze the effect of preheating by laser beam on welding loads and tensile properties. For that purpose, the process is conducted as conventional FSW and LAFSW under identical parameter conditions.

#### 2) Preheating by heating element

The aim of this section is to study the influence of preheating by a heating element on FSW of similar as well as dissimilar joints.

Initially, the research is focused on FSW of the extruded magnesium alloy AZ31. For a general overview about the relation between starting temperature and process force and torque, bead on plate welds are produced. Then, the most beneficial settings are used for FSW in butt weld configuration.

Consecutively, the transferability for FSW of the rolled magnesium alloy AZ31 is examined.

The last part comprises FSW of dissimilar AZ31/AW6016 joint. At first, the conventional process is considered for different welding and rotational speeds. Beneficial settings are subsequently used to compare process loads affected by preheating.

## 4.2 Experimental setup

The welding system used for this work is a Hermle UWF 1000 from 1986. The technical specifications of this universal milling machine are given in table 4.1.

Table 4.1: Hermle UWF 1000 technical specifications /Her86/

| Control                              | Haidenhain TNC155                      |
|--------------------------------------|--|
| Spindle taper                        | SK 40                                  |
| Numer of axes                        | 3                                      |
| Travel X-axes (longitudinal)<br>[mm] | 700                                    |
| Travel Y-axes (cross)<br>[mm]        | 550                                    |
| Travel Z-axes (vertical)<br>[mm]     | 500                                    |
| Rotational speed range<br>[rpm]      | 25 - 3500                              |
| Welding speed range<br>[mm/min]      | 1 -2000                                |
| Maximum process forces<br>[kN]       | X-axes: 10<br>Y-axes: 10<br>Z-axes: 10 |

The experimental setup is shown in figure 4.1. An important component of this work is the analysis of process loads. Therefore, an axial force and torque measurement system (a), supplied by ARTIS GmbH, is used. This system consists of a special tool holder, where the welding tool is clamped in, and an externally attached sensor which transmit the data to an external computer during the process.

The laser used for this investigation is a 3 kW high-power diode laser of the DLS- series built by Rofin. Two wavelengths (940 and 808 nm) are emitted with a focal spot size of 3mm in diameter. The overview of the available laser power is given in appendix. As shown in figure 4.1, the laser (b) is fixed next to the welding tool. An angle of about 60° is formed between laser head and surface of sheets to be welded. Furthermore, the laser beam is focused about 20 mm in front of the tool on the surface. For protection of the laser optic from pollution, a cross-jet (c) is fixed.

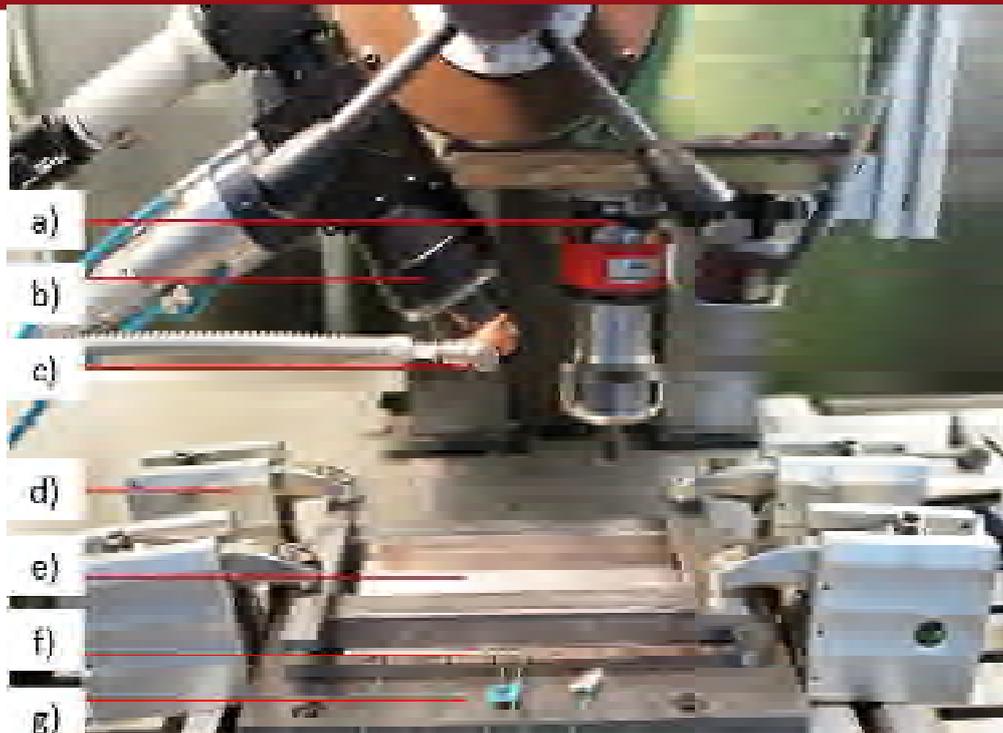


Figure 4.1 : experimental setup welding system: a) axial force and torque measurement system (tool holder; sensor), b) laser, c) crossjet, d) clamping elements, e) workpieces, f) arrestor, g) base plate.

Due to high process forces, the clamping fixture has an important role in FSW. Therefore the joining members (e) are positioned on an arrestor (f) in order to prevent drifting apart. The clamping elements (d) on the left and on the right side generate sufficient contact pressure to retain the materials. Additional downholder arrange an equable force path. The backing plate, consisting of three several steel plates, is located between base plate (g) and workpieces.

The schematic illustration of the temperature measurement during welding is shown in figure 4.2. As mentioned before, the backing plate, consisting of three several steel plates, is located between base plate and workpieces. One of these steel plates serves as channel for thermocouples (type K) up to the central one, which exhibits bore holes provided for the thermocouples. The temperatures are measured at five different points along the weld line. All of these are located 0,8 mm below the surface respective the contact surface between joining members and backing plate. The bore holes BW, MW3 and EW are 15 mm deep whereby the temperature is directly measured under the abutting end. The remaining two are positioned 4 mm besides the center line. Thereby, MW1 measure the temperature on retreating side and MW2 the temperature on advancing side. The produced signals are recorded and sent to an external measurement and analyzing system applied by Dewetron.

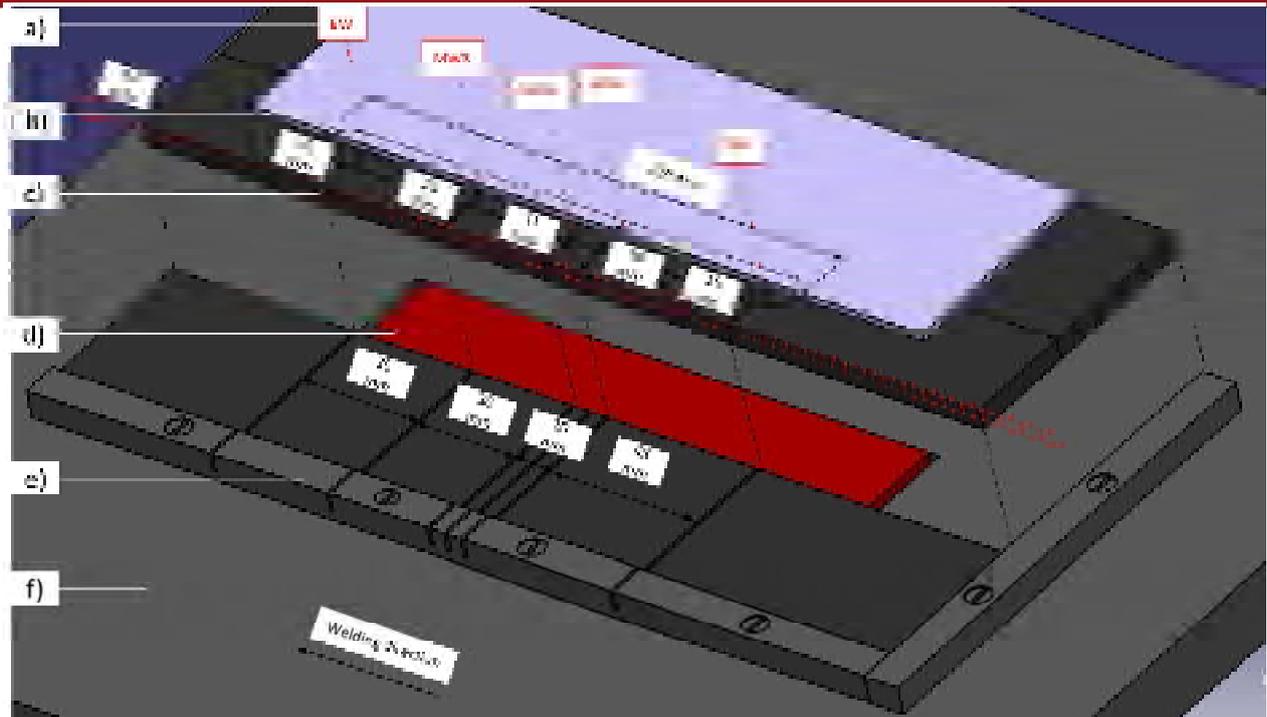


Figure 4.2: schematic illustration of temperature measurement during welding with: a) temperature measuring points (BW; MW1; MW2; MW3; EW), b) workpiece, c) backing plate (three separate steel plates), d) heating element, e) arrestor, f) backing plate.

Another part of the experimental setup, the heating element, is located centrally in the base plate under the backing plate (figure 4.2). For this study, two elements different in size and power are applied, which are respectively fitted in an equivalent copper block. For both, the maximum achievable temperature was determined. The test setup is shown in figure 4.2 and 4.3.



Figure 4.3: schematic illustration of measuring points for the performance test of the heating elements

The heating element is located directly under the backing plate. Above, the joint members are placed. As shown in figure 4.3, the generated temperatures are measured along the center line in five different points. Two of them are situated in the backing plate (BW; EW). The remaining three (S1; S2 and S3) are arranged direct on the top surface of the workpieces.

The results for the measurement of heating element 1 are shown in figure 4.4. It can be seen that the temperature on the surface is lower than in the backing plate. The variation between BW and EW is 6,38 °C in average. For the measurement points on the workpiece surface, the maximum variation is about 21 °C in average. After duration of about 60 minutes, the heating element reaches a constant temperature level of about 150 °C. Meanwhile, the surface temperature is 86,5 °C in average.

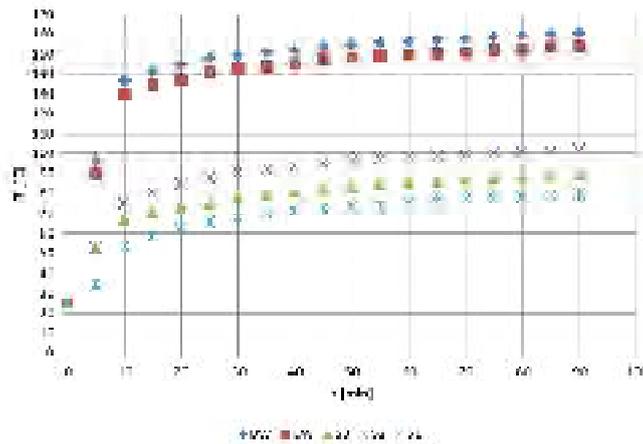


Figure 4.4: measurement of temperature for heating element 1

Heating element 1 is used for the investigation regarding extruded AZ31 sheets with a thickness of 2,2 mm. Because of the number of experiments, a waiting period of 10 minutes was defined between each experiment. At this point, the temperature in the backing plate is about 130 °C. This was appointed to be the initial temperature for FSW under preheating conditions.

The studies regarding rolled AZ31 sheets a thickness of 1,8 mm are made with heating element 2. The recorded temperatures are shown in figure 4.5. The reached temperature after 60 minutes is remarkable higher than for heating element 1. In backing plate, an average temperature of about 311 °C is obtained. The surface exhibits a temperature of 253 °C in average. Identical to FSW of the extruded AZ31, a waiting time of 10 min was also defined for welding of the rolled AZ31. This corresponds to about 225 °C in the backing plate. This value is classified as the initial temperature.

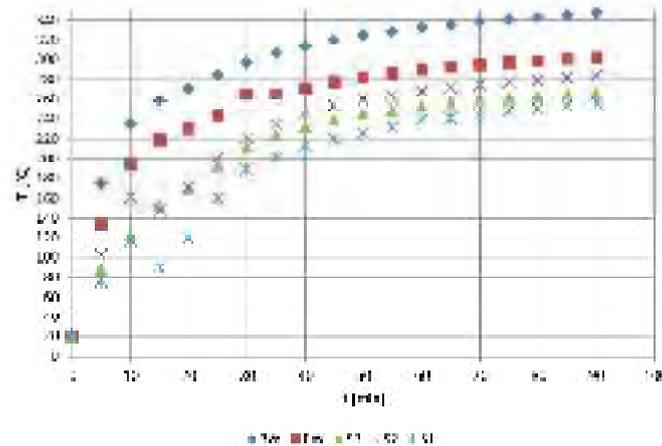


Figure 4.5: measurement of temperature for heating element 2

To investigate the laser influence on the magnesium, a simulation model, generated in Comsol Multiphysics, is used. This software provides to simulate complex physical processes.

An already existing simulation model is used and adapted to the present problem as shown in figure 4.6. To receive comparable results, the experimental setup with corresponding dimensions is transferred to the model. It is important to mention, that the simulation program assume a symmetrical setup for the calculation. For this reason, the generation of the half setup is sufficient. Besides the base plate (a), the backing plate (b) and the workpiece (c) are displayed.

The interaction of laser beam and material is realized by the illustration of a cylinder with a diameter of 3 mm (d), which corresponds to the laser beam diameter. The measurement of the temperatures is carried out by orthogonal work planes (e). These are located in the center of the laser spot as well as 10 mm and 20 mm distant. The chosen positions are important regarding to the distance between tool and laser spot.



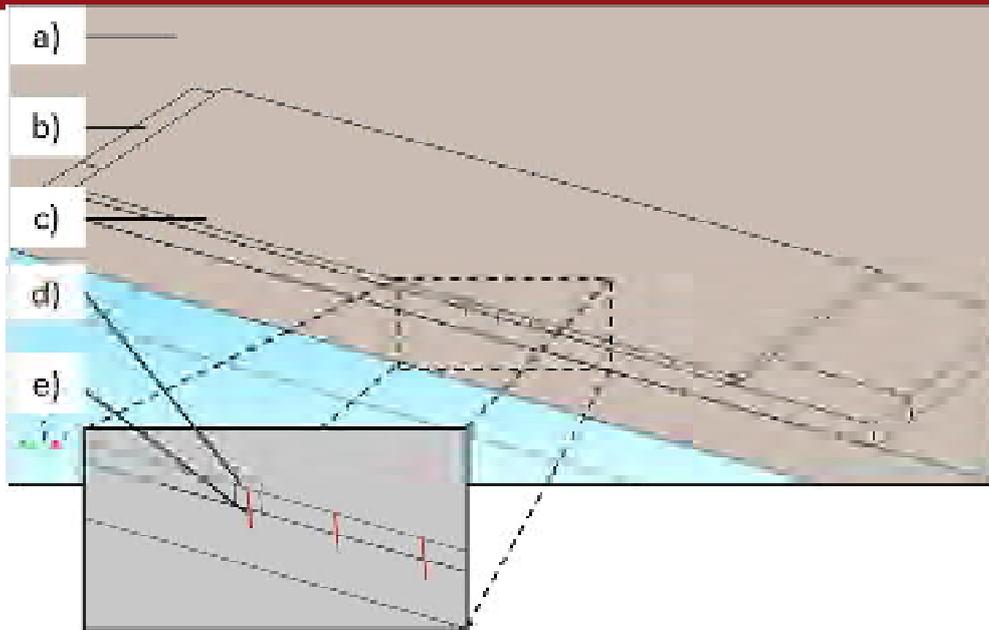


Figure 4.6: schematic illustration of the simulation model

To simulate the welding movement, the laser spot is defined as a fix point. The velocity is applied to the other parts. The quantitative description of the laser power is achieved by the following equation:

$$q_{tot} = \frac{P_{real}}{2} A_{ab} \quad (4-1)$$

with  $P_{real}$  as the real laser power in [W] and  $A_{ab}$  as the coefficient of absorption. Due to the symmetric setup, the power is reduced by half. Moreover, the material initial temperatures as well as the ambient temperature are defined. In the program, conditions for conductive cooling, surface-to ambient radiation, heat transfer in solids and thermal insulation can be defined. Thereby the program uses characteristic properties of the material (given in the data base of the program).

### 4.3 Welding tool

The choice of the welding tool contributes significantly to the quality of welding result. As already mentioned, the literature indicates a multiplicity of tools for FSW. The variation in geometry as well as material depends on the characteristics, like material and thickness, of the sheets to be weld. The welding tools used for the current work are presented in table 4.2 (technical drawing in appendix).

Table 4.2: used welding tools.

| tool                             | 1  | 2  |
|----------------------------------|--|--|
| <b>Shoulder diameter</b><br>[mm] | 12   | 12   |
| <b>Pin diameter</b><br>[mm]      | 5  | 5  |
| <b>Pin length</b><br>[mm]        | 1,7  | 1,5  |
| <b>Material</b>                  | 1.2343   | 1.2343   |
| <b>Characteristics</b>           | monolithic; concave shoulder; conical,<br>unthreaded pin | monolithic; concave shoulder; conical,<br>unthreaded pin |

As described in the chapter about the state of the art, an unthreaded pin is useful for FSW of thin sheets. According to /Lea08/, an improvement of mixing and compression of material can be reached by a threaded pin profile, but this is only necessary in case of thick plates. The thread produces a vertical movement of the material along the pin. For material of low thickness, the shoulder generates a sufficient material flow. Since the investigated materials possess a thickness of 2,2 mm (extruded AZ31; rolled AW6016) or 1,8 mm (rolled AZ31), both tools are made with unthreaded pin. Indeed, the material flow is enhanced by the conical shaped pin. The concave shoulder supports the material flow to the pin additionally.

Tool 1 is used for FSW of the 2,2 mm thick extruded magnesium alloy AZ31 and for FSW of dissimilar AZ31/AW6016 joints.

Based on a thinner plate thickness, the tool manufactured for FSW of the rolled AZ31 (tool 2) have a pin length of 1,5 mm. Thereby, the contact of tool and backing plate is prevented.

#### 4.4 Material

In the scope of this work, the magnesium wrought alloy AZ31 and the aluminum wrought alloy AW6016 are applied. Concerning the magnesium, there are differences in the manufacturing method. AZ31 with a thickness of 1,8 mm are rolled sheets, whereas the 2,2 mm thick plates are manufactured by extrusion. There is no information available about the as-fabricated conditions of both. The rolled aluminum wrought alloy AW6016 is existent in a

solution annealed, naturally aged condition (T4). The delivery condition for the material was different. The extruded AZ31 was existent in the form of H- profiles of which sheets with a width of 60 mm were produced. The length of the profiles was 200 mm. Sheets of the same dimensions were cut off from the rolled alloys AW6016 and AZ31.

The chemical composition of the used materials is given in table 4.3.

Table4.3: chemical composition of the alloys AZ31 and AW6016 in wt-% /Kam00/,/Nor04/

| denotation    | Al      | Mg      | Zn      | Mn  | Si    | Cu   | Fe    | Ni    |
|---------------|---------|---------|---------|-----|-------|------|-------|-------|
| <b>AZ31</b>   | 2,5-3,5 | Vol.    | 0,6-1,4 | 0,2 | 0,3   | 0,05 | 0,005 | 0,005 |
| <b>AW6016</b> | Vol.    | 0,2-0,6 | 0,2     | 0,2 | 1-1,5 | 0,2  | 0,5   | 0     |

A list of several important physical properties of the alloys is displayed in table4.4.

Table4.4: physical properties of the alloys AZ31 and AW6016 /Kam00/,/Nor10/

| property                      | AZ31 (at 20 °C)         | AW6016 (at 23 °C)     |
|-------------------------------|-------------------------|-----------------------|
| <b>Density</b>                | 1,77 g/cm <sup>3</sup>  | 2,7 g/cm <sup>3</sup> |
| <b>Solidus temperature</b>    | 420 °C                  | 610 °C                |
| <b>Liquidus temperature</b>   | 620 °C                  | 650 °C                |
| <b>Thermal conductivity</b>   | 76,9 W/(m*K)            | 195 W/(m*K)           |
| <b>Specific heat capacity</b> | 1010 J/(kg*K)           | 890 J/(kg*K)          |
| <b>Elasticity modulus</b>     | 45 GPa                  | 69,5 GPa              |
| <b>Tensile strength</b>       | 251,2 N/mm <sup>2</sup> | 230 N/mm <sup>2</sup> |

An important aspect in analyzing weld results is the evaluation of tensile properties of the joints in comparison to the base material. Therefore, it is important to determine the properties of base material by tensile tests. Specimens with a length of 90 mm and a width of 12 mm were produced. According to DIN 50123 and DIN EN ISO 6892-1, the specimens should have a length of 120 mm. The adaption of specimens dimension was necessary in regard to the welded joints. With a total width of 120 mm they accord exactly the requested length. Indeed, the preparation of the tensile specimen was carried out by wire-electro discharge machining. Therefore some space was needed to clamp the joints in the machine.

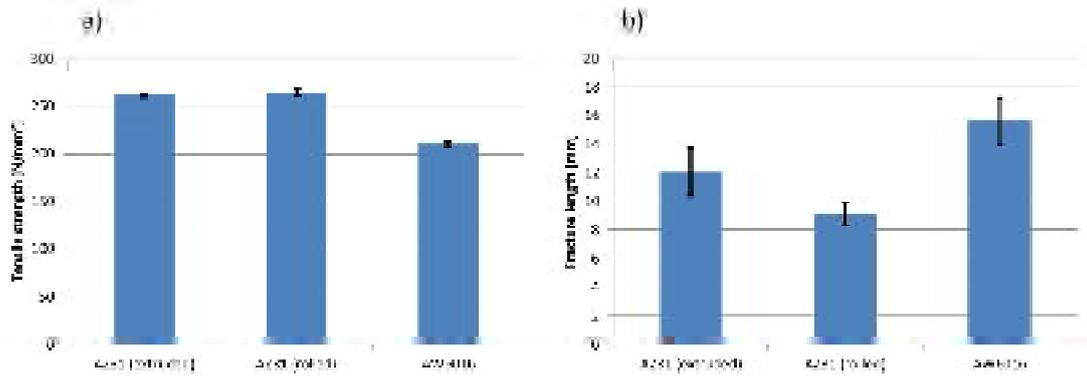


Figure 4.7: tensile properties of the alloys AZ31 and AW6016 a) tensile strength; b) fracture length

The results of tensile tests of the base material are shown in figure 4.7. It can be seen that AZ31 possesses remarkable higher tensile strength than the AW6016 alloy. In contrary, the received fracture lengths are significantly lower for magnesium, which indicate brittle fracture. The fracture appearance (figure 4.8) confirms this assumption. In case of AW6016, a local necking is clearly recognizable.

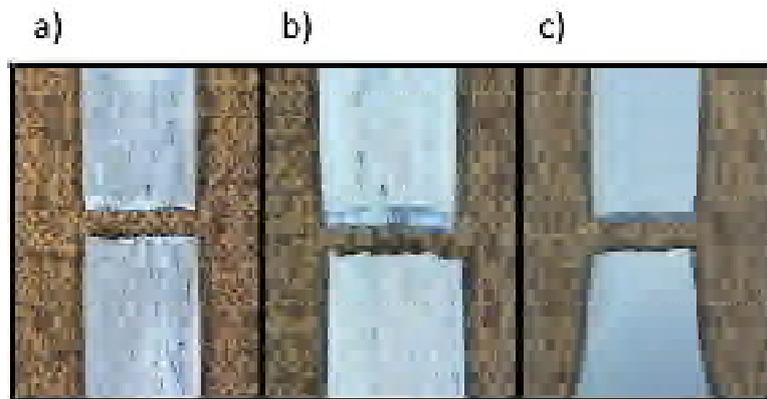


Figure 4.8: fracture appearance a) AZ31 (extruded); b) AZ31 (rolled); c) AW6016

Based on the calculated tensile strengths and by using equation (2-5) of page 20 the flow curves for the used materials can be compiled. The results are presented in figure 4.9. In comparison with literature (figure 2.3 on page 19), the determined curve progressions exhibit comparable values. A lower yield stress for the aluminum alloy AW6016 is observable. As a result, the materials resistance against plastic deformation is less compared to the magnesium alloys, which means superior flow properties and in conclusion lower required process loads during the FSW process.

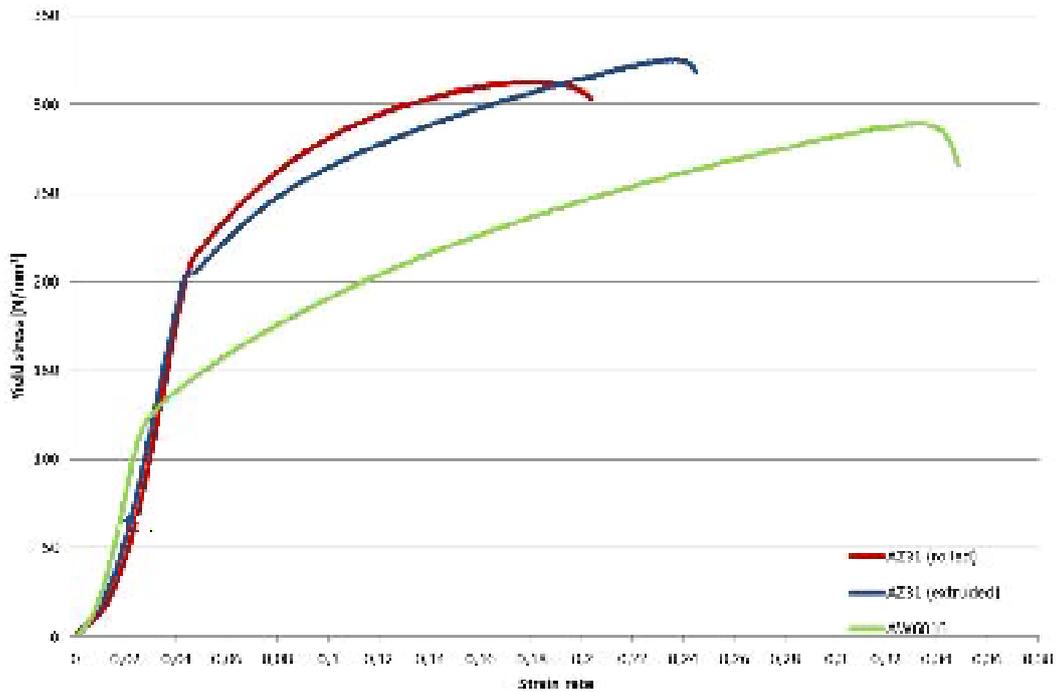


Figure 4.9: calculated flow curves for the used alloys

#### 4.5 Analyze evaluation of the welding results

The optical evaluation of the welded joints is the first step in analyzing the results. Important aspects are:

- Location of defects on the surface
- Formation of pinhole at the end of weld
- Formation of welding burr
- Roughness of the surface

Subsequently, the measured process force and torque are considered and compared for equal as well as unequal parameter settings. On the basis of these curves, a statement about the influence of parameters can be done. As described in the state of the art, the occurring forces significantly affect the welding result. Moreover, the repeatability of weld can be checked.

Already before the plunging of the tool into the joint members, the measurement system generates a signal (noise). The variation for force and for torque is from 0 up to 78 N and from -0,39 Nm up to 0,39 Nm, respectively. In addition, the generated curves are very noisy in some cases, whereby they must be filtered as exemplary shown in figure 4.10. For the comparison of loads occurring during plunge phase, the maximum values of the filtered curves are used.

These curves exhibit for force and torque a relative constant level (during welding phase), which represent the considered value.

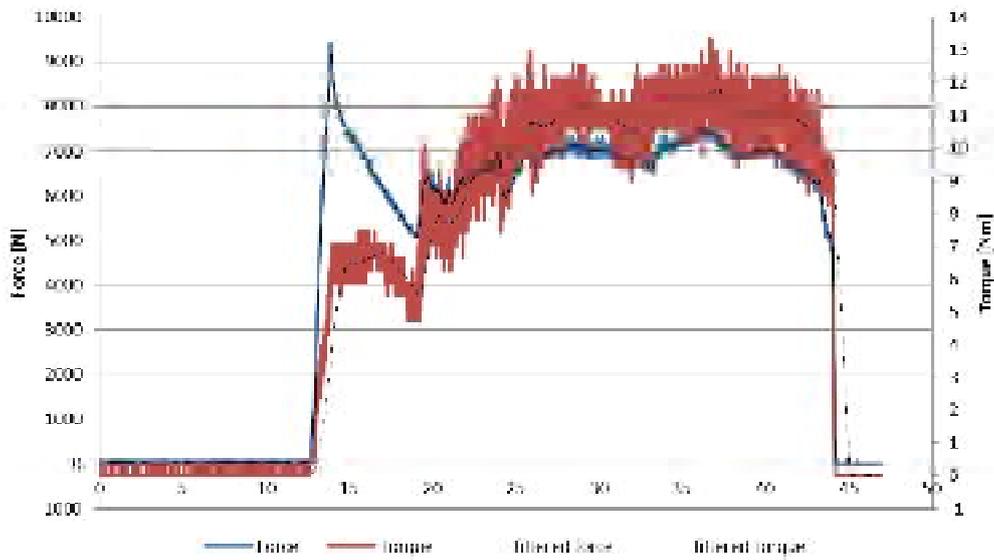


Figure 4.10: exemplary diagram of the measured force and torque

The following step in analyzing the welded joints is the tensile test. For that purpose three samples (beginning, middle and end of weld) for every joint are produced (figure 4.11 a). This enables an overview about the tensile properties along the whole joint. The blanking of the samples is carried out by wire-electro discharge machining. This procedure is characterized by high precision concerning to form and dimensional accuracy. The specimen for microscopic analyzes are processed in the same way.

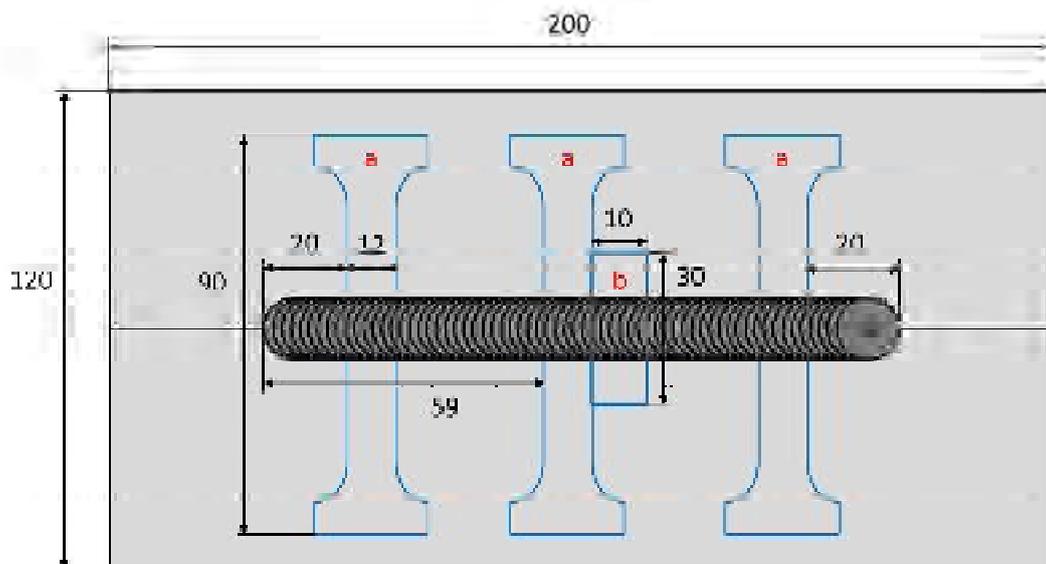


Figure 4.11: schematically illustrations of the specimens for a) tensile test b) microscopic analyze

With a clamping length of 50 mm, the manufactured samples are gripped into a Zwick material testing machine 1455. Among a constant testing speed of 10 mm/min, the machine record tensile force over crosshead travel until the fracture of the sample. By implying the cross-section of the reference geometry, it is possible to calculate the tensile strength.

Explanations for fracture behavior during tensile tests can be indicated by the microstructural analysis with a light microscope Zeiss Axio Scope.A1. Before, the eroded samples are fixed in a specimen holder and positioned in an embedded form. Afterwards, a two-component-cold-embedding-resin is added. After hardening, the specimens are removed and faced on both sides, which improve the surface and enable to start the grinding process with P600 wet sand paper. A Buehler Phoenix 4000V is used for all grinding as well as polishing processes. A summarize of the several steps of grinding and polishing is presented in table 4.5. Every probe was manually grinded at a constant rotational speed of 225 rpm under constantly water supply to avoid scratching of the probes by residual particles. After each grinding step, the duration of processing was duplicated. Between the several preparation phases, the metallographic probes were cleaned in the ultrasonic bath with isopropanol for 5 minutes. After grinding with P4000, the probes were polished by using the automatic grinding head under a constant force of 15 N and supply of waterless alcoholic lubricant to avoid corrosive effects. The rotational movement occurred in counter direction. Polishing by 3  $\mu\text{m}$  grains results in scratching in case of similar magnesium joints. Indeed, a granulation of 1  $\mu\text{m}$  exhibited superior surfaces. Regarding to dissimilar magnesium/aluminum joints, the best results are achieved by a polishing with 3  $\mu\text{m}$ . Afterwards, all probes were cleaned in the ultrasonic bath and subsequently etched with Nital for 8 seconds. After thoroughly rinsing with water, the cleaning in the ultrasonic bath for 5 minutes was carried out. Etching with Nital do not results in visible effects on the aluminum alloy. In general, for etching the AW6016 alloy are etched with Kroll's reagent. However, the etching of dissimilar joints with Kroll's reagent results immediately in over-etching of the magnesium alloy, even for a short duration of 1 second. There is no information about an adequate etching reagent for dissimilar joints. As a result the magnesium/aluminum joints were also etched with Nital for 8 seconds.

Table 4.5: process steps of wet grinding and polishing.

| Process           | specification  | steps          | Parameters             |              | Specimen |             |
|-------------------|--|----------------|------------------------|--------------|----------|-------------|
|                   |  |                | Rotational speed [rpm] | Duration [s] | AZ31     | AZ31/AW6016 |
| Wet grinding      | - water supply<br>- manual processing  | P600           | 225                    | 10           | X        | X           |
|                   |  | P1200          | 225                    | 20           | X        | X           |
|                   |  | P2500          | 225                    | 40           | X        | X           |
|                   |  | P4000          | 225                    | 80           | X        | X           |
| Polishing         | - lubricant supply<br>- automatic processing<br>(counter direction; F= 15 N) | 3 μm - Diamond | 150                    | 300          |          | X           |
|                   |  | 1 μm - Diamond | 150                    | 240          | X        |             |
| Immersion etching |  | Nital          |                        | 8            | X        | X           |

After the light microscopic analyze, several probes are selected and checked for hardness. The test was conducted by a nanointender, which determine the Martens hardness in accordance to DIN EN ISO 14577. The approach is similar to the hardness measurement by Vickers (HV). However, the Martens hardness is specified in N/mm<sup>2</sup> and includes elastic fractions. For this reason a converting from Martens in Vickers hardness is not possible. Indeed, the Martens hardness can be assumed to be ten times higher than the corresponding Vickers hardness. (Bar08)



## 5. Results

### 5.1. LAFSW

#### Influence of laser on extruded AZ31

In preparation for the investigations concerning LAFSW, it was important to consider the influence of laser power on the extruded AZ31 separate. The object of this part is to determine “optimum” values of laser power for different welding speeds, which are used in the following study of LAFSW. “Optimum” values mean the level of power where the material begins to melt or burn. This criterion was chosen because of the definition of FSW. This process is characterized by welding at solid state. Therefore a melting of material due to laser would not be consistent with the nature of process.

The procedure for studying the influence of laser power is given in figure 5.1. The schematic illustration shows the electrical current as setting parameter because the amount of laser power is adjusted by it. The corresponding values for power  $P$ , specified by producer, are presented in the appendix. These values are reduced by 20 % (loss at optical elements) to obtain the real available laser power  $P_{real}$ .

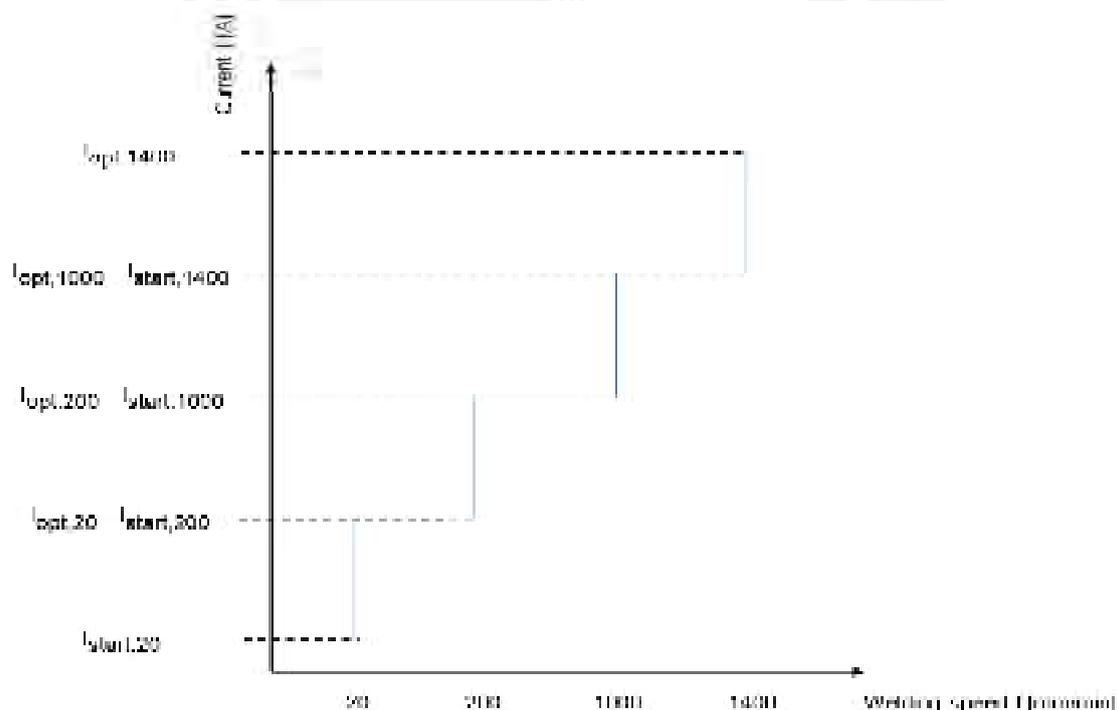


Figure 5.1: schematic illustration of procedure for the investigation of laser power on extruded AZ31

The investigation starts with a welding speed of 20 mm/min and an electrical current of 12 A. Subsequently, the value of current is increased in certain steps (see appendix) up until a change in surface appearance is observable. The adjusted value is defined as optimum value for a welding speed of 20 mm/min  $I_{opt,20}$ . Concurrently it corresponds to  $I_{start,200}$ , the start value of electric current for a speed of 200 mm/min. This procedure is repeated for transverse speeds of 1000 and 1400 mm/min. The results are presented in table 5.1.

Table 5.1: determination of values for electrical current for different welding speeds

| Welding speed [mm] | Electrical current [A] | Laser power [W] |
|--------------------|------------------------|-----------------|
| 20                 | 20                     | 191,2           |
| 200                | 30                     | 474,4           |
| 1000               | 50                     | 1040            |
| 1400               | 50                     | 1040            |

The next step was the evaluation of these results. Therefore the procedure for the different welding speeds and their corresponding “optimum” values of laser power was repeated three times. Meanwhile, the occurring temperatures in the backing plate were measured by the method described in the experimental approach. From these five measuring points, the highest value was chosen. For every parameter setting, the average of the three temperatures was formed and used for the comparison to the simulation model.

The surface appearance of the used magnesium alloy varied between the sheets. This results in differing influence of laser power on surface despite identical parameter settings. For darker surfaces, the laser beam affects the material more than for bright surfaces caused by a higher absorption.

The received values for electrical current are used for the investigation of LAFSW. Furthermore, the measured process temperatures serve to evaluate the simulation model described in the experimental approach. The aim is to predict surface temperatures during the interaction of laser beam and material. This serves the determination of an ideal initial temperature of the joining members with regard to reducing process loads during LAFSW.

As mentioned in the state of the art, there are no exact values for absorption of magnesium. Indeed, a calculation method is given in [Mor05]. For a wavelength of 1,06  $\mu\text{m}$  an absorption coefficient of 0,08 can be calculated. Values of about 0,9 are obtained by an investigation of

Nd:YAG- laser ( $\lambda=1,06 \mu\text{m}$ ) interaction on the magnesium alloy WE43. Due to the widely variation, the simulation is carried out for different absorption coefficient (table5.2).

Table5.2: settings for simulation of laser interaction on magnesium

| Welding speed<br>[mm/min] | electrical current<br>[A] | coefficient of absorption |      |      |      |     |
|---------------------------|---------------------------|---------------------------|------|------|------|-----|
|                           |                           | 0,08                      | 0,09 | 0,16 | 0,25 | 0,5 |
| 20                        | 20                        | 0,08                      | 0,09 | 0,16 | 0,25 | 0,5 |
| 200                       | 30                        | 0,08                      | 0,09 | 0,16 | 0,25 | 0,5 |
| 1000                      | 50                        | 0,08                      | 0,09 | 0,16 | 0,25 | 0,5 |
| 1400                      | 50                        | 0,08                      | 0,09 | 0,16 | 0,25 | 0,5 |

The temperatures in the experiment were measured 0,8 mm under the surface of the backing plate. To compare the results of the simulation with the experiment, it was necessary to consider the simulated temperatures at the same position (figure5.2). Additionally, the analysis of temperatures at different distances (10; 20 mm) to the point of laser interaction is made. This is based on the position of laser focus during LAFSW. In the present study, the beam is focused (on surface) about 20 mm in front of the welding tool. Both, the laser and the welding tool, are moved with identical transverse speed during process. That means the local heated area is cooling down until the welding tool has reached it. For this reason information about the residual temperature is important.

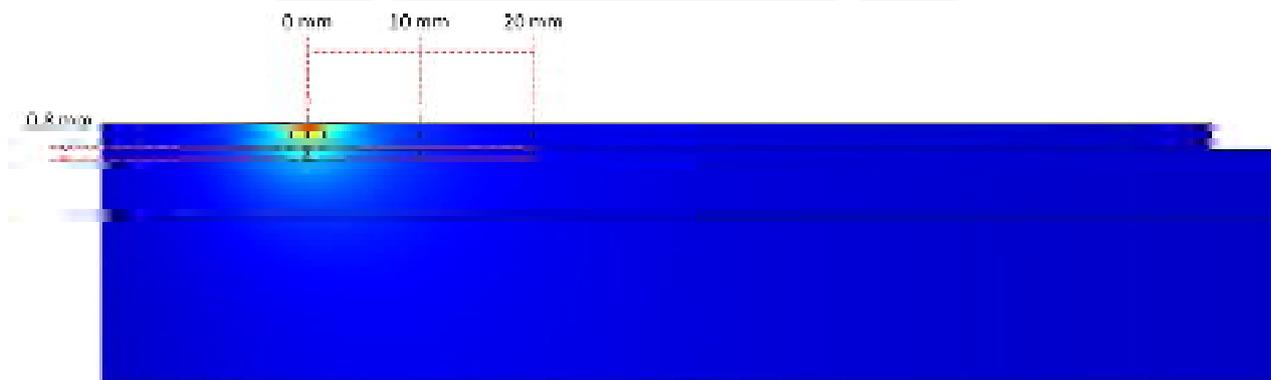


Figure5.2: measuring points of temperature in the simulation model

The comparison of measured and simulated temperatures at different distances to the point of laser interaction is presented in figure52. For a high transverse speed of 1400 mm/min, it can be seen that the reached temperatures are slightly above the initial temperature (about 26 °C). The short interaction time is not sufficient to generate high heat. The level of temperature is nearly equal for the considered distances. In contrast, the temperatures in simulation decrease

with increasing distance from the point of laser interaction. This effect gets larger at higher absorption coefficients. The diagram (figure5.3 a) indicates that the similarity of values is higher for a low absorption coefficient. Indeed, the exact replication of measured temperatures was not possible. The variations between simulation and experiment are remarkable higher for low transverse speed (figure5.3 b). In case of low absorption (0,8 and 0,9), the level of temperature is too low, but the behavior by increasing distance is similar. A clearly higher maximum temperature at the point of interaction is generated by simulation for an absorption coefficient of 0,5. At 10 mm distance, the value almost correlates with the experiment.

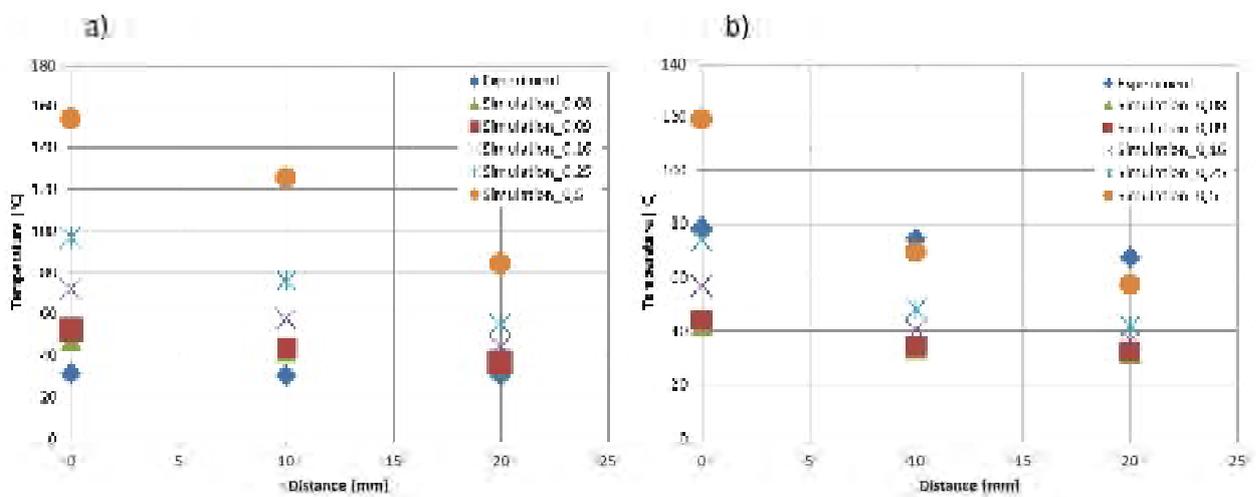


Figure5.3: comparison of temperatures between simulation and experiment for different transverse speeds: a) 1400 mm/min and b) 20 mm/min.

In conclusion, the exact replication of experimental recorded temperatures by simulation was not possible. The variation of absorption coefficient leads to approximately the same gradient of temperatures only for high transverse speed.

## FSW of extruded AZ31

To review the influence of initial workpiece temperature, it was important to get an overview of the characteristics of conventional FSW at first. Considered aspects were force, torque and temperature occurring during welding as well as surface appearance, tensile properties and microstructure. Afterwards, the knowledge obtained serves as reference for the comparison of process properties in LAFSW as well as the tests concerning to preheating by heating elements.

### **Experimental settings**

The experimental settings are given in table 5.3. For butt joint configuration the welding process was investigated at a constant rotational speed of 2000 rpm for a wide range of welding speeds. In addition to low speeds of 20 and 200 mm/min, welds are also made at higher welding speeds of 1000 and 1400 mm/min. This approach enabled an overview about process characteristics. Three welds were made for each parameter setting with constant plunging depth (0,2 mm) and speed (100 mm/min) as well as tool tilt angle (2°). To generate sufficient heat at the beginning of the weld, a dwell time of 5 seconds after plunging was chosen. Each welding process started at an initial temperature (measured in backing plate) of about 28 °C in order to compare the received results at different initial temperatures of workpiece in the following chapters. As mentioned in the experimental approach, welding tool 1 was used for FSW of the extruded magnesium alloy AZ31. According to /Lea08/, tools with a concave shoulder and a conical, unthreaded pin generate sufficient frictional heat in order to produce high quality welds for FSW of thin plates. Concerning to the adhesive behavior of the magnesium, a simple machining with lathes is required.

Table 5.3: experimental settings for FSW of extruded AZ31

| Form of weld                                 | Butt joint    |     |      |      |
|--|---------------|-----|------|------|
| Material                                     | Extruded AZ31 |     |      |      |
| Rotational speed<br>[rpm]                    | 2000          |     |      |      |
| Welding speed<br>[mm/min]                    | 20            | 200 | 1000 | 1400 |
| Number of experiments                        | 3             |     |      |      |
| Plunging depth<br>[mm]                       | 0,2           |     |      |      |
| Plunging speed<br>[mm/min]                   | 100           |     |      |      |
| Dwell time<br>[s]                            | 5             |     |      |      |
| Tool tilt angle<br>[°]                       | 3             |     |      |      |
| Weld length<br>[mm]                          | 130           |     |      |      |
| Initial temperature in backing plate<br>[°C] | 28            |     |      |      |
| Welding tool                                 | Tool 1        |     |      |      |

### Surface appearance

Figure 5.4 shows the surface appearance for FSW of extruded AZ31 overall the welding speed. Defect free welds with a completely formed pinhole are made for all settings, independent of the welding speed. It can be seen that with increasing rotational speed, a welding burr occurs. Due to the higher rotational speed the heat input increases whereby the plasticized material is pushed to the edge of the weld and consolidate in the form of welding burr.

For  $f = 20$  mm/min, the weld possesses a high welding burr on retreating and advancing side. In accordance to /Völ09/, this appearance occurs due to an excessive heat input into weld. As a result, the plasticized material is released from the weld bottom to the upper surface and afterwards pushed out of the weld where the material consolidates and forms the welding burr. As a result, the weld cross section is reduced which leads to inferior tensile properties.

By increasing welding speed the welding burr reduce considerably, which point to less heat input. For  $f = 20$  and  $200$  mm/min, smooth surfaces are produced. Observably the surface is rough at high welding speeds due to less heat input.

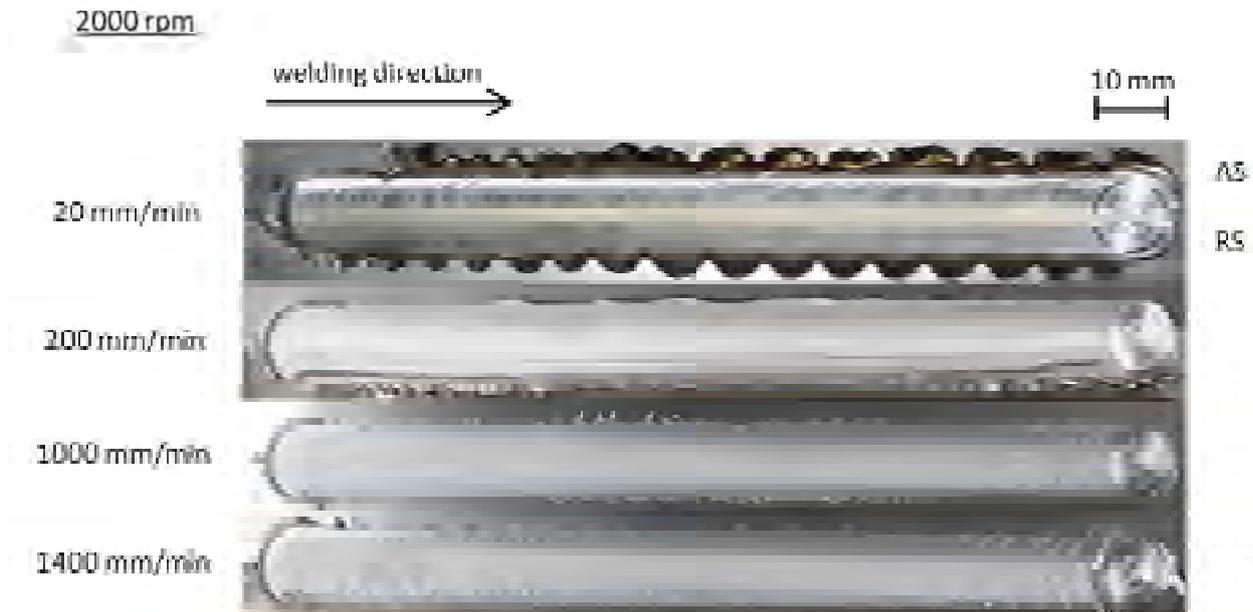


Figure 5.4: surface appearance of FSW of extruded AZ31 for different welding speeds at constant rotational speed.

### Process temperatures

The measured maximum temperatures during FSW as function of welding speed are presented in figure 5.5. The values were measured according to the test setup described in experimental approach. The reached temperature level for a welding speed of  $20$  mm/min is obviously higher than for  $1000$  and  $1400$  mm/min. For  $20$  mm/min, the temperature increases from beginning to center of the weld. At the end of the weld, the temperature reduces drastically. These effects can be constituted as follows: During the plunging phase, the occurring friction leads to heat and an increase in temperature. A slow welding speed causes a long interaction between tool and workpiece whereby a large quantity of heat is produced. After reaching a maximum value the temperatures decline.

By contrast, the maximum temperatures for higher welding speeds decrease constantly from beginning to the end of the weld. Due to high welding speeds the heat produced by friction between the tool and the workpiece is low by what the measured temperatures diminish along the welding line.





paths for a weld made at  $N = 2000$  rpm and  $f = 200$  mm/min are given in figure 5.6. It can be seen that the plunging of the tool into the workpiece results in an intense increase in axial force as well as torque. Indeed, the increase of force is sharper in comparison to the torque. This effect is based on the following context: At first, the tool pin is plunged in, which results in a sharply raising axial load. By contrast, the amount of torque depends on friction between tool and workpiece and thereby on the size of friction area. This increased slowly by further plunging of the tool into the material.

If the adjusted plunge depth is reached, the tool dwells for a certain time at the same position. The rotational movement generates heat, whereby the resistance against deformation of the material is reduced. This leads to plasticization and mixing of the material. In the diagram, this behavior is observable by the decrease of process loads after the peak value. Subsequent to this, the translational movement along the weld line is initialized. A slight rise of loads up to a certain level is observable. This level is relatively constant up to the end of the welding process. A short dwell time before pulling out the tool is represented by a slight decline of loads. In comparison to the axial force, the torque path is noisier caused by changing friction conditions between tool and workpiece. The material in front of the tool is in a solid condition whereby more loads are necessary. By contrast, the material behind the tool is already in a plasticized form.

In figure 5.7 the paths for axial force and torque for a weld made at  $N = 2000$  rpm and  $f = 1400$  mm/min are presented. These curves show the same characteristics as described before. Peak values are reached at the end of plunging phase. The following dwell time leads to the reduction of the loads. In contrast to figure 5.6, the levels of axial force and torque rise drastically after dwell time. This effect is caused by the high welding speed of 1400 mm/min which results in less generated heat and finally a higher level of required force for the material's plasticization. Due to the high welding speed, the duration of interaction between tool and workpiece decreases. For this reason the level of occurred loads while the actual welding phase, is less constant than for lower speeds as shown in figure 5.6.

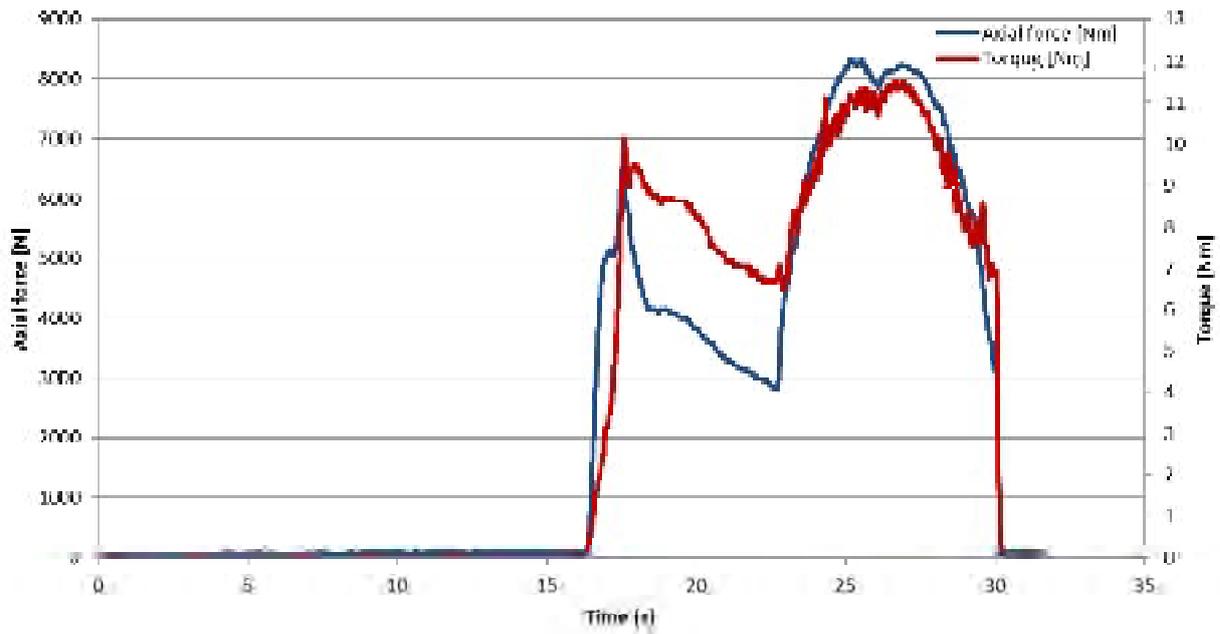


Figure 5.7: axial force and torque path for FSW of extruded AZ31 at  $N = 2000$  rpm and  $f = 1400$  mm/min. (filtered curve)

The forces and torques appear while different process phases are summarized in figure 5.8 and 5.9 for all welds. During the plunging phase, the level of force and torque (figure 5.8) are relatively constant. The force and torque varied between 6600 N and 7200 N and 8,2 Nm and 11,5 Nm overall welds. According to /Ath09/ the variation of these values can be explained by the flow behavior of material while interaction between tool and workpiece. Although the process parameters and material are the same, the repartition around the welding tool is different from one experiment to another. Furthermore there could be differences between the tool speed and the set speed of the milling machine.

A remarkable increase of welding force and torque occurs when raising welding speeds (figure 5.9). As described before, the generated heat is low in case of high speeds. Thereby the material possesses a higher resistance against deformation which results in larger force and torque.

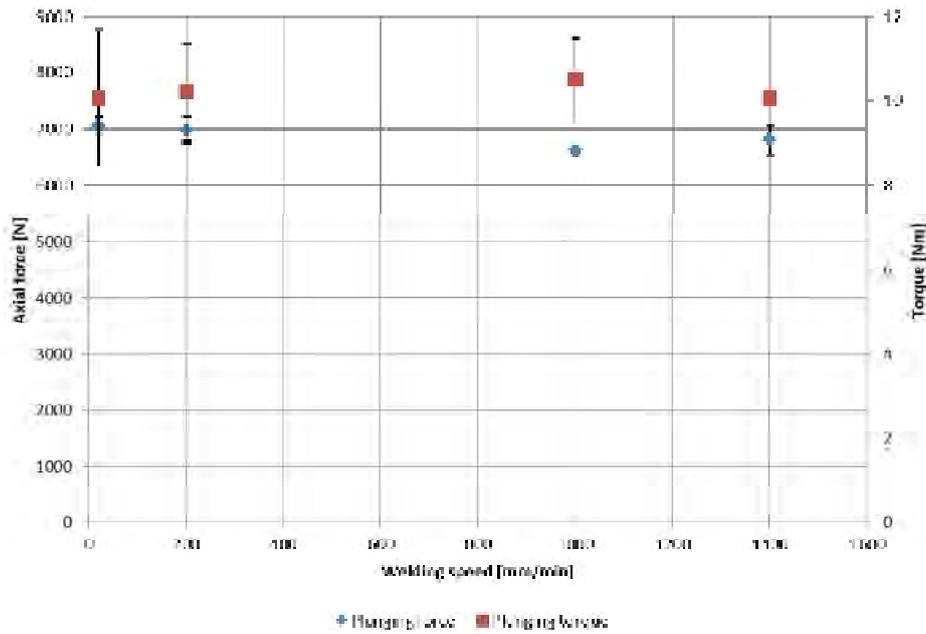


Figure 5.8: measured forces and torques for FSW of extruded AZ31 subject to different welding speeds at constant rotational speed. (plunging phase)

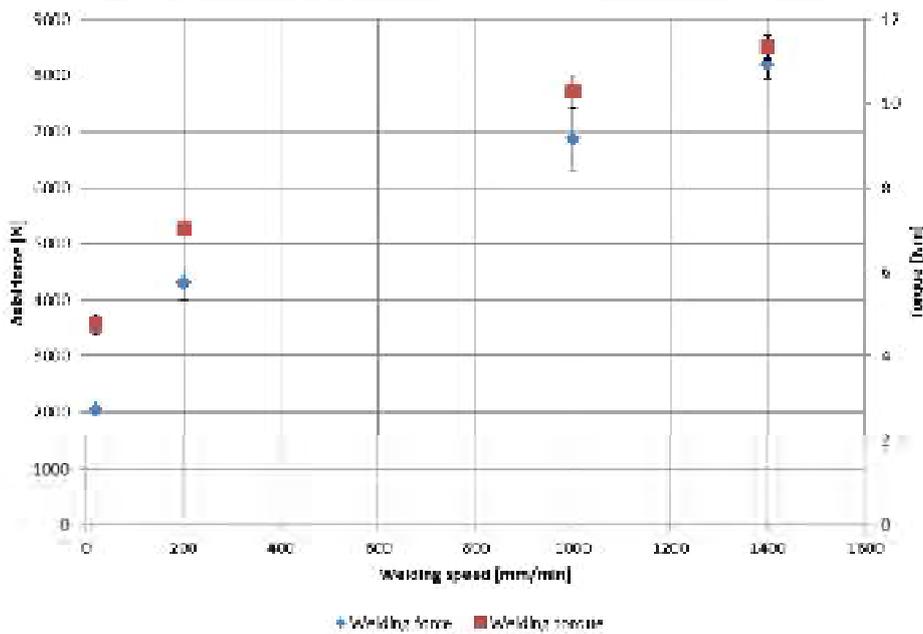


Figure 5.9: measured forces and torques for FSW of extruded AZ31 subject to different welding speeds at constant rotational speed. (welding phase)

### Tensile tests

The tensile strength as function of welding force and torque is given in figures 5.10. To evaluate the results the knowledge about the base materials tensile strength is important. The extruded magnesium alloy AZ31 reached an average strength of 260,8 N/mm<sup>2</sup> in tensile tests. The highest value (about 77 % of base material) is reached for the condition of 200 mm/min while the specimen made with a welding speed of 20 mm/min affords the lowest tensile strengths (about 56 % of base material). It is recognizable that increasing welding speed – and thereby the process force and torque – up to 200 mm/min results in stronger joints. As mentioned before, the low speeds results in excessive heat input which can affect the tensile properties in a negative way. For welding speed over 200 mm/min, the tensile strength decline clearly. Indeed, the values are higher than 60 % of the base material tensile strength. The probable reason for this effect is the insufficient heat generation. From the state of the art’s chapter, it is known that the weld pitch is an important indicator for heat input in welds. A low weld pitch (“hot weld”) means higher generated heat and eventually higher tensile properties. In contrary, a high weld pitch (“cold weld”) indicates a low level of heat input (figure 5.11 b).

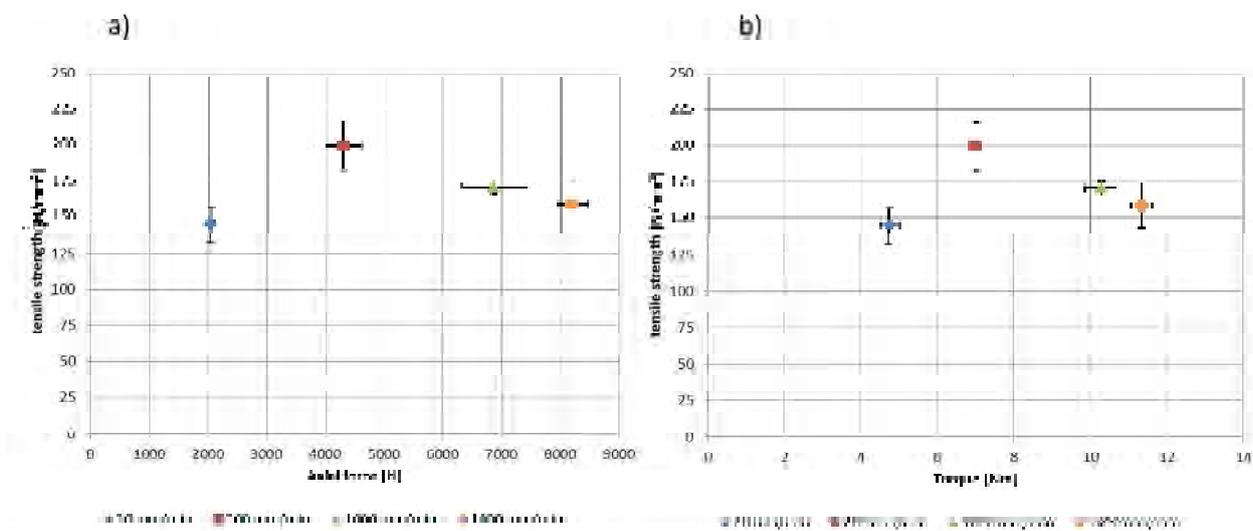


Figure 5.10: tensile strength for FSW of extruded AZ31 for different welding speeds at constant rotational speed subject to: a) axial force; b) torque.

In regard to fracture length (figure 5.11 a), it can be concluded that FSW leads to a significant reduction. A fracture length of about 4,1 mm (about 34,6 % of base metal) was reached in case of welds made at  $f = 200$  mm/min. The other joints exhibit a fracture length under 25 % of those of the base material.

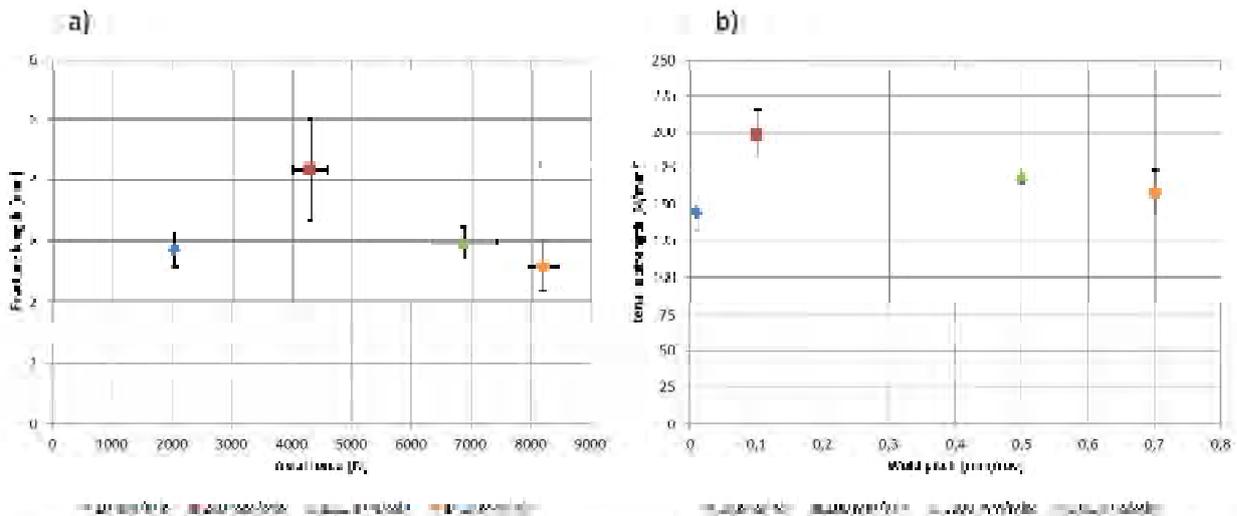


Figure 5.11: tensile properties for FSW of extruded AZ31 for different welding speeds at constant rotational speed:  
 a) fracture length as function of axial force; b) tensile strength as function of weld pitch.

From figure 5.10 and 5.11 it can be concluded that process loads of about 4500 N axial force and 7 Nm torque results in high tensile properties because of adequate heat input which is indicated by the weld pitch. Furthermore it shows that excessive and low heat input deteriorates the properties.

Fracture appearances that occurred in consequence of tensile tests, are presented in figure 5.12. Specimen for joints welded at 20 and 200 mm/min fractured at the advancing side. In contrast, the fracture appearance of welds made under condition of higher welding speeds is located in the middle of the weld.

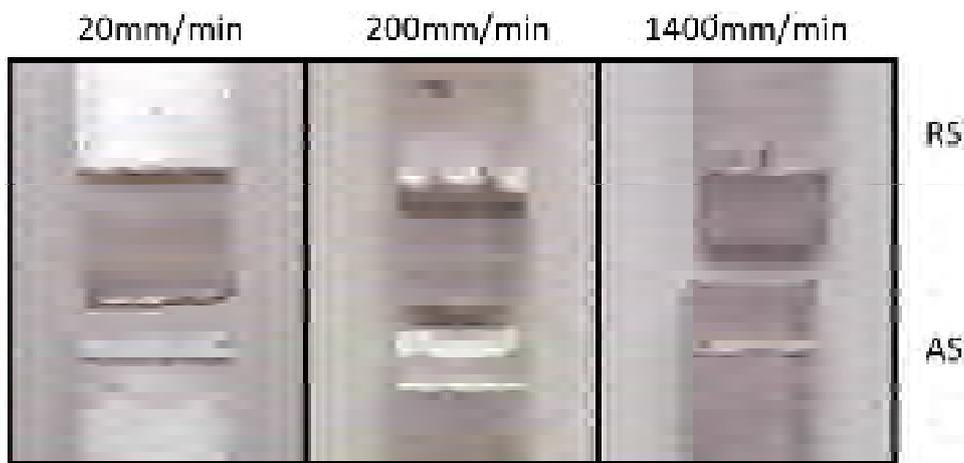


Figure 5.12: fracture appearance for FSW of extruded AZ31 for 20; 200 and 1400 mm/min at constant rotational speed.

## Metallographic analysis

Possible explanations for the received values of tensile strength and the position of fracture can be found by consideration of the micrographs which are shown in figure 5.13 and 5.14. Although all joints were made under same conditions, except welding speed, the plunging depth, especially on advancing side, varied clearly. For a welding speed of 20 mm/min the plunging depth is about 0,5 mm and 0,2 mm on the advancing side and retreating side, respectively. Due to the low speed, the generated heat is high whereby the plasticized material is pushed to the edge of the weld (bulk on advancing side) and consolidates in the form of welding burr. Thereby the material is missing in the weld joint. The reduced cross-section is the weak point of the joint and therefore the most likely fracture point in tensile test.

For welds with 200 mm/min, the measured plunging depth account about 0,2mm for both sides of the center line while there are differences in depth for joints made at a welding speed of 1400 mm/min. About 0,2 mm and 0,1 mm were measured on retreating and advancing side, respectively. These differences influence also the size and form of the stirring zone as shown in figure 5.14. The size decreases with the rising of welding speed which also indicates a decreasing heat input. This relation is also made by /Mis07/. An asymmetrical form of stirring zone can be observed for a welding speed of 200 mm/min. A lack of heat input and plunge depth can lead to a lack of penetration defect at the bottom of the weld, which can be seen for joint with 1400 mm/min. This crack possesses a length of about 490  $\mu\text{m}$ . A possible reason for the lack of penetration defect depth is the system deformation based on the high force during process. /IWB10/

A comparison of the micrographs also shows differences in surface appearance of the welds. While the surface is smooth for lower welding speeds, it can be seen that a rougher surface is revealed for 1400 mm/min.

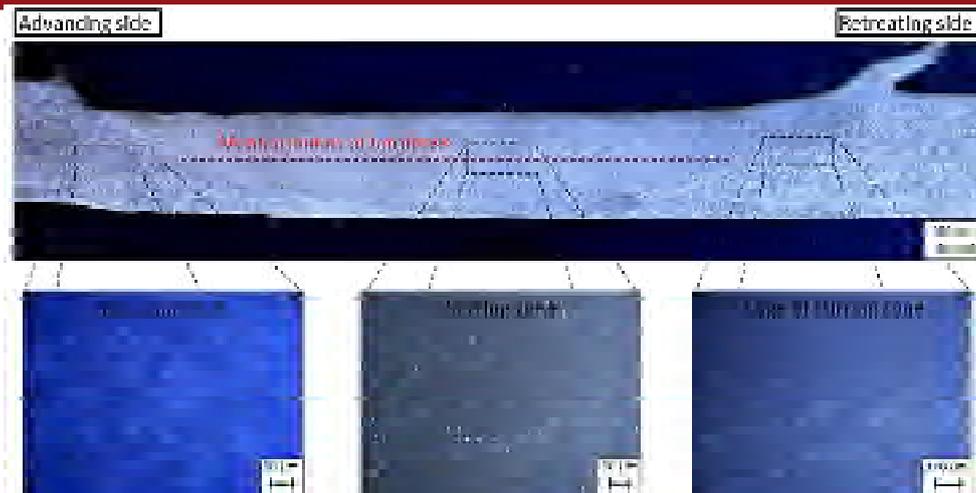


Figure 5.13: micrograph for FSW of extruded AZ31 for 20 mm/min at constant rotational speed.

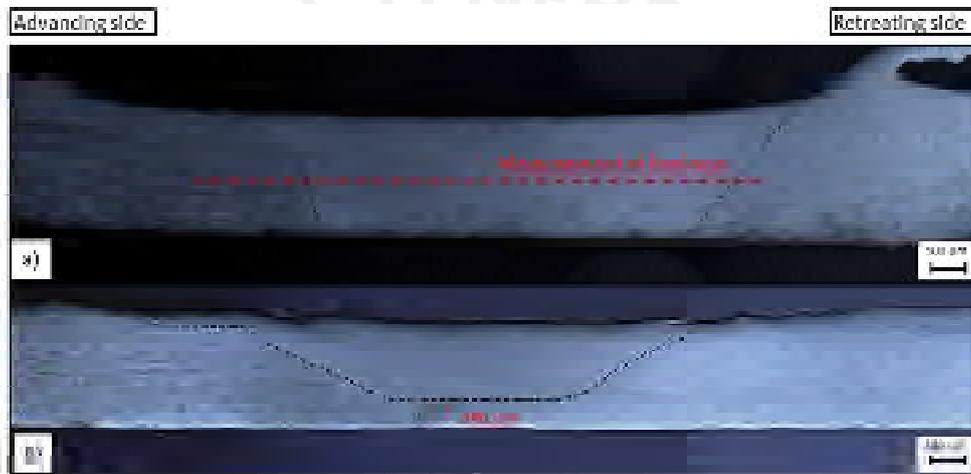


Figure 5.14: micrographs for FSW of extruded AZ31 for 200 and 1400 mm/min at constant rotational speed.

An additional explanation for differences in tensile strengths is provided by the diagram in figure 5.15. It shows the hardness profiles for joints made at 20 and 200 mm/min. The measuring points run along the marked lines in figure 5.13 and 5.14 at a distance of 500  $\mu\text{m}$ . For 200 mm/min, it is obvious that the softest regions are located on the advancing side. The maximum hardness value of 67,6 HV is reached in the weld center. Almost all measured points exhibit a higher hardness than the base metal (55,8 HV). This circumstance is caused by the dynamic recrystallization that take place during FSW. The heat input leads to the reduction of dislocations and generation of refined grains. In accordance to the Hall-Petch-relation, these grains results in a higher hardness and finally in higher tensile properties. This effect is confirmed by the measurement of grain size. The average grain size in base metal is about 62  $\mu\text{m}$ . On the contrary the grains in the stir zone exhibit a size of about 29  $\mu\text{m}$ . This corresponds to a grain refinement of about 53 %.

For lower welding speeds the regions are softer with a minimum at the advancing side. The measurement of grain size in the stir zone proved an average size of about  $45\ \mu\text{m}$ . The reason for this is the excessive heat input during welding. Pursuant to /Pad10/, higher temperatures and slower cooling rates due to low welding speeds leads to grain growth. Thereby the hardness declines and lower tensile properties are the consequence.

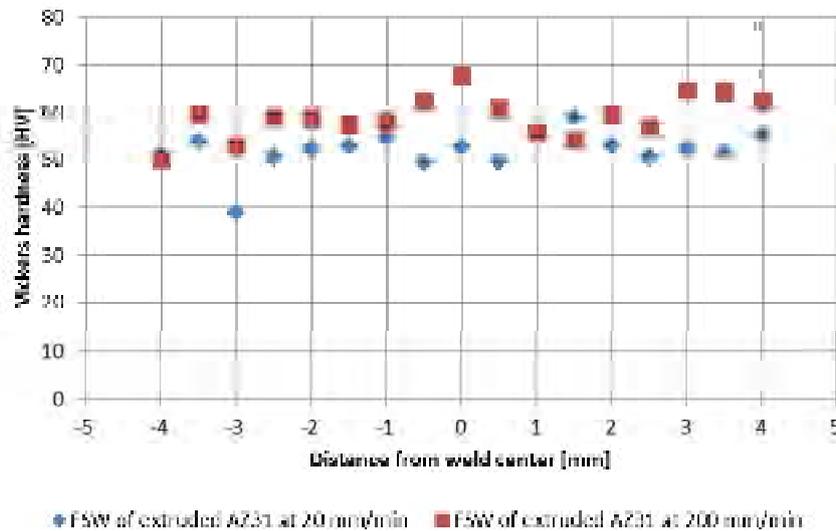


Figure 5.15: hardness profile for FSW of extruded AZ31 for 20 and 200 mm/min at constant rotational speed.

Both profiles indicate that the hardness is lower on the advancing side whereby a fracture while tensile test is probable on this side. Furthermore, it can be seen that the regions, in case of low welding speeds, are softer which results in less tensile properties.

### Laser assisted friction stir welding

The described potential of laser used to improve the FSW process is considered in the following chapter. The main object of this investigation is to rate the influence of an additional heating source, in the form of laser power, on the process force and torque as well as the tensile properties. A decrease in load is expected, whereby the welding speed could increase without raising the process loads in comparison to conventional FSW.



**Experimental settings**

Table5.4 contains the experimental settings. To compare the results with those of the conventional FSW, the same settings for rotational and welding speed as well as number of experiments, plunging depth and speed, dwell time, tool tilt angle and weld length are selected. Additionally, values for laser power are chosen from the investigation relating to influence of laser power on the material.

Table5.4: experimental settings for LAFSW of extruded AZ31.

| <b>Form of weld</b>                                 | <b>Butt joint</b>                        |       |      |      |
|---|--|-------|------|------|
| <b>Material</b>                                     | Extruded AZ31                            |       |      |      |
| <b>Rotational speed</b><br>[rpm]                    | 2000                                     |       |      |      |
| <b>Welding speed [mm/min]</b>                       | 20                                       | 200   | 1000 | 1400 |
| <b>Current</b><br>[A]                               | 20                                       | 30    | 50   | 50   |
| <b>Laser power</b><br>[W]                           | 191,2                                    | 474,4 | 1040 | 1040 |
| <b>Number of experiments</b>                        | 3  |       |      |      |
| <b>Plunging depth</b><br>[mm]                       | 0,2                                      |       |      |      |
| <b>Plunging speed [mm/min]</b>                      | 100                                      |       |      |      |
| <b>Dwell time</b><br>[s]                            | 5  |       |      |      |
| <b>Tool tilt angle</b><br>[°]                       | 2  |       |      |      |
| <b>Weld length</b><br>[mm]                          | 130                                      |       |      |      |
| <b>Initial temperature in backing plate</b><br>[°C] | 28                                       |       |      |      |
| <b>Welding tool</b>                                 | Tool 1                                   |       |      |      |
| <b>Position of laser focus point</b>                | Abutting edges between the joint members |       |      |      |

## Surface appearance

The surface appearance of the welded blank sheets, shown in figure 5.16, exhibits defect free and smooth joints for all tested welding speeds. A completely formed pinhole at the end of the weld is obtained. The surface for  $f = 1400$  mm/min is slightly rough. As expected, a high welding blur also occurs for LAFSW for  $f = 20$  mm/min, which can be ascribed to the excessive heat input. Raising the welding speed results in a considerably reduction of welding burr.

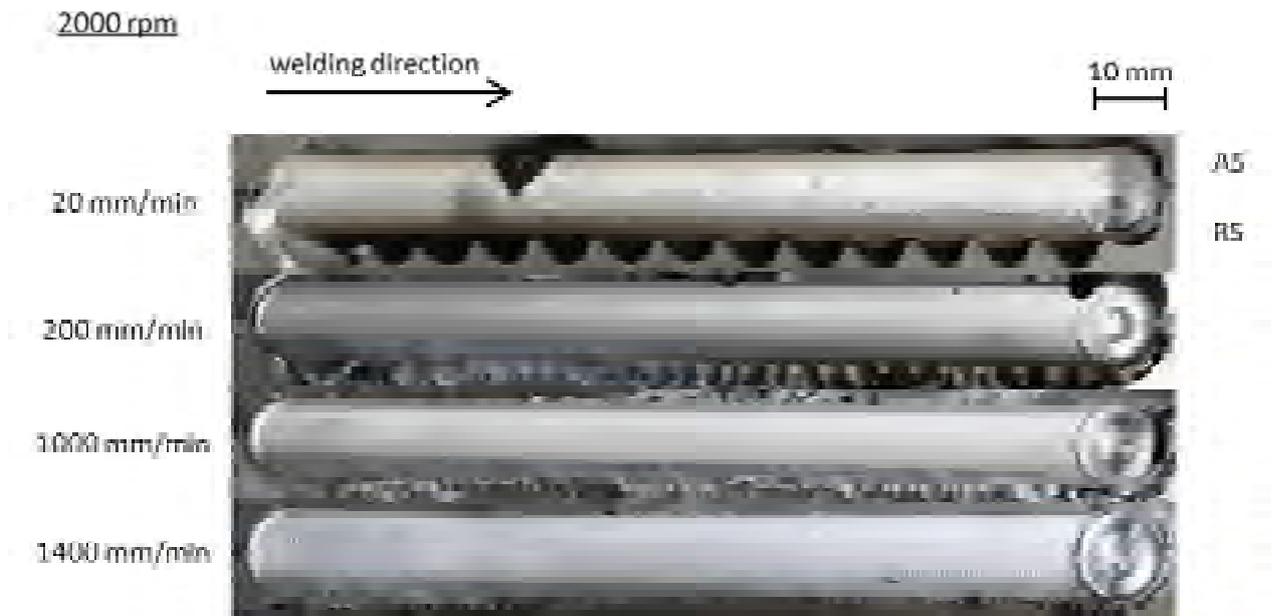


Figure 5.16: surface appearance of LAFSW of extruded AZ31 for different welding speeds at constant rotational speed.

A comparison of welding surfaces for FSW and LAFSW is given in figure 5.17. Joints made at constant rotational speed of 2000 rpm with different welding speeds (1000; 1400 mm/min) are displayed. It can be seen that there are remarkable differences between welds made by conventional FSW and those made by LAFSW. Without preheating materials, the joints possess an obvious rougher surface. The laser assistance increase the heat input into workpiece locally, whereby the plasticization of the materials is easier and the flow behavior is improved. Indeed, the additional heat results in welding burr.

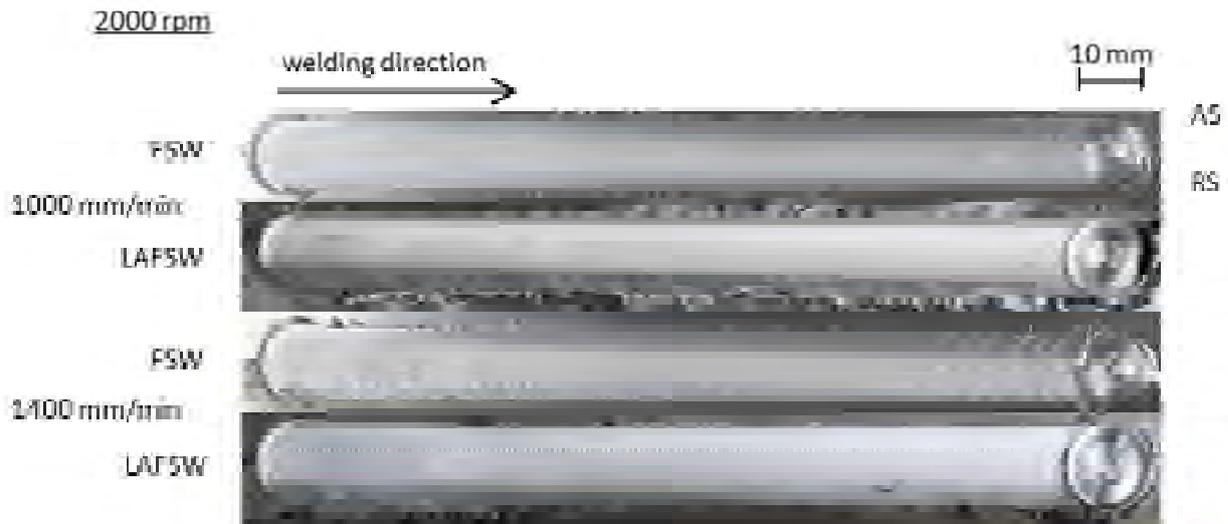


Figure 5.17: comparison of surface appearance of LAFSW and FSW of extruded AZ31 for different welding speeds at constant rotational speed.

### Process loads

Process force and torque were measured during LAFSW and compared to those of conventional FSW. The results are presented in figure 5.18 and 5.19. Since the laser is switching-on if the plunging phase is finished, the tool starts to move along the weld line. For this reason, there are no large variations in loads between the procedures during plunging phase (figure 5.18). From figure 5.19 a) the effect of preheating can be seen concerning forces during welding phase. A reduction of about 11,4 % is reached for a welding speed of 20 mm/min. For  $f = 200$  mm/min the force is decreasing by about 25,5 %. Joints made by  $f = 1000$  mm/min and  $f = 1400$  mm/min exhibit a force reduction of 12,6 % and 14,6 %, respectively. Overall, an average reduction of 16 % is achieved. The diagram indicates that an increase of welding speed without larger force is possible. Preheating by laser reduce the force level for welding with 1400 mm/min to those levels recorded during FSW for a welding speed of 1000 mm/min.

The influence on welding torque is even larger (figure 5.19 b). Differences of 28,8 % for  $f = 20$  mm/min, 24,7 % for  $f = 200$  mm/min, 25,3 % for  $f = 1000$  mm/min and 24,9 % for  $f = 1400$  mm/min are reached. That corresponds to a total average decline of 25,9 %.

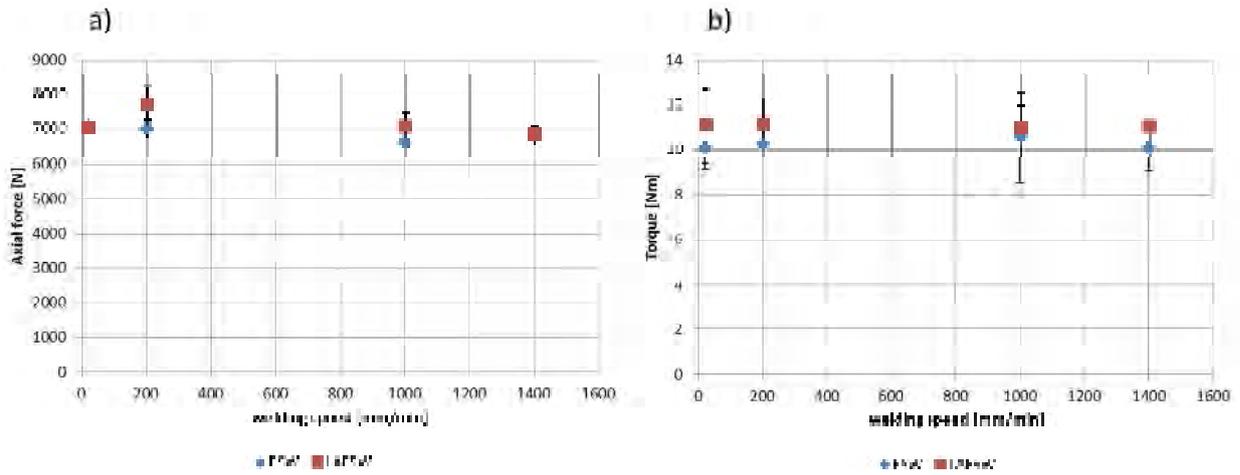


Figure 5.18: comparison of loads for LAFSW and FSW of extruded AZ31 at constant rotational speed: a) axial force as function of welding speed; b) torque as function of welding speed. (plunging phase)

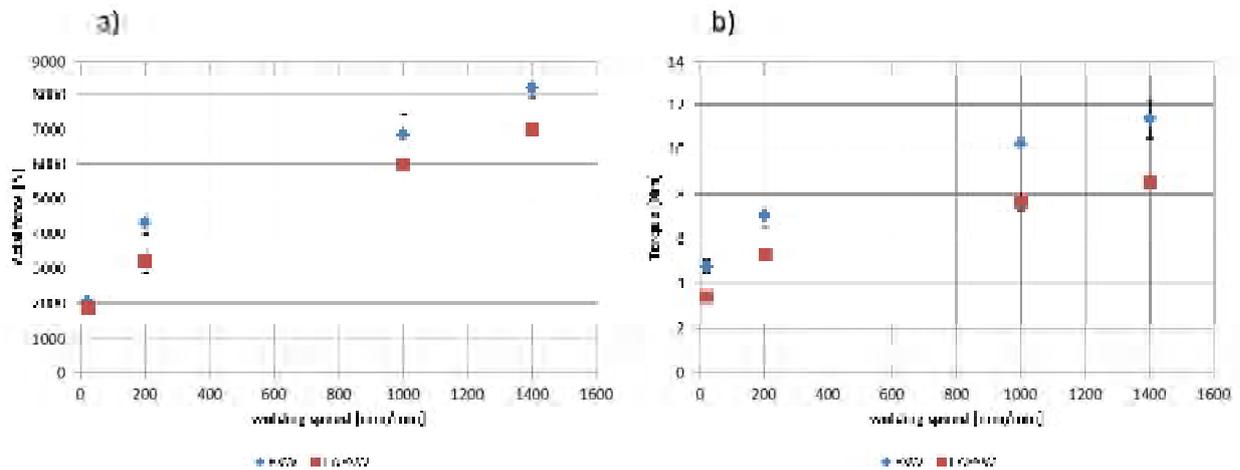


Figure 5.19: comparison of loads for LAFSW and FSW of extruded AZ31 at constant rotational speed: a) axial force as function of welding speed; b) torque as function of welding speed. (welding phase)

### Tensile tests

Concerning tensile strength, figure 5.20 shows that the determined values are lower for LAFSW (compared to FSW) for all welding speeds, except for  $f = 20$  mm/min. These welds reached an average strength of  $160 \text{ N/mm}^2$  (61,6 % of base material). Tensile strengths for welding speeds of 200, 1000 and 1400 mm/min are respective 149, 149,9 and  $137,3 \text{ N/mm}^2$ . That corresponds to less than 60 % tensile strength of the base material. A dependency of tensile properties on welding force (a) and torque (b) can hardly be asserted. In case of LAFSW, a rise of welding force from 1800 N to 7000 N results in a decrease of tensile strength.

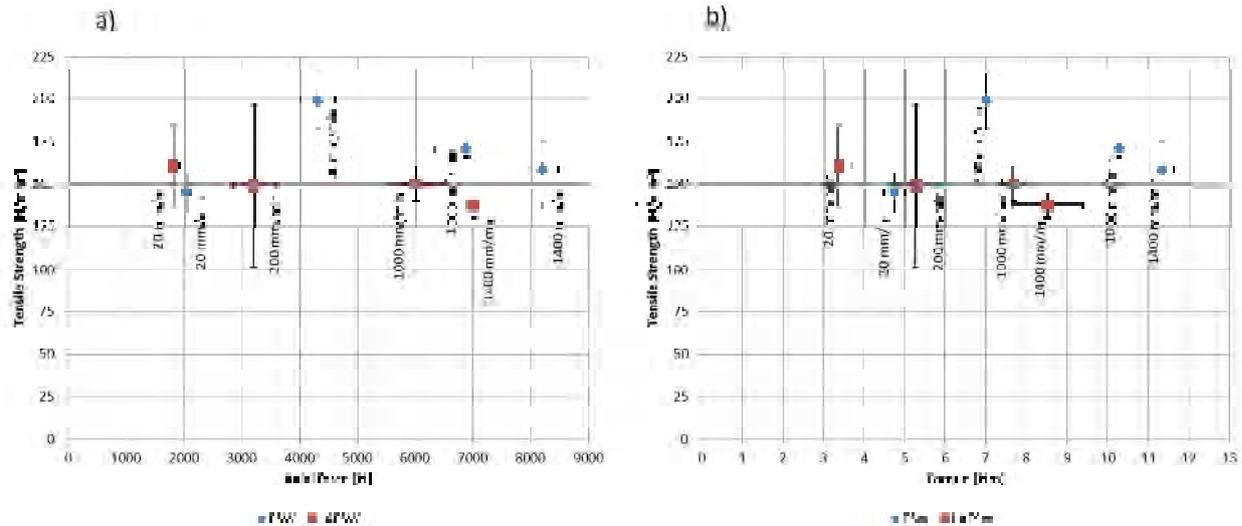


Figure 5.20: comparison of tensile strength for LAFSW and FSW of extruded AZ31 for different welding speeds at constant rotational speed subject to: a) axial force; b) torque.

The tensile strength as function of weld pitch is shown in figure 5.21 (a) and demonstrate a similar result. In consequence of the peak value of FSW for 200 mm/min, it can be assumed that a low pitch weld leads to high tensile strength. However, a clear trend over all conditions is not recognizable. Figure 5.21 (b) represent the fracture length subject to axial force. In comparison to FSW, the values for LAFSW are lower. The best values are obtained by 20 and 200 mm/min with 3,1 and 3,2 mm, respective. That corresponds about 26 % of the base material's fracture length. In contrast to tensile strength, a general trend is visible. Increase welding speed up to 200 mm/min (corresponds increasing force up to 4300 N) leads to higher fracture length. Subsequent, a remarkable reduction of fracture length is caused by higher speeds than 200 mm/min.

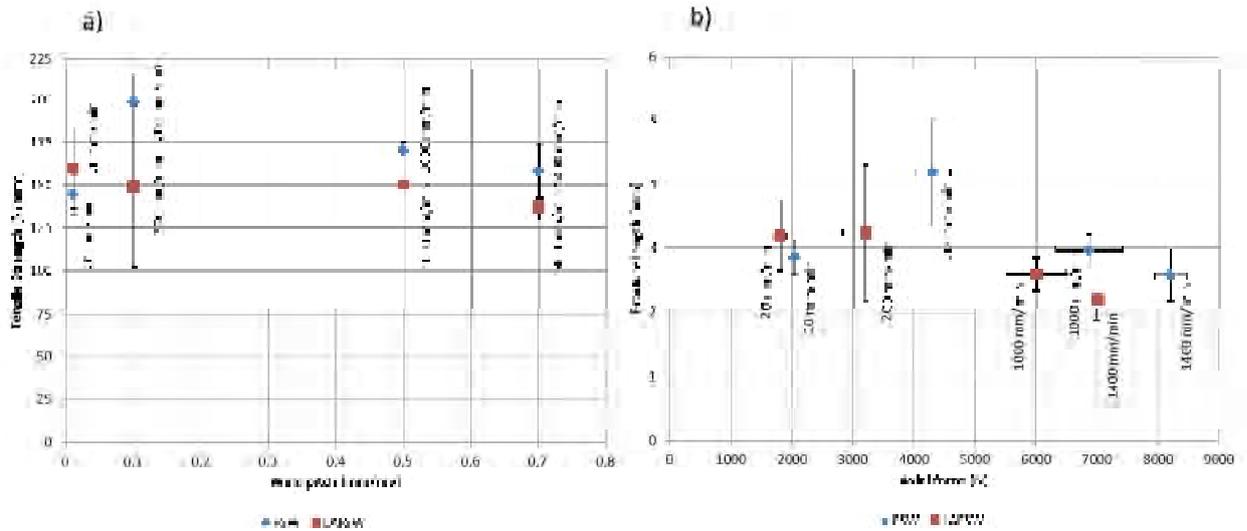


Figure 5.21: comparison of tensile properties for LAFSW and FSW of extruded AZ31 for different welding speeds at constant rotational: a) fracture length as function of axial force; b) tensile strength as function of weld pitch.

In figure 5.22 the fracture appearances for tensile tests of joints welded at different welding speeds are presented. For  $f = 1400$  mm/min the sample fractured in the middle of the weld. Specimens for joints welded at 20 and 200 mm/min fractured at the advancing side. This observation accords with the fracture appearance of conventional FSW. Therefore similarities in micrographs are expected.

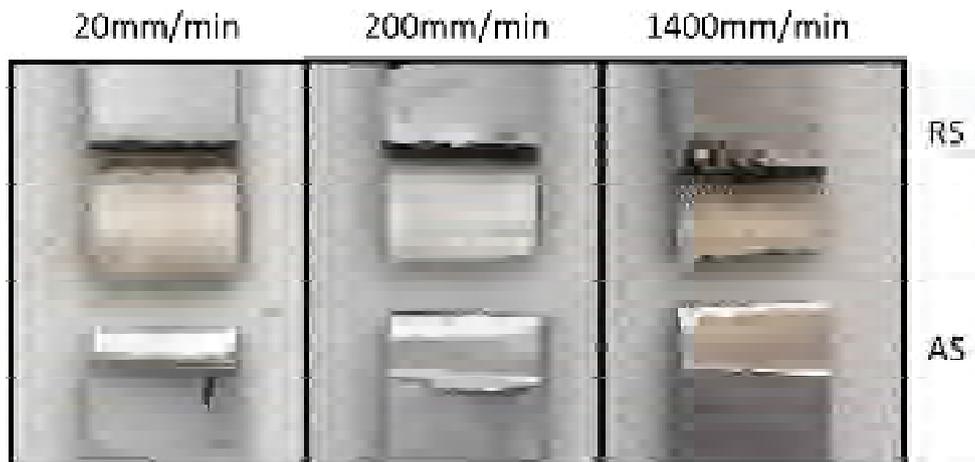


Figure 5.22: fracture appearance for LAFSW of extruded AZ31 for 20; 200 and 1400 mm/min at constant rotational speed

## Metallographic analysis

In contrary to conventional FSW, the micrograph for LAFSW at 20 mm/min (figure 5.23) does not exhibit a deeper plunging on advancing side which is the reason for a higher tensile strength. Indeed, near the top surface small cracks appear, probably caused by the laser beam interaction. The reduced tensile strength of joints for  $f = 200$  mm/min can be explained by the defect occurring on the advancing side. From the micrograph it can be seen that a *wormhole* defect appears on the edge of stirring zone. This effect is caused by an inadequate material flow. In general this defect is observable for “cold welds” (high weld pitch) due to insufficient heat input. In the present case, a sufficient amount of heat should be implemented by the adequate welding speed. Based on this fact, there must be a negative influence of the laser. It can be assumed that the laser power results in melting and burning of the material during welding. Thereby fractions of the material are missing in the stirring zone which results in defect production.



Figure 5.23: micrographs for LAFSW of extruded AZ31 at constant rotational speed for a) 20 mm/min; b) 200 mm/min.

For high welding speeds, the results are comparable to those of the conventional FSW process. Due to insufficient heat input, high process forces are generated. In consequence, the plunging depth is decreasing and a lack of penetration defect appears at the weld bottom.

The comparison of micro hardness for LAFSW and FSW of extruded AZ31 at a welding speed of 200 mm/min (figure 5.24) exhibits few differences. The maximum hardness values

are reached in the weld center with 67,6 HV for FSW and 63,78 HV for LAFSW. The similarity of the hardness is expected in regard to the average grain size in the stirring zone. The measurement revealed 29  $\mu\text{m}$  and 28  $\mu\text{m}$  for FSW and LAFSW, respectively. Corresponding to the Hall-Petch-relation, the grain refinement of about 53 % leads to higher hardness values and superior tensile properties. In case of preheating by laser, the produced joint for  $f = 200$  mm/min possesses a poor tensile strength (figure 5.20). The reason is a wormhole defect located on the edge of the stirring zone (on advancing side).

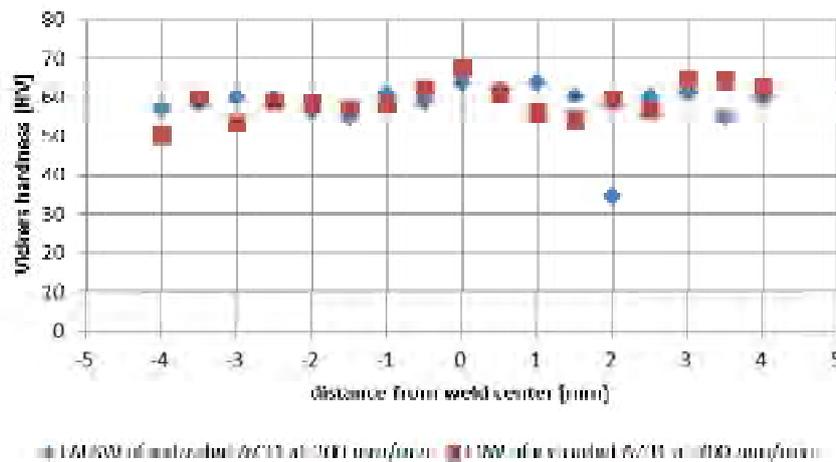


Figure 5.24: comparison of hardness profile for LAFSW and FSW of extruded AZ31 for 200 mm/min at constant rotational speed.

The previous analyses show the beneficial effect of LAFSW. A remarkable improvement of the surface quality could be reached for high welding speeds. The produced joints are smooth and defect free. Moreover, the process loads are reduced drastically, whereby the possibility of increase welding speed without a rise of the forces and loads is shown. Indeed, a negative effect of the laser is obtained regarding tensile properties. The determined tensile strengths and fracture lengths are lower compared to FSW at 28 °C initial temperature. For a welding speed of 200 mm/min, the metallographic analysis shows a defect formation on the edge of the stirring zone.



## 5.2 Preheating by heating element

### Heating element: bead on plate weld

The investigation of preheating the material by a heating element was conducted with a bead on plate weld at first. On the one hand it was important to consider the influence of different starting temperatures on the welding loads and surface appearance for several welding speeds, on the other hand this approach economize material.

### Experimental settings

Table 5.5: experimental settings for FSW of extruded AZ31 with heating element in bead on plate weld configuration.

| Form of weld                                  | Bead on plate weld |     |     |      |      |
|---|--------------------|-----|-----|------|------|
| Material                                      | Extruded AZ31      |     |     |      |      |
| Rotational speed<br>[rpm]                     | 2000               |     |     |      |      |
| Welding speed<br>[mm/min]                     | 20                 | 200 | 800 | 1000 | 1400 |
| Starting temperature in backing plate<br>[°C] | 28                 | 28  | 28  | 28   | 28   |
|   | 50                 | 50  | 50  | 50   | 50   |
|   | 100                | 100 | 100 | 100  | 100  |
|   | 130                | 130 | 130 | 130  | 130  |
| Number of experiments                         | 3                  |     |     |      |      |
| Plunging depth<br>[mm]                        | 0,2                |     |     |      |      |
| Plunging speed<br>[mm/min]                    | 100                |     |     |      |      |
| Dwell time<br>[s]                             | 5                  |     |     |      |      |
| Tool tilt angle<br>[°]                        | 2                  |     |     |      |      |
| Weld length<br>[mm]                           | 130                |     |     |      |      |
| Welding tool                                  | Tool 1             |     |     |      |      |

The experimental settings are shown in table 5.5. Joints were made at constant rotational speed of 2000 rpm with different welding speeds (20; 200; 800; 1000 and 1400 mm/min). Moreover, the starting temperature in the backing plate was varied (28; 50; 100 and 130°C) for each welding speed. Settings as the number of experiment, plunging depth and speed,

dwelt time as well as angle of incidence and weld length were identical to the previous chapters.

### Surface appearance

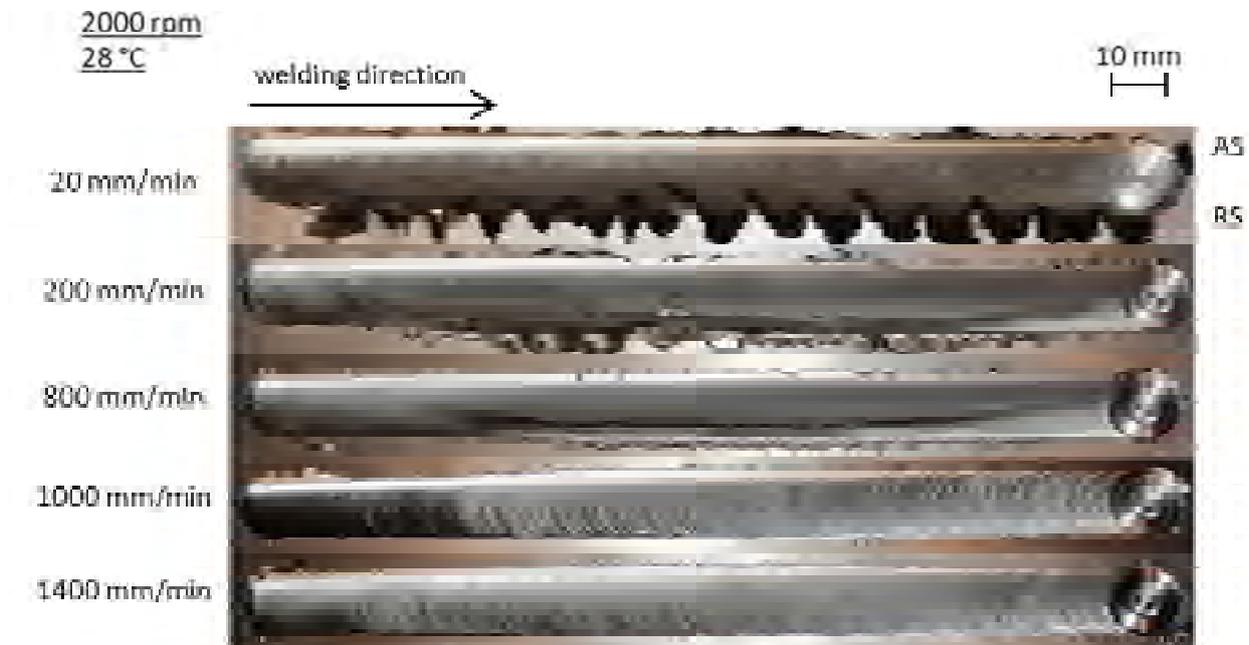


Figure 5.25: surface appearance of FSW of extruded AZ31 (bead on plate weld) for different welding speeds at constant rotational speed and a starting temperature of 28 °C.

As already known from previous tests, a welding speed of 20 mm/min leads to large welding burr, which is shown in figure 5.25 for a starting temperature of 28 °C. Because of less heat input, the welding burr decreases by increasing welding speed. Moreover, it can be seen that all welds are defect free but with significant differences in surface quality concerning roughness. Up to a welding speed of 800 mm/min the surfaces are smooth. A further rising of speed results in rough surfaces. For  $f = 200$  mm/min and 800 mm/min the appearance of welding burr in the welding line can be observed. This effect only occurred in case of bead on plate weld. This welding burr runs from the center line (at beginning of weld) to the retreating side (at middle of weld) and back to the center line (at end of weld). The respective area is larger for  $f = 200$  mm/min. Hence, a dependency of flow behavior on heat input can be assumed. At the beginning of weld, the generated heat results in pushing the material from centerline to the retreating side. Towards to the middle of the weld, the heat input increases and the material is pushed closer to retreating side. If the heat input decreases towards the end of weld, the welding burr moves to the centerline.

Overall starting temperatures, the widest differences in surface appearance exist between 28 and 130 °C. In figure 5.26, it is recognizable that preheating also leads to excessive heat input

for  $f = 200 \text{ mm/min}$ , which is expressed by high welding burr on the retreating side. Furthermore, the higher starting temperature caused an adhesion of the sheet on the backing plate for a welding speed of  $20 \text{ mm/min}$ . When removing the sheet, a defect occurred. Another effect of preheating is the shifting of the described welding burr (in welding line) to higher welding speeds.

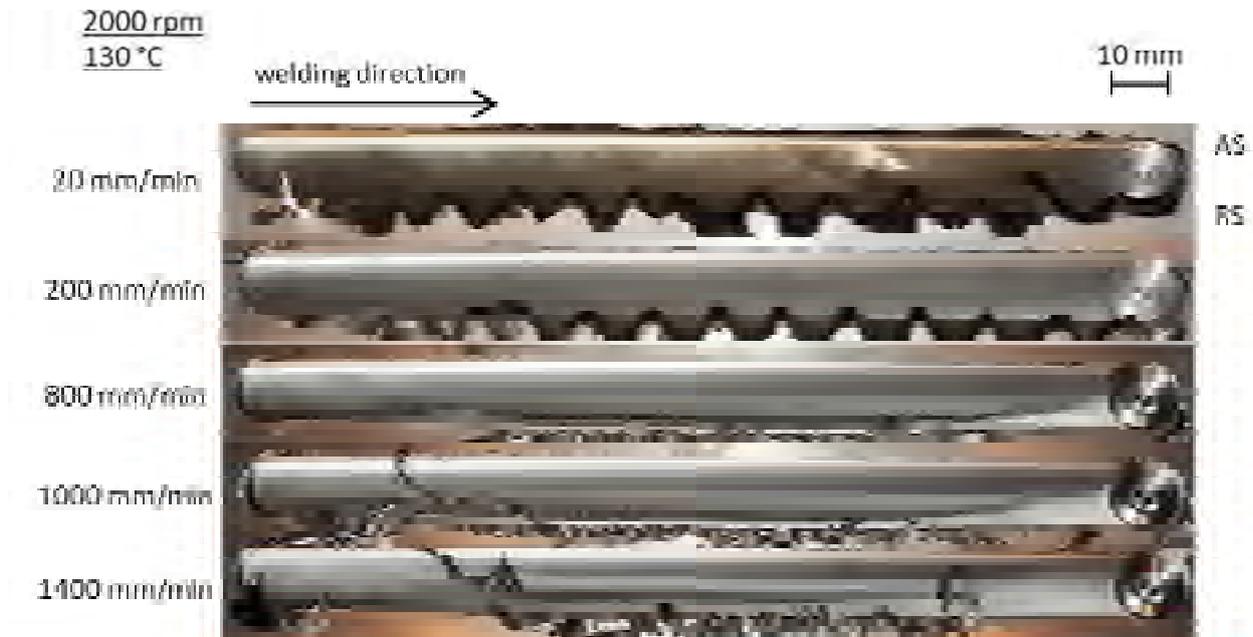


Figure 5.26: surface appearance of FSW of extruded Mg (bead on plate weld) for different welding speeds at constant rotational speed and a starting temperature of  $130 \text{ }^\circ\text{C}$ .

### Process loads

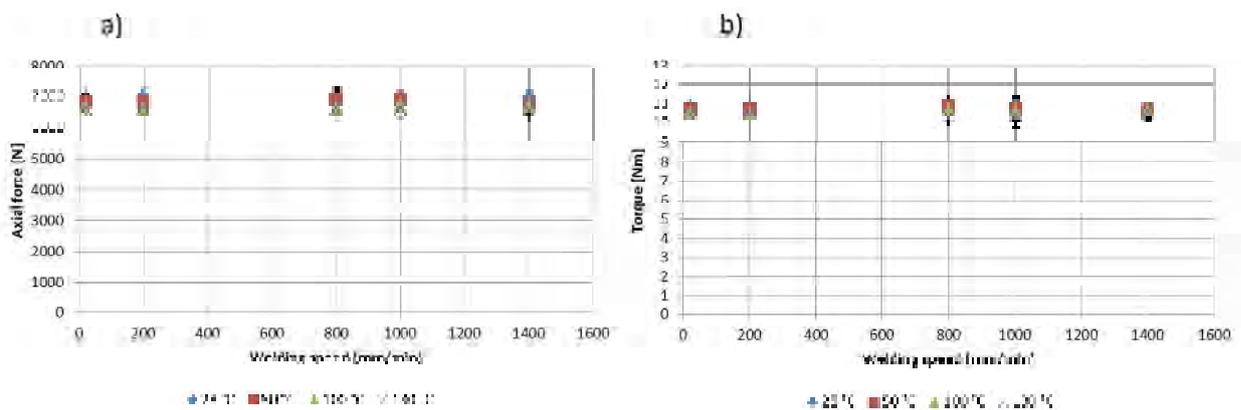


Figure 5.27: comparison of measured forces and torques for FSW of extruded AZ31 (bead on plate weld) at constant rotational speed: a) axial force as function of welding speed; b) torque as function of welding speed. (plunging phase)

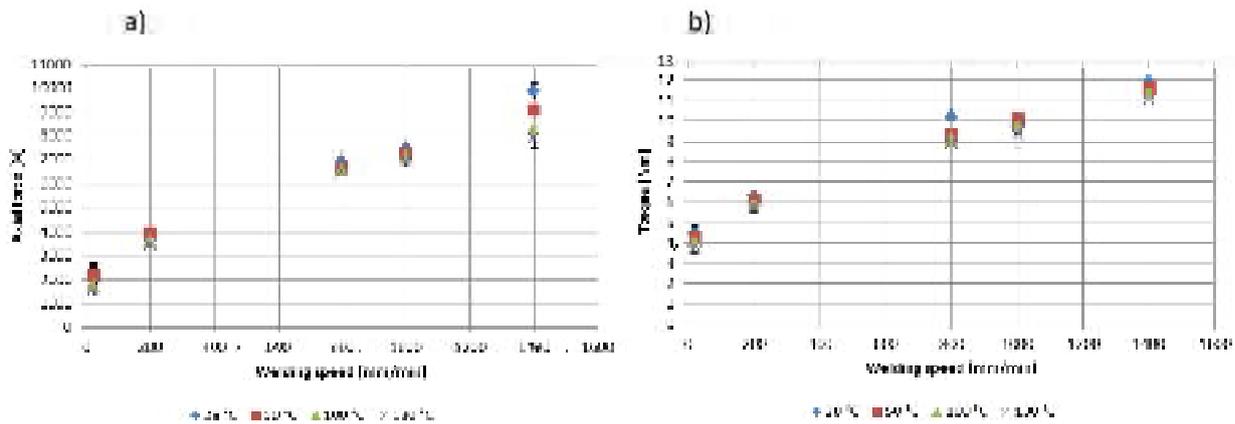


Figure 5.28: comparison of measured forces and torques for FSW of extruded AZ31 (bead on plate weld) at constant rotational speed: a) axial force as function of welding speed; b) torque as function of welding speed. (welding phase)

A beneficial effect on process force and torque is caused by the higher starting temperature. The measured loads are presented in figure 5.27 and 5.28. In general, it can be concluded that raising the welding speed results in higher force and torque during welding phase (figure 5.28). Similar load levels are received for  $f = 800$  and  $1000$  mm/min.

During plunging phase (figure 5.27), an average force of  $6893,1$  N and an average torque of  $10,83$  Nm are obtained for the welds made at  $28$  °C starting temperature. These values could be reduced by  $4,5$  % (force) and  $4,1$  % (torque) due to preheating.

As expected, the largest reduction of process loads is obtained for a starting temperature of  $130$  °C. Concerning force during welding phase (figure 5.28 a), the force for  $f = 20$  mm/min decreased by about  $30,8$  %. Diminishment of  $12,7$ ;  $6,25$ ;  $8$ ; and  $20$  % were achieved for  $f = 200$ ;  $800$ ;  $1000$  and  $1400$  mm/min, respectively. The results for torque during welding phase, shown in figure 5.28 (b), are also beneficial.  $17,7$  % lower torque for a welding speed of  $20$  mm/min,  $9,9$  % for  $200$  mm/min,  $13$  % for  $800$  mm/min,  $4$ % for  $1000$  mm/min and  $7,3$  % for  $1400$  mm/min are reached.

Heating element: butt weld

The previous conclusions are now used to limit the experimental extend for FSW of extruded magnesium alloy AZ31 in butt weld configuration. Besides the relation of initial temperature and process loads, this part focuses on the occurred temperatures as well as tensile properties and metallographic analysis. The results gained are compared to those of conventional FSW.

## Experimental settings

From the previous study it is noted that the lowest process loads are obtained at the highest tested temperature, whereby the following welds were made at a starting temperature of 130 °C in backing plate. The other settings are identical to those of the conventional FSW (see 5.1). Thereby, a comparison of loads and tensile properties can be done.

Table 5.6: experimental settings for FSW of extruded AZ31 with heating element in butt weld configuration.

| Form of weld                                  | Butt weld     |     |      |      |
|---|---------------|-----|------|------|
| Material                                      | Extruded AZ31 |     |      |      |
| Rotational speed<br>[rpm]                     | 2000          |     |      |      |
| Welding speed<br>[mm/min]                     | 20            | 200 | 1000 | 1400 |
| Starting temperature in backing plate<br>[°C] | 130           |     |      |      |
| Number of experiments                         | 3             |     |      |      |
| Plunging depth<br>[mm]                        | 0,2           |     |      |      |
| Plunging speed<br>[mm/min]                    | 100           |     |      |      |
| Dwell time<br>[s]                             | 5             |     |      |      |
| Tool tilt angle<br>[°]                        | 2             |     |      |      |
| Weld length<br>[mm]                           | 130           |     |      |      |
| Welding tool                                  | Tool 1        |     |      |      |

## Surface appearance

As expected, the surface appearance of the joints is similar to the previous investigations as demonstrated in figure 5.29. Sound welds are produced for all parameter settings, excepted for a welding speed of 200 mm/min. During the welding phase a surface lack of fill defect is recognizable on the advancing side. This defect can be ascribed to an inadequate material flow across the weld surface and a lack of pressure. /Arb13/

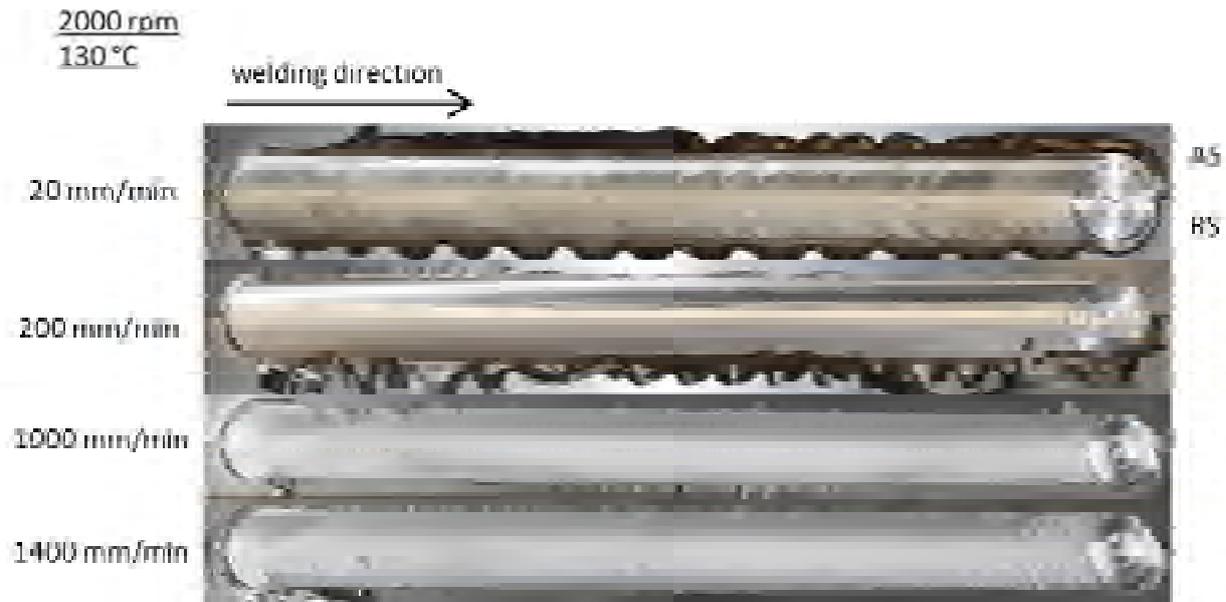


Figure 5.29: surface appearance of FSW of extruded AZ31 for different welding speeds at constant rotational speed and initial temperature of 130 °C.

Due to low welding speed and the additional inserting heat, joints welded at  $f = 20 \text{ mm/min}$  and  $200 \text{ mm/min}$  exhibit a high welding burr. Moreover, the previously described observation of adhesion of the welded joint on the backing plate could also be noted. Up to a welding speed of  $1400 \text{ mm/min}$  the surfaces are smooth. The low heat input results in a rougher surface for high welding speeds.

In comparison to FSW at  $28 \text{ °C}$  initial temperature, there are variations in surface appearances for higher welding speeds. A smoothing of the surface can be seen without generation of welding burr.

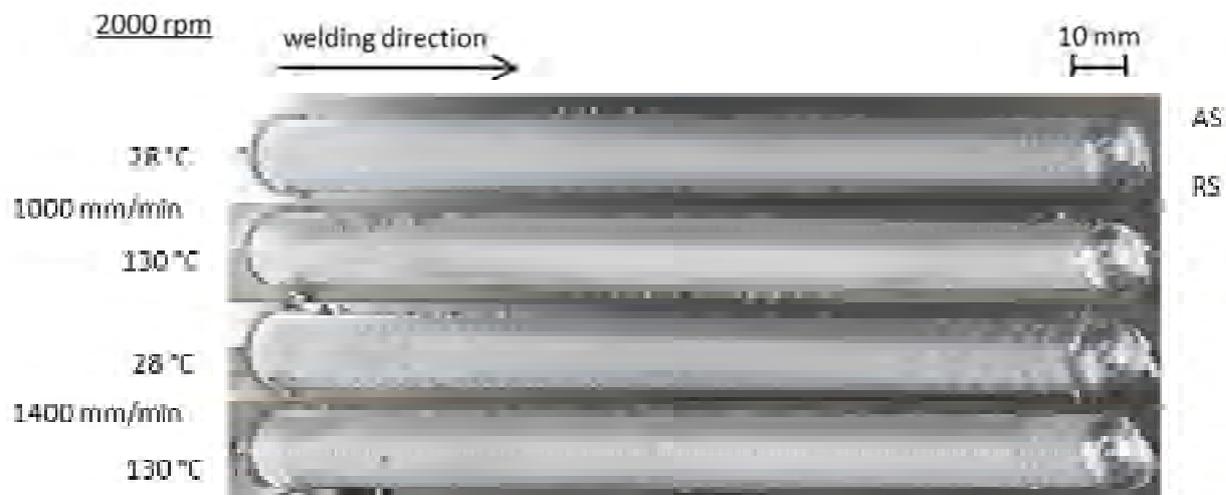


Figure 5.30: comparison of surface appearance of FSW of extruded AZ31 for different welding speeds and initial temperatures at constant rotational speed.

## Process temperatures

The temperature progressions for the welding at elevated starting temperature are presented in figure 5.31 for a welding speed of 20 mm/min (a) and 1400 mm/min (b). Additionally, the measured temperatures of FSW at 28 °C initial temperature are charted, too. This enables a comparison of both processes. For a low welding speed, the temperatures increase up to the middle of the weld. Subsequently the appearing heat is reduced up to the end of the weld. The higher initial temperature exhibits a slight higher level of process temperatures (average of 55 °C for all measurement point). In case of  $f = 1400$  mm/min, the progressions are relative similar and characterized by diminished temperatures up to the end of weld. Thereby, the average variation is about 101 °C between the processes.

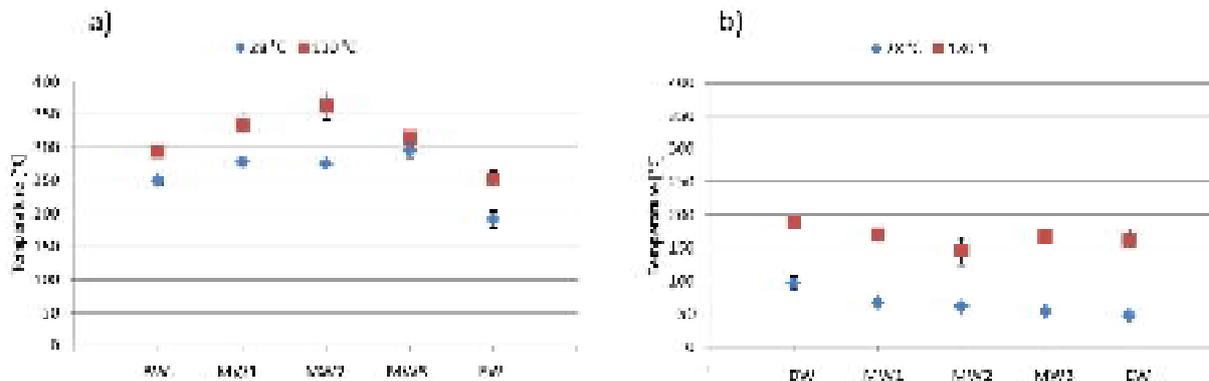


Figure 5.31: comparison of occurring temperature during FSW of extruded AZ31 for different initial temperatures at constant rotational speed for welding speeds of a) 20 mm/min and b) 1400 mm/min. BW- beginning of weld; MW- middle of weld; EW- end of weld

## Process loads

The comparison of process loads (during plunging phase) for FSW of extruded AZ31 at different initial temperatures is presented in figure 5.32. Regarding to axial force subject to welding speed, figure 5.32 (a) shows that a relative constant level is reached independent of speed. Furthermore, an effect of the temperature is not visible. The average axial force for FSW at 28 °C is about 6858 N. In comparison, a starting temperature of 130 °C causes about 150 N less in average. This corresponds only 2,1 %. The effect concerning torque (figure 5.32 b) is even small (about 1 %).

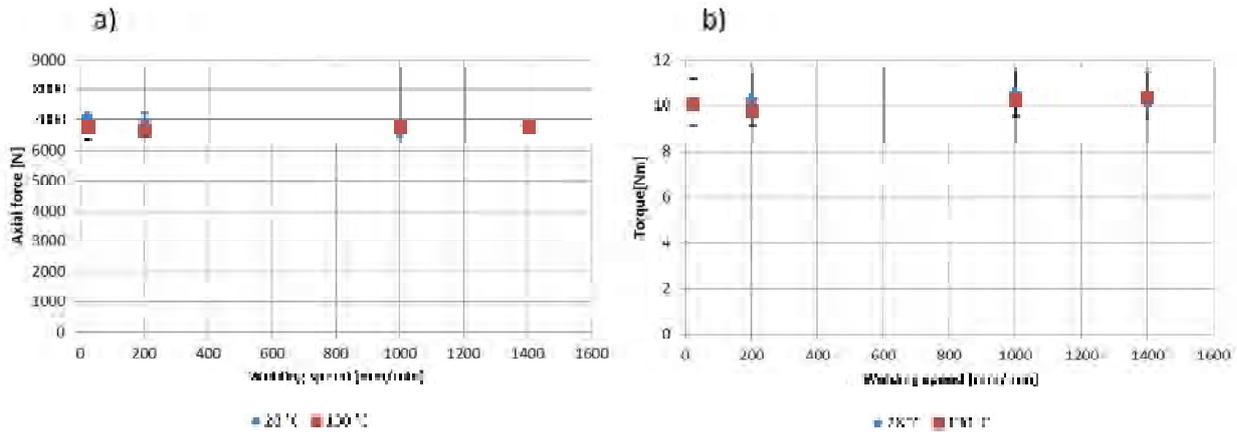


Figure 5.32: comparison of measured forces and torques for FSW of extruded AZ31 at constant rotational speed: a) axial force as function of welding speed; b) torque as function of welding speed. (plunging phase)

The analysis of the loads during welding phase shows an effect of the temperature over all welding speeds. As presented in figure 5.33 (a), the axial force could be reduced from 2033 N to 1533 N for a welding speed of 20 mm/min. This corresponds a decline of 24,5 %. Compared to LAFSW (11,4 %), the effect is higher. For  $f = 200$ ; 1000 and 1400 mm/min, it could be achieved a reduction of axial force by 20,9; 8,25 and 13,4 %, respectively. In case of LAFSW, the decline of forces was higher with 25,5 % for  $f = 200$  mm/min, 12,6 % for  $f = 1000$  mm/min and 14,6 % for 1400 mm/min. Overall, the level of average force reduction is with 17,7 % almost identical to LAFSW (16 %).

Figure 5.33 (b) gives an overview of the process torque as function of welding speed for 28 °C and 130 °C initial temperature. However, the effect of temperature is slight. The highest difference is achieved by a welding speed of 20 mm/min. The torque could be reduced by 17,6 %. By increasing welding speed, the effect diminishes. For  $f = 200$  mm/min, a decline of 9,5 % is reached. In case of welding speeds of 1000 and 1400 mm/min, the torque is reduced by 6,4 and 6,1 %, respectively. The determined values correspond 9,9 % average torque diminish. In case of LAFSW, the torque reduction was remarkable higher for each parameter set (average 25,9 %). The loads were reduced by over 20 % for every welding speed.



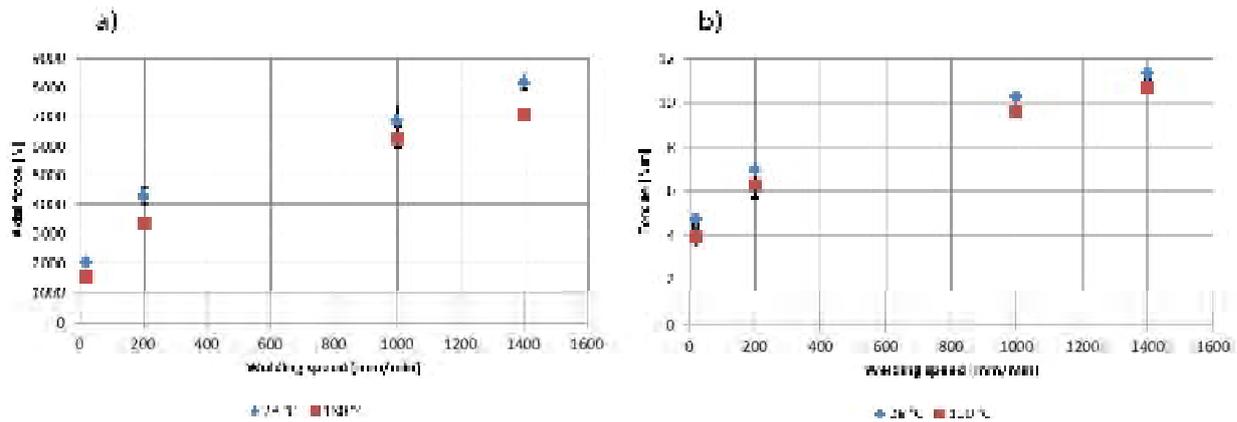


Figure 5.33: comparison of measured forces and torques for FSW of extruded AZ31 at constant rotational speed:  
a) axial force as function of welding speed; b) torque as function of welding speed. (welding phase)

### Tensile tests

A summarize of tensile properties on different factors is given in figure 5.34 and 5.35. The tensile strength as function of the axial force for different welding speeds and initial temperatures is presented in figure 5.34 (a). It can be seen that the welds made under a higher starting temperature of 130 °C exhibit lower strength compared to the FSW at 28 °C. The highest value, in case of the preheated material, is 160,1 N/mm<sup>2</sup> (about 61,5 % of the base material). This is reached for  $f = 1000$  mm/min. The poorest strength is achieved by a welding speed of 200 mm/min. With 105,5 N/mm<sup>2</sup>, it corresponds to 40,5 % of the base material's strength. Moreover, it can be seen that the variation of this value is high. As mentioned before, the weld made at 200 mm/min exhibit a surface lack of fill defect in the middle of the weld. This results in very poor tensile strength in this area. In general, the values for higher forces (welding speeds) are higher than for a low level of force (welding speed). The same conclusion can be made regard to figure 5.34 (b). There, the tensile strength subject to torque is illustrated.

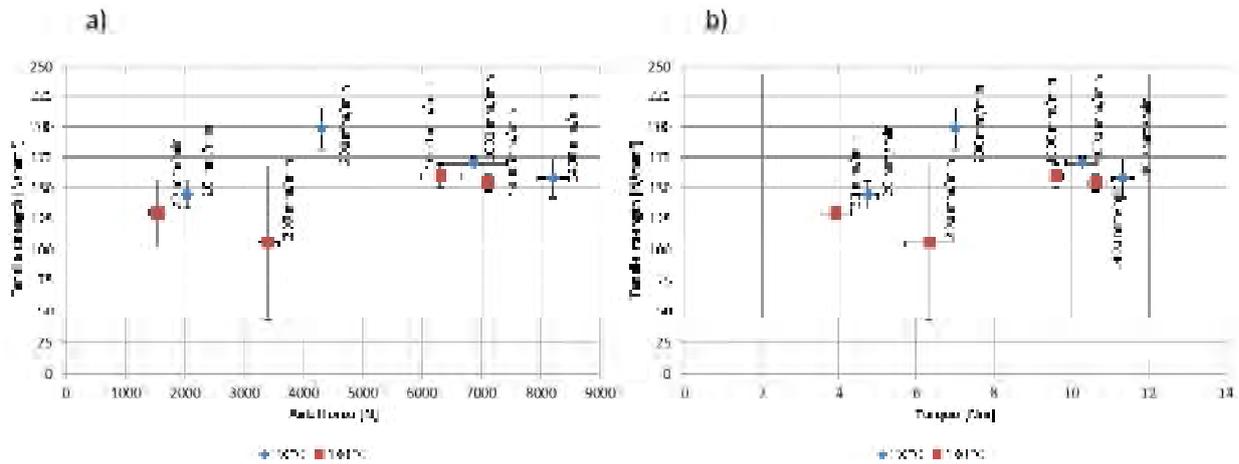


Figure 5.34: comparison of tensile strength for FSW of extruded AZ31 for different welding speeds and initial temperatures at constant rotational speed subject to: a) axial force; b) torque.

Concerning to figure 5.35 (a), the effect of preheating on fracture length can be seen. In case of  $f = 20$  and  $200$  mm/min, the higher temperature results in a lower fracture lengths. For welding speeds of  $1000$  and  $1400$  mm/min the values possess a similar level compared to FSW at  $28$  °C initial temperature.

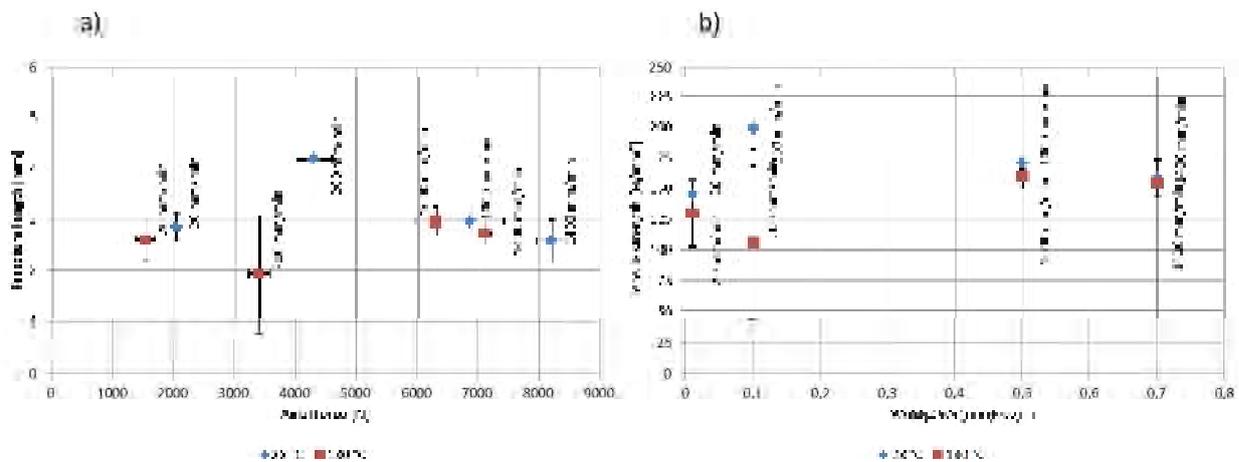


Figure 5.35: comparison of tensile properties for FSW of extruded AZ31 for different welding speeds and initial temperatures at constant rotational speeds: a) fracture length as function of axial force; b) tensile strength as function of weld pitch.

Due to the high strength reached by FSW at  $28$  °C and a welding speed of  $200$  mm/min, it can be assumed that a certain level of force and torque is required to produce strong joints. The reason could be an adequate heat input that is indicated by the weld pitch, which is shown in figure 5.36 (b).

The fracture appearance of the welds possesses shows identical properties to the previous results. In case of low speeds ( $20$  and  $200$  mm/min), the probes fracture on the advancing side.

For a welding speed of 1400 mm/min, the fracture position is located in the middle of the weld line.

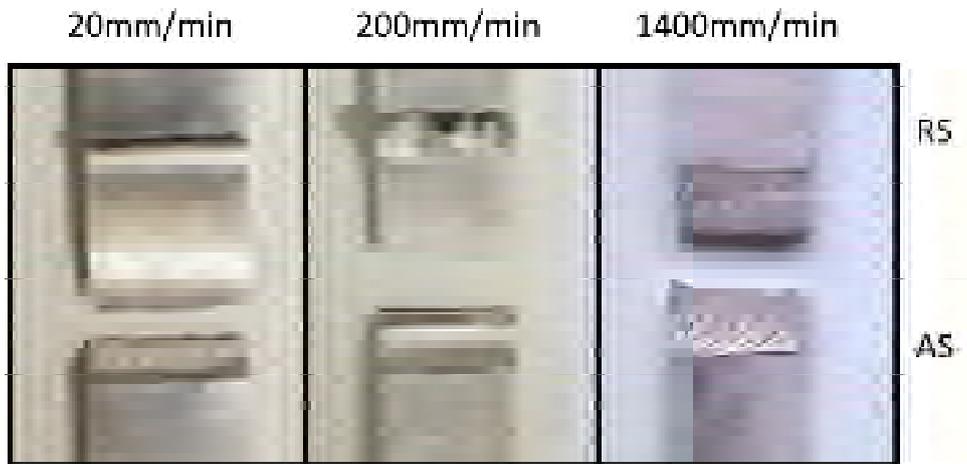


Figure 5.36: fracture appearance for FSW of extruded AZ31 for 20; 200 and 1400 mm/min at constant rotational speed and an initial temperature of 130 °C

### Metallographic analysis

Concerning to LAFSW, similar observations can be made by the metallographic analysis. For  $f = 20$  mm/min, the deeper plunging depth on the advancing side, caused by the excessive heat input, can be seen. At this point, the cross section is weak. Thereby, the fracture at this point is probable.

Analog to the results of LAFSW, the joints for  $f = 200$  mm/min exhibits a wormhole defect on the edge of stirring zone on the advancing side (figure 5.37). As mentioned before, this defect is caused by an inadequate material flow. As a result, the joint is weak and fracture at lower forces during tensile test.

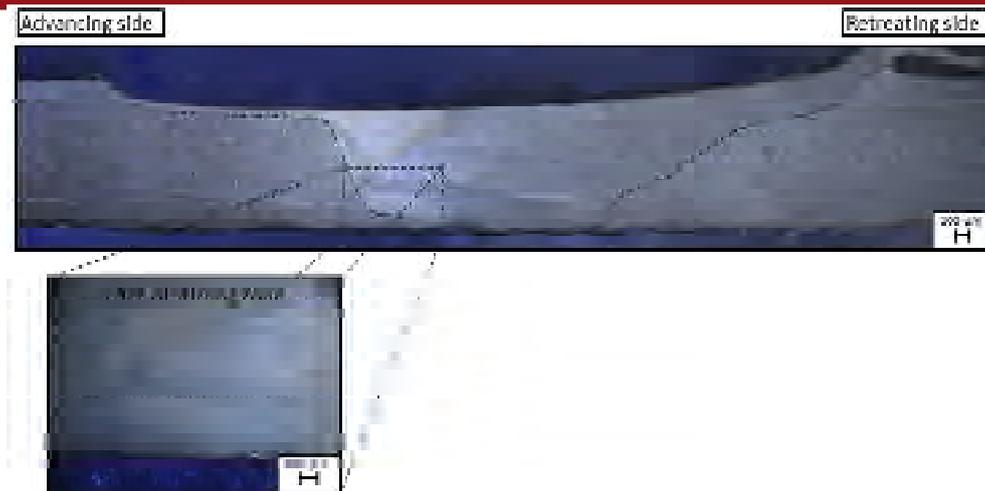


Figure 5.37: micrograph for FSW of extruded AZ31 for 200 mm/min at constant rotational speed and an initial temperature of 130 °C.

The analysis of welds made at a welding speed of 1400 mm/min (figure 5.38) addicted, that a lack of penetration defect appears with a length of about 367  $\mu\text{m}$ . The additional heat is not sufficient to adjust the high welding loads. As mentioned before, the deformation of the system could be a possible reason.

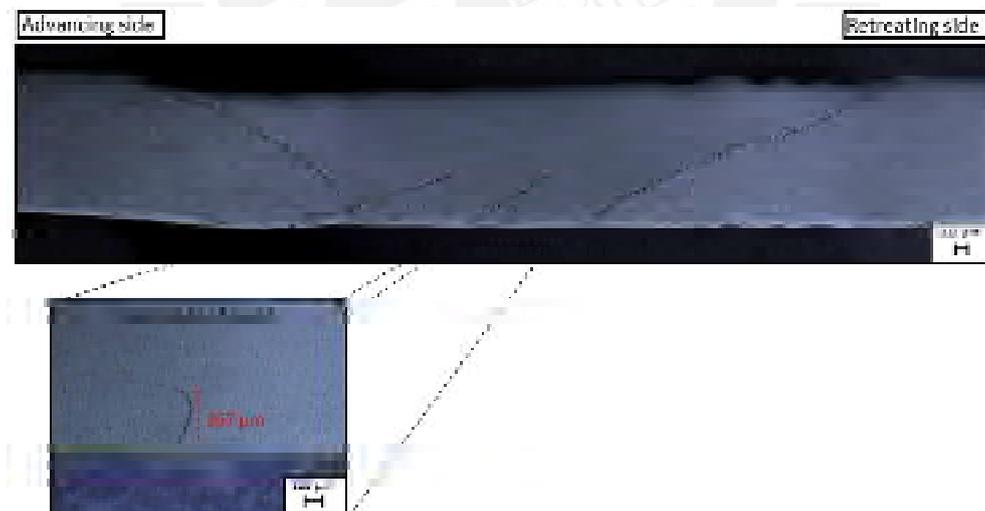


Figure 5.38: micrograph for FSW of extruded AZ31 for 1400 mm/min at constant rotational speed and an initial temperature of 130 °C.

The hardness profiles for FSW of extruded AZ31 at different initial temperatures and a welding speed of 200 mm/min are given in figure 5.39. The comparison shows that the hardness is lower in case of preheated workpieces, which can be an additional reason for lower tensile strength. However, the measurement of the grain size in the stirring zone results in only few

differences of about 1  $\mu\text{m}$ . The peak values for both are located in the middle of the weld followed by values in both directions. The minimum hardnesses can be found on the advancing side, which is a possible explanation for the fracture position.

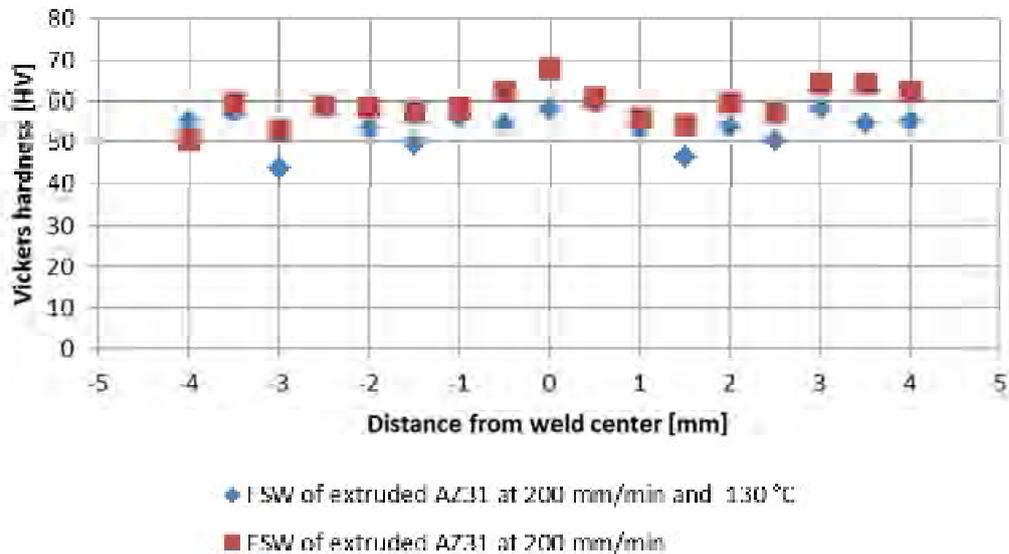


Figure 5.39: comparison of hardness profile for FSW of extruded AZ31 at different initial temperatures for 200 mm/min at constant rotational speed.

It can be concluded that preheating by a heating element leads to the reduction of process loads and improved surfaces. The materials are softer which results in a lower level of forces required for the plastic deformation. However, the effect on loads during plunging phase is less than for the welding phase. Moreover, the comparison with preheating by laser shows that the effect is remarkable lower in case of the torque. The differences could be explained by differences in the appearing temperatures by the preheating elements. Probably, these are higher for LAFSW due to the local heat input. At this point, the material is very soft whereby the coefficient of friction is low. As a result, the torque decrease.

Although the higher initial temperature leads to fewer loads, the received tensile tests indicate a worsening of tensile strength. In case of a welding speed of 200 mm/min, the joint exhibit defects on the surface as well as at the edge of the stirring zone. Furthermore, the comparison of hardness shows that preheating results in softer material. However, the differences in grain size in the stirring zone are low. The described defect also occurred during LAFSW for the same welding speed. For this reason a negative influence on the material flow by preheating can be assumed.

### FSW of rolled AZ31

The previous investigation of different initial temperatures of the joining members indicated a positive effect on the process loads during FSW of extruded AZ31 sheets with a thickness of 2,2 mm. The highest reduction of force and torque was caused by a starting temperature of 130 °C in backing plate. Indeed, the influence on loads during the welding phase was higher than for plunging phase. The metallographic analysis indicated the increased appearance of defects and differences in plunge depth for higher starting temperature. As a result inferior tensile properties were observable.

The aim of this chapter is to review the transferability of the results on the rolled magnesium alloy AZ31. The plates possess a thickness of 1,8 mm. The investigation includes the analysis of process temperatures, loads, surface appearance, tensile properties as well as micrographs.

For comparability, the experimental settings (table5.7) are mostly identical to those of the previous tests. Variations exist with regard to starting temperature and welding tool. Because of the positive effect of an initial temperature of 130 °C, it is assumed that a further increase of temperature can result in superior process loads. Thereby the tests are preceded for 27; 130 and 225 °C starting temperature in backing plate. For this purpose a more powerful heating element is used.

In comparison to the extruded magnesium alloy, the rolled AZ31 has a thickness of 1,8 mm. To prevent a contact of tool and backing plate, the used welding tool possesses a pin length of 1,5 mm. However, the generated heat should be sufficient to produce sound welds. This assumption is based on the fact that shoulder is mostly responsible for the heat generation.

Table 5.7: experimental settings for FSW of rolled AZ31 with heating element in butt weld configuration.

| Form of weld                                  | Butt weld   |     |      |      |
|---|-------------|-----|------|------|
| Material                                      | rolled AZ31 |     |      |      |
| Rotational speed<br>[rpm]                     | 2000        |     |      |      |
| Welding speed<br>[mm/min]                     | 20          | 200 | 1000 | 1400 |
| Starting temperature in backing plate<br>[°C] | 27          | 27  | 27   | 27   |
|   | 130         | 130 | 130  | 130  |
|   | 225         | 225 | 225  | 225  |
| Number of experiments                         | 3           |     |      |      |
| Plunging depth<br>[mm]                        | 0,2         |     |      |      |
| Plunging speed<br>[mm/min]                    | 100         |     |      |      |
| Dwell time<br>[s]                             | 5           |     |      |      |
| Tool tilt angle<br>[°]                        | 2           |     |      |      |
| Weld length<br>[mm]                           | 130         |     |      |      |
| Welding tool                                  | Tool 3      |     |      |      |

### Surface appearance

The results concerning surface appearance are presented in figure 5.40 up to figure 5.42. For a starting temperature of 27 °C (figure 5.40), the surfaces exhibit a similar condition to FSW of extruded AZ31. A high welding burr can be observed for  $f = 20$  mm/min. Indeed, the occurred excessive heat input leads to a surface galling defect on the weld surface (retreating side). Thereby the material under the tool shoulder is galled and teared which results in the present appearance. In addition, a root flow defect could be observed on the backside surface in the form of a chevron pattern. This is also caused by the excessive heat input during the process.

Due to an adequate heat input, joints made at a welding speed of 200 mm/min possess a smooth surface without any defects and a completely formed pinhole. As expected, the weld quality worsens by increasing welding speed. For  $f = 1000$  mm/min, the surface is smooth at

the beginning of the weld and is getting rougher from a certain point. The reason is the generation of a sufficient temperature level at the beginning of the weld due to the dwell time. Subsequently, the welding speed is too high to produce the required heat which causes the present defects. This effect is intensified in case of a welding speed of 1400 mm/min. The surface is extremely rough and teared from the start. During the welding phase, the magnesium adheres to the tool which leads to a defective pinhole at the end of weld.

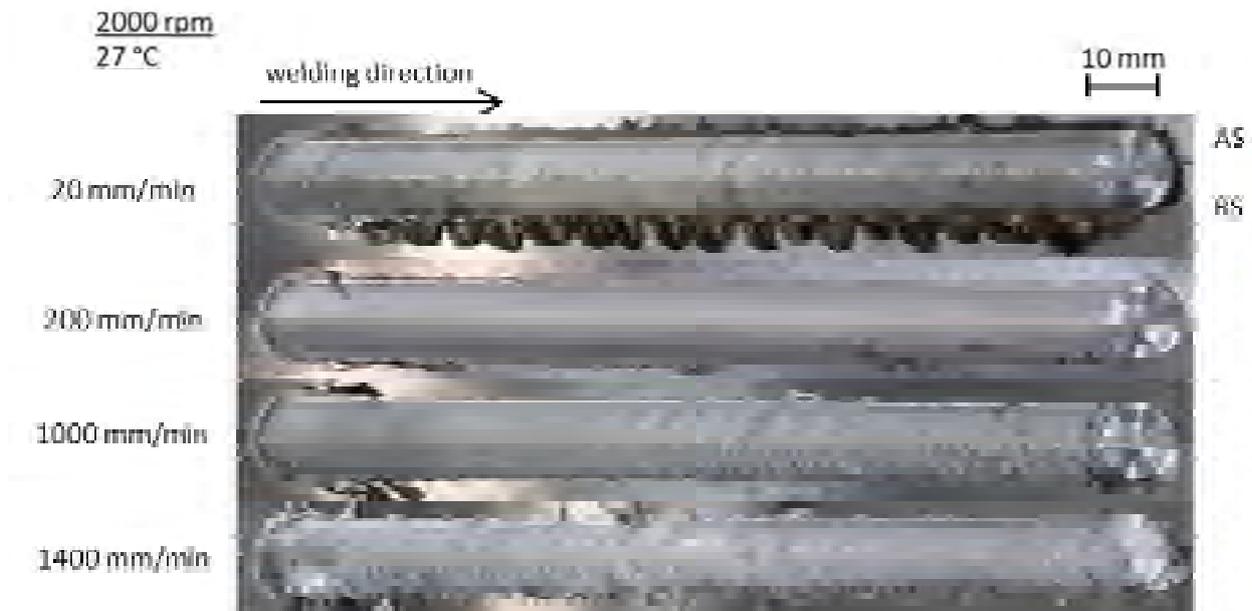


Figure 5.40: surface appearance of FSW of rolled AZ31 for different welding speeds at constant rotational speed and initial temperature of 27 °C.

The pictures in figure 5.41 illustrate the surface appearance for FSW of rolled AZ31 at the highest starting temperature of 225 °C. The higher temperature results in the formation of an accurate pinhole over all welding speeds. It can be seen that the surface galling defect also occurs for  $f = 200$  mm/min. Moreover, a high welding burr appeared which indicates the excessive heat input. A positive effect of the elevated temperature is considerable for higher speeds (1000 and 1400 mm/min). The surfaces are smooth and defect free from the beginning to the end of the weld.





### Process temperature

The analysis of the process temperatures show similarities to FSW of the 2,2 mm thick sheets. For a welding speed of 20 mm/min (figure 5.43 a), the measured temperatures increase at first, followed by decline (for all starting temperatures). The average difference of the measured values between 25° C and 225 °C starting temperature is about 78 °C. In comparison, a difference of about 149 °C is calculated for a welding speed of 1400 mm/min (figure 5.43 b). Independent of the initial temperature, the progression indicates a decreasing trend from the beginning to the end of the weld.

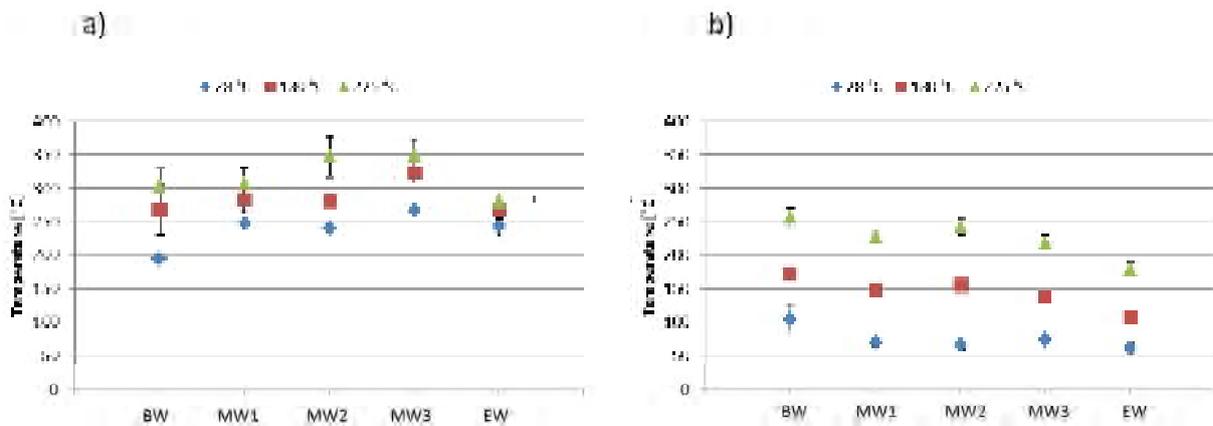


Figure 5.43: comparison of occurrence temperature during FSW of rolled AZ31 for different initial temperatures at constant rotational speed for welding speeds of a) 20 mm/min and b) 1400 mm/min. BW- beginning of weld; MW- middle of weld; EW- end of weld

### Process loads

The process loads for plunging and welding phase overall welding speeds and initial temperatures are summarized in figure 5.44 and 5.45. As expected, the greatest reduction is observed for an initial temperature of 225 °C. In case of plunging force and torque (figure 5.44), an average decrease of 4,3 % and 5,2 % is reached. Regarding the welding force (figure 5.45 a), a remarkable difference of 33,33 % could be achieved for  $f = 20$  mm/min. The corresponding torque (figure 5.45 b) was reduced by 22,4 %. Preheating of the workpieces enabled the decline of welding force for  $f = 200$  mm/min by 23,1 %, for  $f = 1000$  mm/min by 21,8 % and for  $f = 1400$  mm/min by 17,1 %. This means an average reduction of welding force of about 23,8 %. Regarding the welding torque, the values could be diminished by 27,7 %, 12,8 % and 4,8 % for the welding speeds 200 mm/min, 1000 mm/min and 1400 mm/min, respectively. This leads to mean 16,9 % less torque during welding phase.

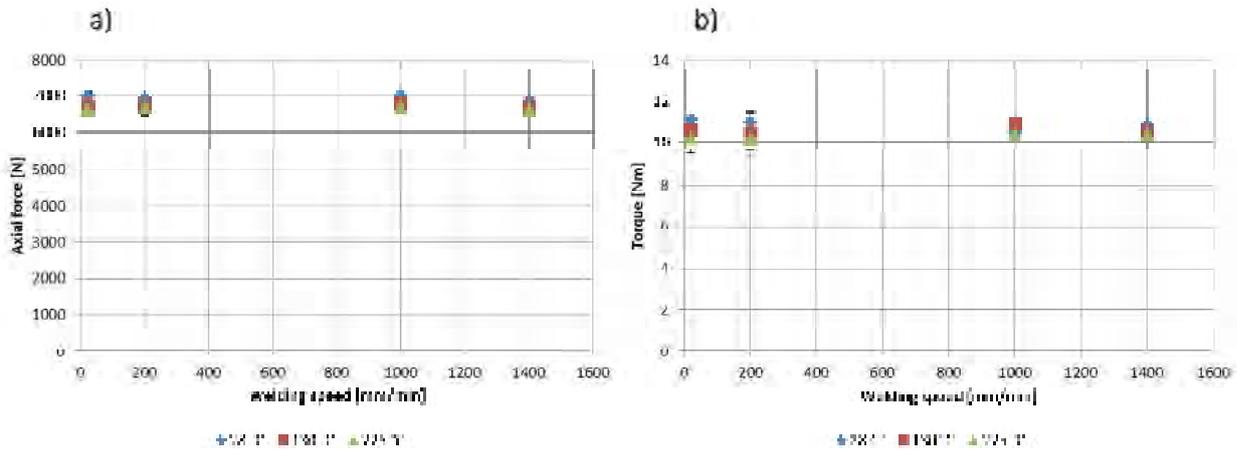


Figure 5.44: comparison of measured forces and torques for FSW of rolled AZ31 at constant rotational speed:  
 a) axial force as function of welding speed; b) torque as function of welding speed. (plunging phase)

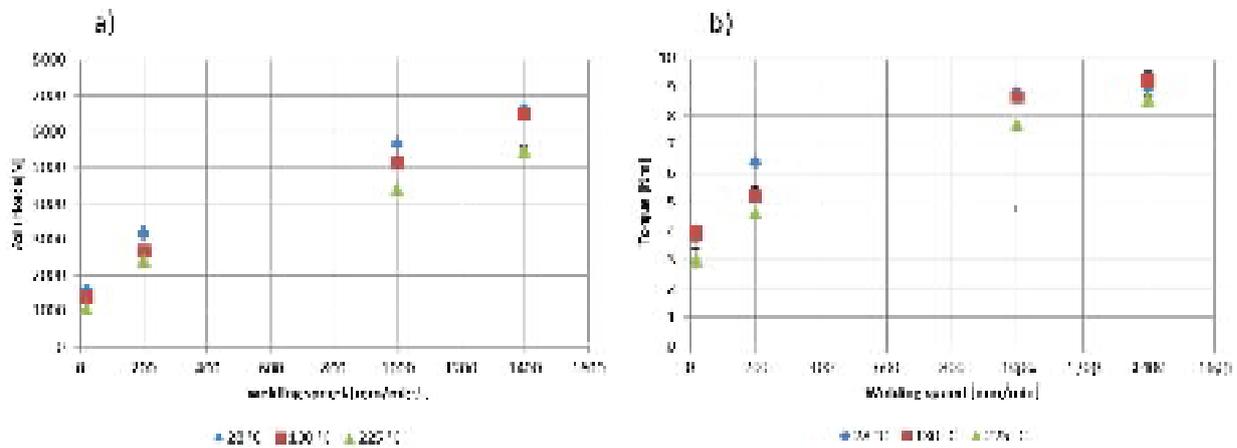


Figure 5.45: comparison of measured forces and torques for FSW of rolled AZ31 at constant rotational speed:  
 a) axial force as function of welding speed; b) torque as function of welding speed. (welding phase)

### Tensile tests

The results of the tensile tests are given in figure 5.46 and 5.47 and indicate analogies to the studies concerning the extruded AZ31. From figure 5.47 it can be seen that the highest tensile strength of 194,5 N/mm<sup>2</sup> (73,6 % of the base material) is reached by a welding speed of 200 mm/min and an initial temperature of 27 °C. The remaining values are less than 60 % of the base materials tensile strength, except the joints made at 130 °C and a welding speed of 200 mm/min. Under the condition of 225 °C initial temperature and  $f = 20$  mm/min, the weakest joint was produced (31,6 % of the base material). In general, it can be seen that the low welding speed results in low tensile strength. A relatively constant level of strength (between 52 % and 59 % of the base material), independent of the initial temperature and level of loads, is observable for the welding speeds of 1000 mm/min and 1400 mm/min. In contrast, the ob-

tained values for tensile strength vary significantly for low welding speeds. A tendency of decreasing strength by superior starting temperature can be noted.

The tensile strength as function of welding force (figure 5.46 a) respectively welding torque (figure 5.46 b), shows a clear correlation. Low process loads (about 1000 N and 3 Nm) result in poor values for tensile strength. A continuing rise of tensile strength is noticeable by increasing the welding force and welding torque up to a certain point. Subsequently, the joints become weaker. The optimum tensile strength is reached at a welding force of about 3200 N and a welding torque of about 6 Nm. Large deviations from this point lead to clearly lower values for tensile strength. When regarding the tensile strength as function of weld pitch (figure 5.47 b), it can be concluded that low values of about 0,1 mm/rev (“hot weld”) are indicators for high strength due to adequate heat input. Indeed, a weld pitch of 0,01 mm/rev indicates excessive heat input which causes a decreasing strength. Analog, a high weld pitch (“cold weld”) means an insufficient heat input and thereby lower tensile strength.

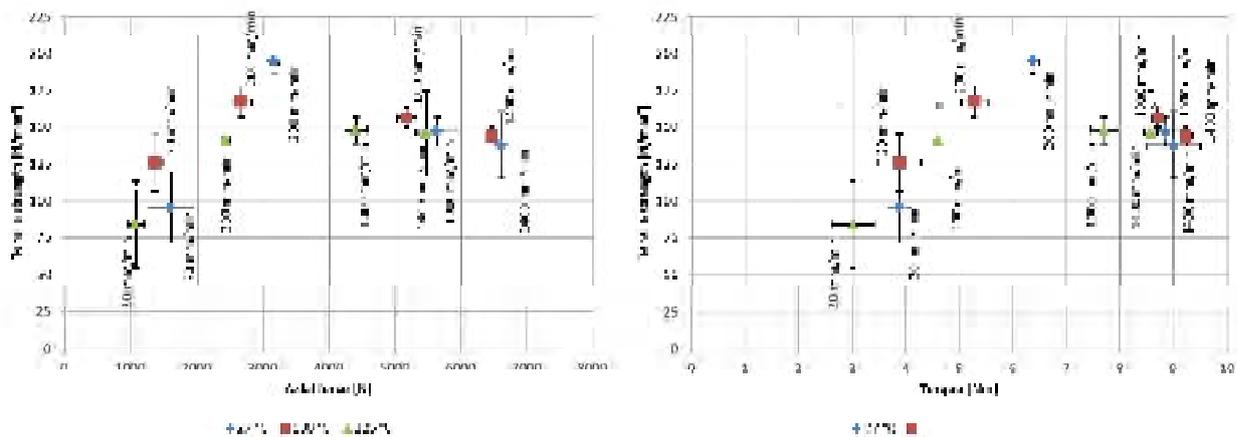


Figure 5.46: comparison of tensile strength for FSW of rolled AZ31 for different welding speeds and initial temperatures at constant rotational speed subject to: a) axial force; b) torque.

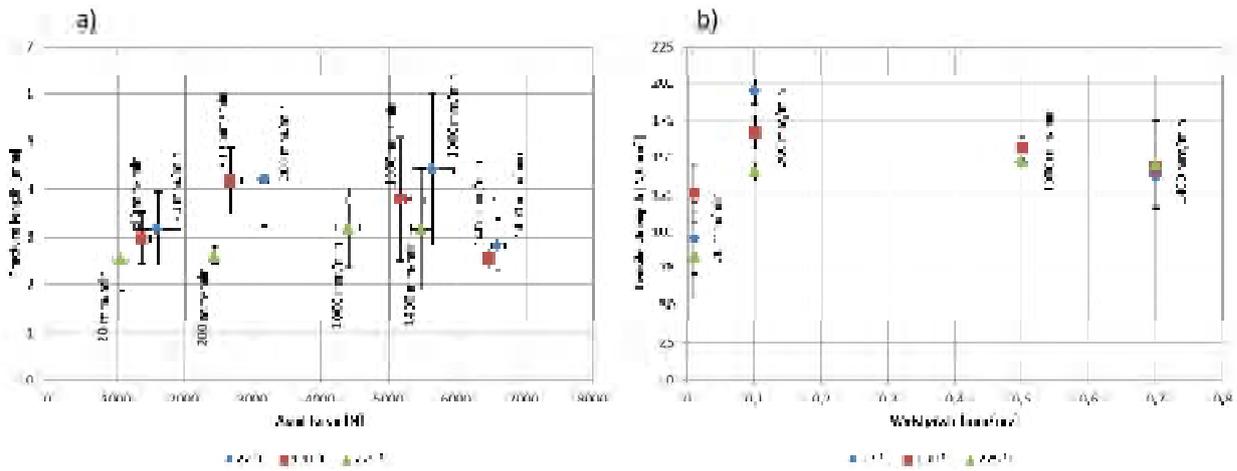


Figure 5.47: comparison of tensile properties for FSW of rolled AZ31 for different welding speeds and initial temperatures at constant rotational speed: a) fracture length as function of axial force; b) tensile strength as function of weld pitch.

Concerning fracture length (figure 5.47 b), preheating the workpieces mostly leads to lower values. In comparison to the base material, the highest fracture length is obtained by a welding speed of 1000 mm/min at 27 °C initial temperature and amount about 4,4 mm (48 % of base metal).

The analysis of the fracture position during tensile test exhibits the same results as for FSW of extruded AZ31. As shown in figure 5.48, the joints made at  $f = 20$  and 200 mm/min fracture on the advancing side. In contrast, the probes welded at higher speeds fracture in the middle of the weld. This behavior is observable over all initial temperatures.

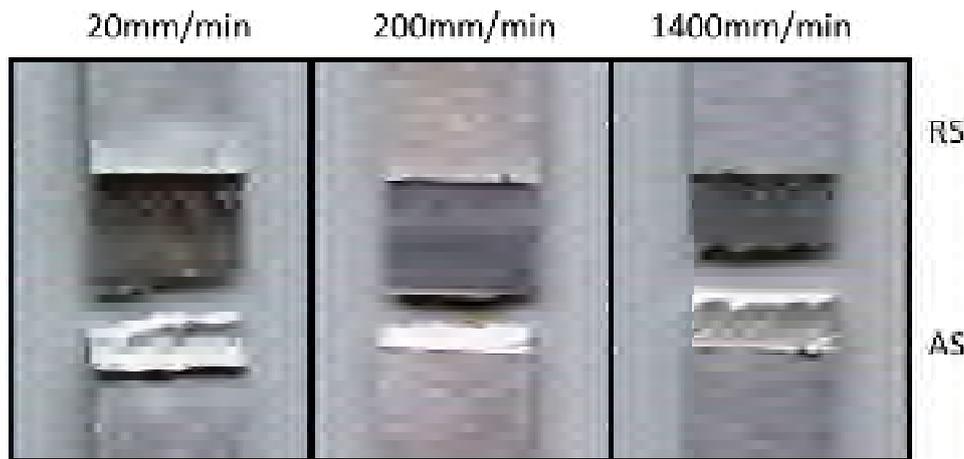


Figure 5.48: fracture appearance for FSW of rolled AZ31 for 20; 200 and 1400 mm/min at constant rotational speed.

## Metallographic analysis

The micrographs for FSW of rolled AZ31 for  $f = 20$ ; 200 and 1400 mm/min are presented in figure 5.49. Besides the surface galling defect on the retreating side of the weld, the reduced cross section caused by formation of welding burr is observable (a). Due to the low welding speed, the amount of generated heat is high. As a result, the material's yield stress decrease and it could be deformed plastically. Moreover, the soft material enables a deeper plunging of the tool. In case of the 1,8 mm thick sheets, this effect leads to excessive material flow at the root of the weld direct under the pin. The black bar at the bottom indicates contact of the pin with the backing plate.

The cross-section of a joint made at a welding speed of 200 mm/min is displayed in figure 5.49 (b). Indicated by the high surface quality and the high tensile properties, no defect is observable in the micrograph.

As mentioned before, a high welding speed results in low heat generation and an extremely rough and torn surface, which is recognizable in figure 5.49 (c). In addition, a decline of cross-section is caused that affect the tensile properties in a negative way.

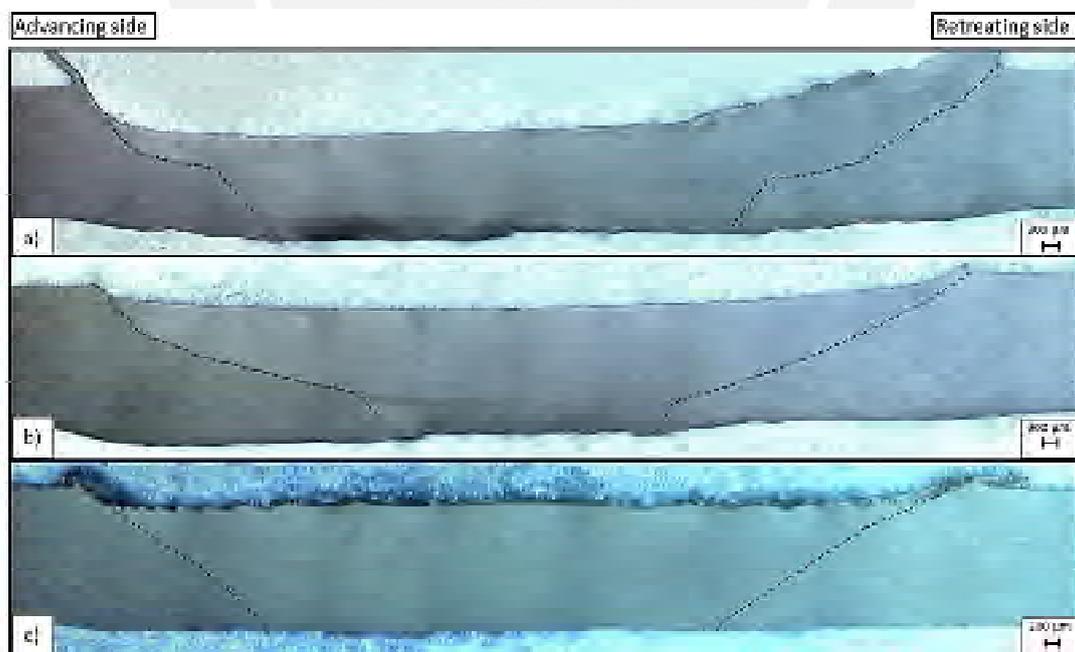


Figure 5.49: micrographs for FSW of rolled AZ31 at constant rotational speed for a) 20 mm/min; b) 200 mm/min and c) 1400 mm/min.

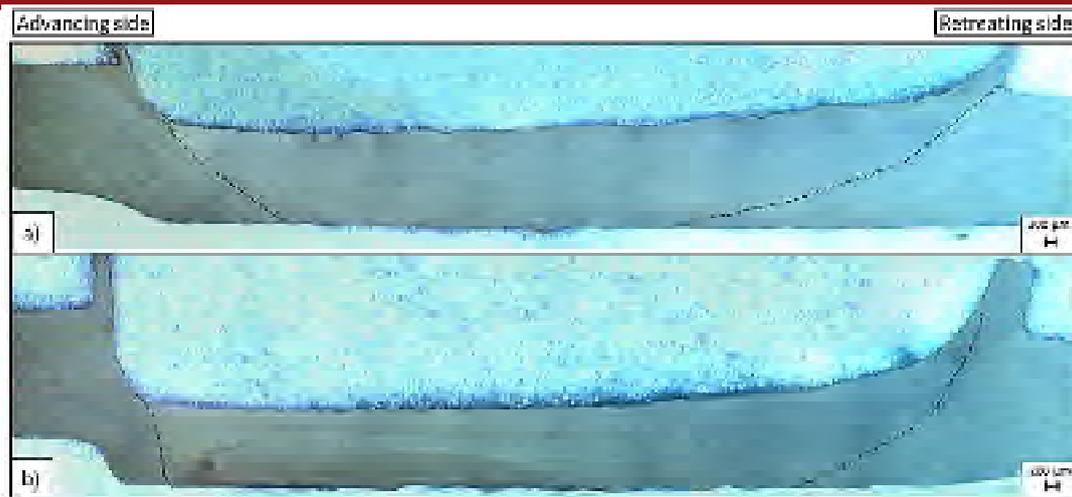


Figure 5.50: micrographs for FSW of rolled AZ31 at constant rotational speed for 20 mm/min and a) 130 °C and b) 225 °C.

Concerning tensile properties, the slightest influence of preheating was achieved for high welding speeds of 1000 and 1400 mm/min. In contrast, preheating up to 225 °C (in backing plate) strongly affect the tensile strength of welds made at  $f = 20$  and 200 mm/min in a negative way. A possible explanation is achieved by the micrographs, presented in figure 5.50. The cross-sections of FSW for 20 mm/min and 130 °C (a) as well as 225 °C (b) are shown. The increased initial temperature results in a softening of the material, whereby the tool is enabled to plunge deeper and to interact with the backing plate. As a result, the cross-section is significant reduced on the advancing side, which leads to inferior tensile properties. The same effect is observable for  $f = 200$  mm/min, but in a weakened form.

The results indicate the positive effect of preheating during FSW and confirm the results on the extruded AZ31. An initial temperature of 225 °C leads to significant lower process forces during the welding phase. However, the effect on torque is lower. The reduction of loads during the plunge phase is also comparable low. In contrast to previous tests, the joint 1,8 mm thick sheets possess no defects caused by welding at higher initial temperatures. Indeed, the material is strong soften, which enable a deeper plunging of the tool. This reduces the cross-section significant and as a result, the tensile properties are worse.

### FSW of dissimilar extruded AZ31/rolled AW6016

The previous chapters showed the positive effect of higher initial temperatures of the joint members on process loads during FSW of similar magnesium joints. In the following part, this effect should be investigated for FSW of dissimilar magnesium/ aluminum joints. The rolled aluminum alloy AW6016 and the extruded magnesium alloy AZ31 are used for the research.

### Parameter settings for FSW of extruded AZ31/rolled AW6016

From the literature it can be seen that FSW enables the successful joining of dissimilar magnesium/aluminum materials. Indeed, the range of parameter settings (rotational and welding speed) is rare. For this reason, the investigation on FSW of magnesium/aluminum dissimilar joints starts to compile useful parameter settings for the main experiments. The surface appearances as well as the tensile properties were analyzed.

The experimental settings for this study are presented in table 5.8. As mentioned in the state of the art the generated heat on the advancing side is larger than on the retreating side. Therefore it is useful to arrange the material with worse flow behavior, in this case magnesium, on the advancing side. The investigation of the used material showed that the yield stress is lower for AW6016 (figure 2.3). This indicates a lower level of required force to plasticize the material. Resulting from this fact, the flow behavior of the used aluminum alloy is superior.

For each rotational speed (800; 900; 1000; 1200 rpm), welds are made at different welding speeds (40; 100; 200; 300; 1000 mm/min). To produce statistically validated results, every parameter setting was investigated three times. Under a tool tilt angle of 2 °, the tool is plunged into the material with a speed of 100 mm/min. The adjusted plunge depth is 0,2 mm. The dwell time of 5 s was chosen to generate sufficient heat to prevent surface defect at the beginning of the weld.

Table 5.8: experimental settings for FSW of extruded AZ31/AW6016



| Arrangement of materials       | Advancing side: extruded AZ31 |      |      |      |
|--------------------------------|-------------------------------|------|------|------|
|                                | Retreating side: AW6016       |      |      |      |
| <b>Rotational speed [rpm]</b>  | 800                           | 900  | 1000 | 1200 |
| <b>Welding speed [mm/min]</b>  | 40                            | 40   | 40   | 40   |
|                                | 100                           | 100  | 100  | 100  |
|                                | 200                           | 200  | 200  | 200  |
|                                | (300)                         | 300  | 300  | 300  |
|                                | (1000)                        | 1000 | 1000 | 1000 |
| <b>Number of experiments</b>   | 3                             |      |      |      |
| <b>Plunging depth [mm]</b>     | 0,2                           |      |      |      |
| <b>Plunging speed [mm/min]</b> | 100                           |      |      |      |
| <b>Dwell time [s]</b>          | 5                             |      |      |      |
| <b>Tool tilt angle [°]</b>     | 2                             |      |      |      |
| <b>Weld length [mm]</b>        | 140                           |      |      |      |
| <b>Welding tool</b>            | Tool 1                        |      |      |      |

### Surface appearance

Regarding surface appearance, the best joints are received at a welding speed of 20 mm/min overall rotational speeds (figure 5.51). The joints are defect free and possess smooth surfaces with a complete pinhole at the end of the weld. It can be seen that with increasing rotational speed a welding burr occurs. Due to the higher rotational speed, the heat input increases intensely whereby the plasticized material is pushed to the edge of the weld and consolidate in the form of welding burr.



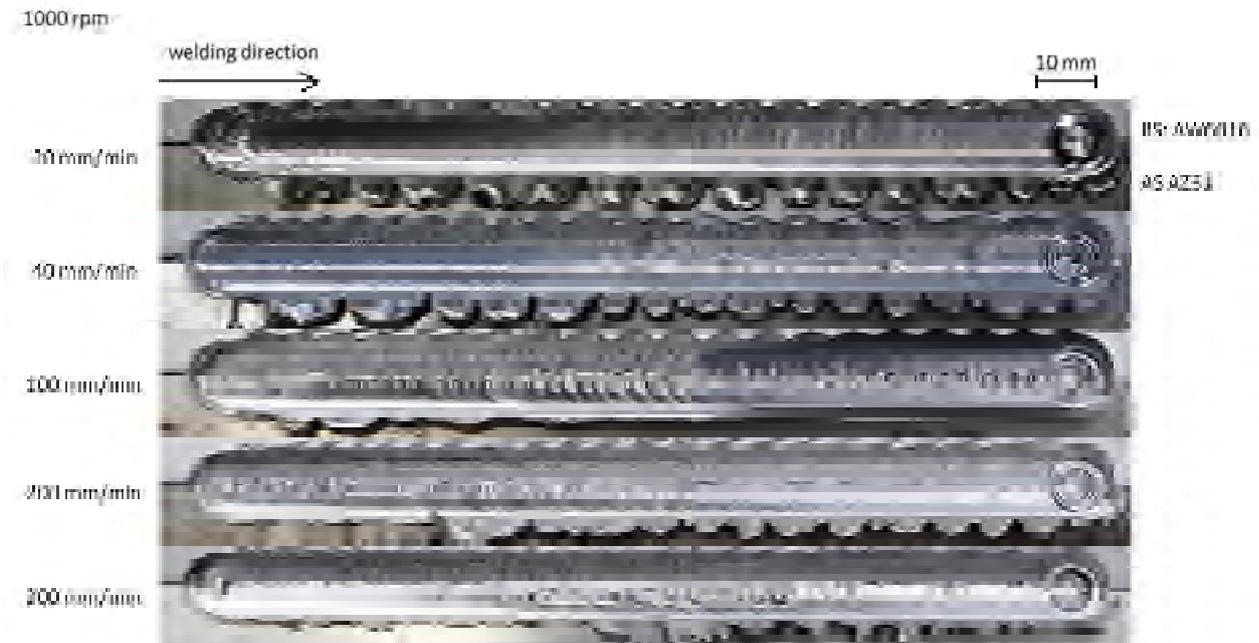


Figure 5.53: surface appearance for FSW of extruded AZ31/AW6016 for different welding speeds at a constant rotational speed of 1000 rpm.

For  $N = 1000$  rpm the results are shown in figure 5.53. As described before the excessive heat input at a welding speed of 20 mm/min causes welding burr. By raising the welding speed up to 300 mm/min, the welding burr diminishes due to less appearing temperature. Meanwhile the surface gets rougher and surface lack of fill defects appear which results in the weakening of the joint.

### Tensile tests

The tensile strength as function of rotational and welding speed is presented in figure 5.54. The evaluation of the obtained values is carried out by the comparison to the base material with the lowest tensile strength. With 209,7 N/mm<sup>2</sup> the aluminum alloy AW6016 possesses a lower strength than the extruded AZ31, whereby it serves as reference. For FSW of dissimilar magnesium/aluminum joints, the highest values are achieved by a rotational speed of 900 rpm independent of the welding speed, except for  $f = 20$  mm/min. With 141,4 N/mm<sup>2</sup> (about 67,4 % of base material) for  $f = 30$  mm/min and 140,5 N/mm<sup>2</sup> (about 67 % of base material) for  $f = 100$  mm/min, the joints at  $N = 900$  rpm provided the best results.

A tendency of decreasing tensile strength is observable for high rotational speeds (1000; 1200 rpm).  $N = 1200$  rpm exhibit a tensile strength of 138,1 N/mm<sup>2</sup> (about 65,8 % of the base material) for  $f = 40$  mm/min. By increasing the welding speed, the joints become weaker and

reach a minimum of 20,9 N/mm<sup>2</sup> for  $f = 300$  mm/min. In general, a low welding speed leads to higher values for tensile strength.

It must be noticed that the range of tensile strength varied strongly for each parameter set. The high dispersion indicates the instability of the process.

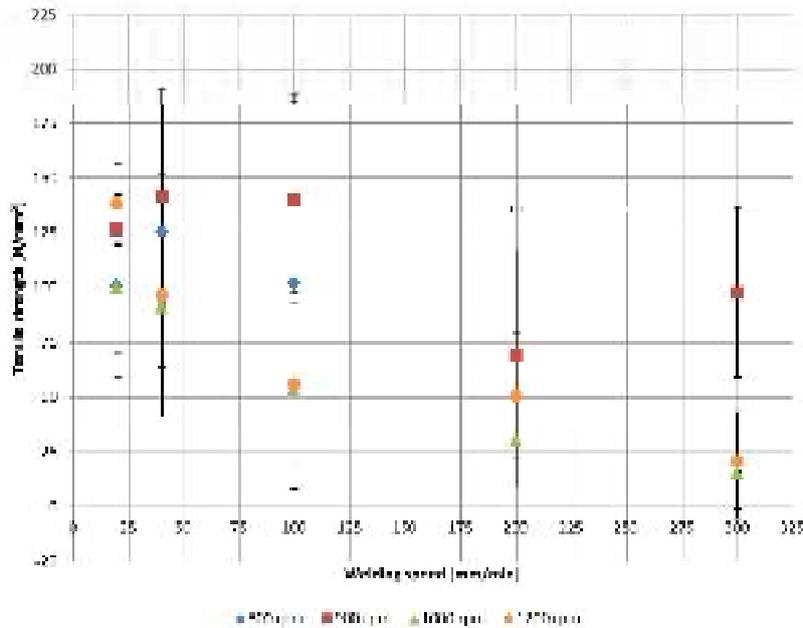


Figure 5.54: tensile strength for FSW of extruded AZ31/AW6016 subject to welding speeds and rotational speeds

The analysis of the fracture length (figure 5.55) exhibits a similar behavior. The best result is generated by  $N = 900$  rpm for a welding speed of 100 mm/min. The fracture length amounts 2,7 mm (17,4 % of base material). By increasing welding speed, a continuing decline of fracture length can be noted for a rotational speed of 1200 rpm. The other joints exhibit an improvement of values at first, followed by a remarkable decrease.

The high dispersion observed for the tensile strength also appears concerning fracture length.

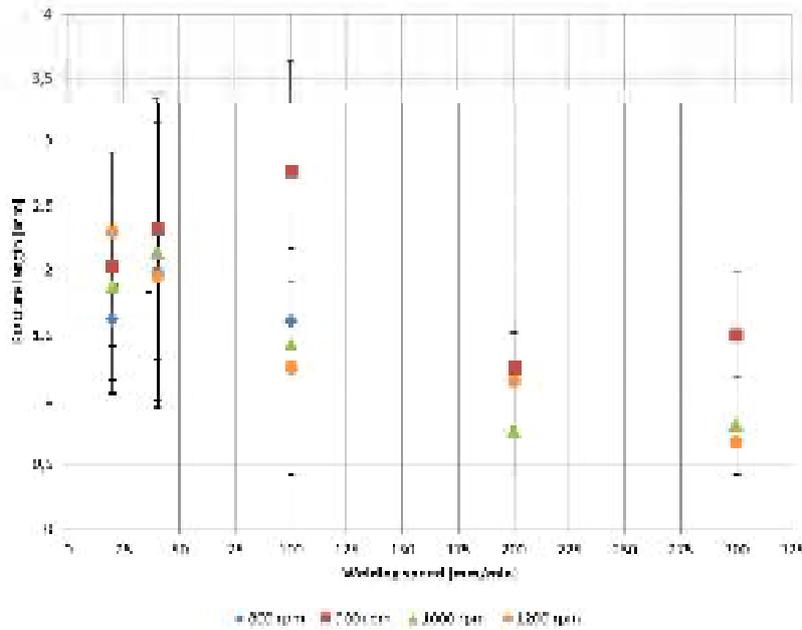


Figure 5.55: fracture length for FSW of extruded AZ31/AW6016 subject to welding speed and rotational speed

A statement about the condition of the produced welds can be made by the analysis of the weld pitch as shown in figure 5.56. The best results in regard to tensile strength are obtained for a low weld pitch which indicates an adequate heat input. An increasing relation of welding speed and rotational speed leads to significant values. As a result, an insufficient generation of heat can be assumed.

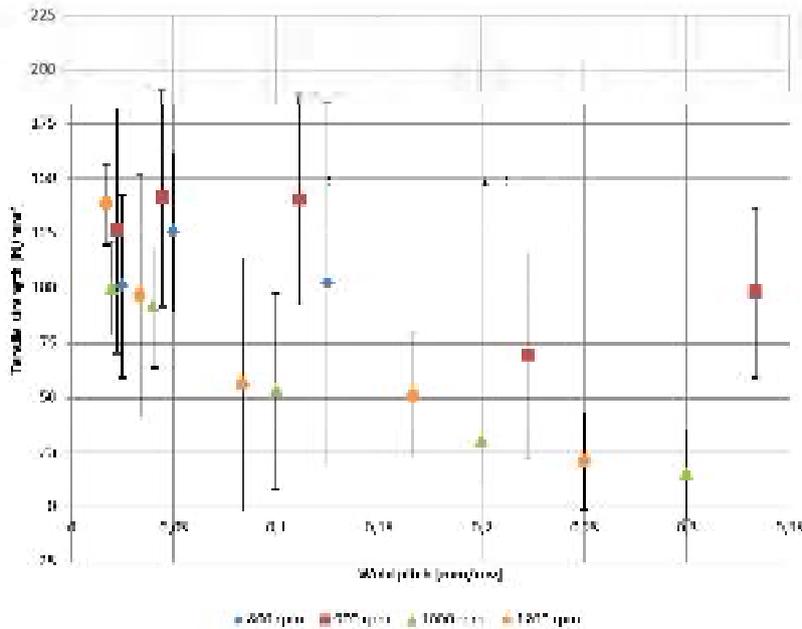


Figure 5.56: tensile strength for FSW of extruded AZ31/AW6016 subject to weld pitch and rotational speeds

In conclusion, joints welded at a rotational speed of 900 rpm received the best results. This setting exhibits over all welding speeds the highest tensile strengths compared to the other test settings. In consideration of the weld pitch, it is indicated that lower welding speeds result in higher strength due to adequate heat input.

#### Heating element: for FSW of Mg/Al

The joining of dissimilar materials represents a crucial point in industrial applications. As described in the state of the art, FSW is capable of achieving this task. However, the high process loads require low welding speeds. By increasing the initial temperature of the workpieces, the forces should be reduced. Due to this, the following part contains tests to review the influence of higher initial temperature on process loads during FSW of magnesium/aluminum dissimilar joints.

#### **Experimental settings**

The experimental settings are presented in table 5.9. As mentioned before, the magnesium alloy is arranged on the advancing side because of poorer flow behavior. Due to the previous tests, a constant rotational speed of 900 rpm is chosen. Five different welding speeds - 40; 100; 200; 300 and 1000 mm/min - are tested. Because of comparability, the settings regarding plunge depth and speed, dwell time, tool tilt angle as well as the welding tool is identical to the previous investigation. The focus of the presented master thesis is on FSW of magnesium similar joints. For this reason the tests concerning dissimilar magnesium/aluminum joints are made once for each parameter setting.

Table 5.9: experimental settings for FSW of extruded AZ31/AW6016 with heating element.

| Arrangement of materials                      | Advancing side: extruded AZ31 |     |     |     |      |
|---|-------------------------------|-----|-----|-----|------|
|   | Retreating side: AW6016       |     |     |     |      |
| Rotational speed<br>[rpm]                     | 900                           |     |     |     |      |
| Welding speed<br>[mm/min]                     | 40                            | 100 | 200 | 300 | 1000 |
| Starting temperature in backing plate<br>[°C] | 22                            | 22  | 22  | 22  | 22   |
| Number of experiments                         | 1                             |     |     |     |      |
| Plunging depth<br>[mm]                        | 0,2                           |     |     |     |      |
| Plunging speed<br>[mm/min]                    | 100                           |     |     |     |      |
| Dwell time<br>[s]                             | 5                             |     |     |     |      |
| Tool tilt angle<br>[°]                        | 2                             |     |     |     |      |
| Weld length<br>[mm]                           | 130                           |     |     |     |      |
| Welding tool                                  | Tool 1                        |     |     |     |      |

### Surface appearance

The surface appearances of the produced joints at 22 °C initial temperature are summarized in figure 5.57. The correspondent welds for 130 °C are shown in figure 5.58.

For  $f = 40$  and  $100$  mm/min at 22 °C starting temperature (figure 5.57), the welds possess a crack at the beginning of the weld caused by insufficient heat generation. Afterwards, the surface is rough, but defect free with the formation of a complete pinhole at the end of the weld. Because of the low speeds, the formation of welding burr on the advancing side is visible. In case of a welding speed of  $200$  mm/min, a slight surface crack is observable at the beginning of the weld. Due to the higher speed, the generated heat is lower and the material is not completely plasticized. It starts to adhere below the tool shoulder and cause a rough welding surface. Besides, the pinhole is not completely formed. By increasing the welding speed up to  $300$  mm/min, the crack appeared at the beginning of the weld gets longer. This indicates a further reduction of generated heat. Due to the adhesive behavior of the material, the surface

is torn up to the end of the weld. The joints made under the condition of  $f = 1000$  mm/min, the process results in a weak bonding between the joining members. The material's plasticization is insufficient due to the low amount of generated heat. As a result, a continuous crack along the weld line is observable.

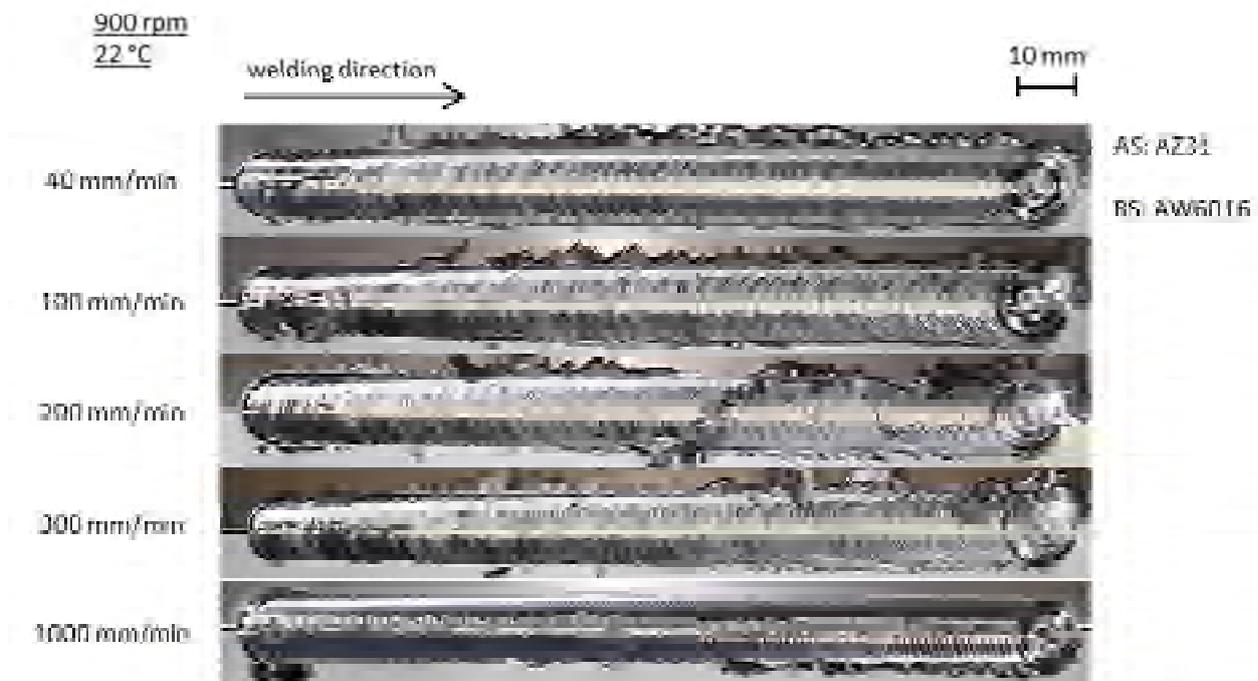


Figure 5.57: surface appearance for FSW of extruded AZ31/AW6016 for different welding speeds at a constant rotational speed of 900 rpm and 22 °C.

The comparison of the weld surfaces with those of an initial temperature of 130 °C (figure 5.58) shows, that the observed cracks at the beginning of the weld are avoided. In case of a welding speed of 40 mm/min, the joint is defect free but exhibits high welding burr on the advancing and retreating side. A defect free joint up to the middle of the weld is obtained for  $f = 100$  mm/min. Afterwards a crack in the center line arises. Similar effects are observable for  $f = 200$  and 300 mm/min. In regard to the remarkable higher initial temperature, the reason for the defective weld could be the difference in thermal conductivity of the materials. The aluminum conducts the heat much faster than magnesium, which indicates a problem in case of high welding speeds and elevated initial temperatures. When the tool moves along the weld line, the material is plasticized by the generated heat. Due to preheating, the temperature is already much higher than in case of FSW at 22 °C. The mixed material begins to cool when the tool is moving away. In this case, the aluminum's temperature is faster on a lower level which means the consolidation of the material, whereby it contracts. Meanwhile, the magne-



sium is still plasticized. As a result the bonding between both materials is weak and cracks occur. This effect is especially visible during FSW with high welding speeds and high initial temperatures, because a larger temperature gradient between the materials is possible. In case of low speeds, the cooling rate is slower because of the slower tool motion, whereby the temperature gradient between the joining members is smaller.

In case of significant higher welding speeds (1000 mm/min), the additional provided temperature is not sufficient to enable the plasticization of the material by the tool. The consequence is continuous crack along the weld line that results in a poor bonding.

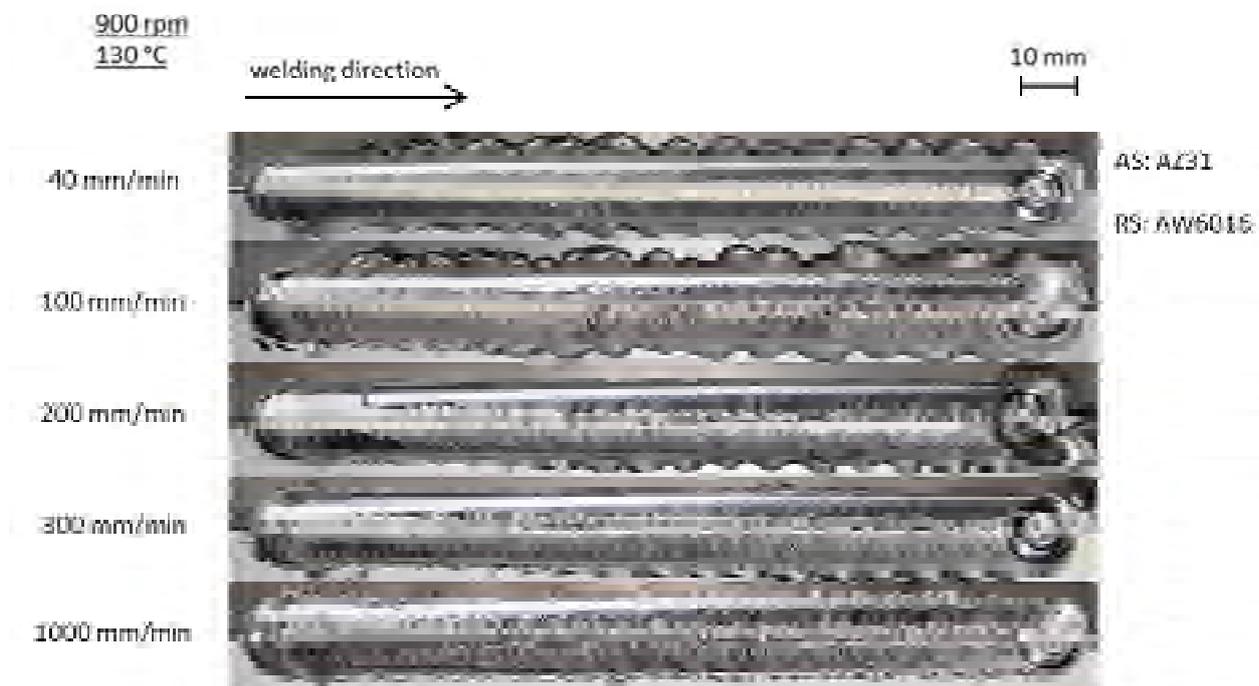


Figure 5.58: surface appearance for FSW of extruded AZ31/AW6016 for different welding speeds at a constant rotational speed of 900 rpm and 130 °C.

### Process temperature

It is important to mention that the following diagrams contain only the results for 4 measurement points. The reason is an error, which occurred during welding. As a result, the measurements of one point were defective.

By consideration of the process temperatures, a similar behavior to FSW of AZ31 is observable. Figure 5.59 shows the comparison of temperature progressions for 22 °C and 130 °C initial temperature at 40 (a) and 1000 mm/min (b) welding speed. In regard to  $f = 40$  mm/min (a), the temperature elevate from the beginning to the middle of the weld. Afterwards, it decreases up to the end of the weld. The curve progressions are identical, independent of the

initial temperature. For 1000 mm/min, the raised temperature level is obtained by the dwell time at the beginning of the weld. Because of the high welding speed, the generated heat diminishes up to the end of the weld.

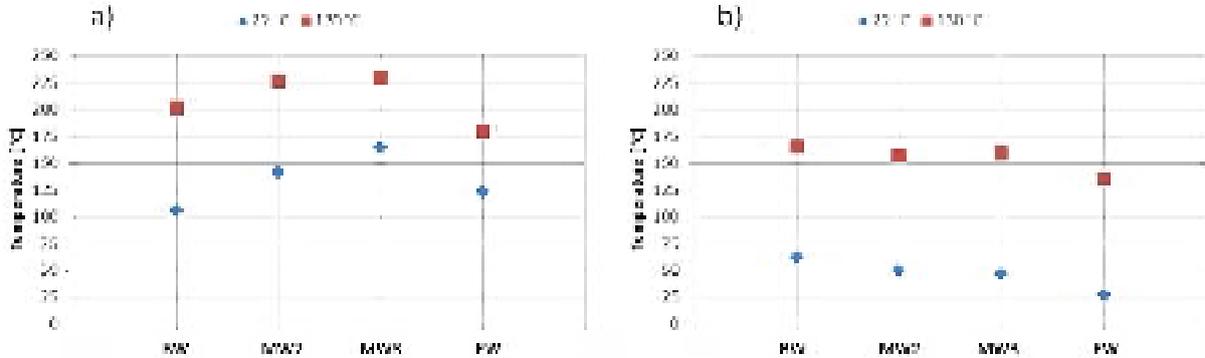


Figure 5.59: comparison of occurring temperature during FSW of extruded AZ31/AW6016 for different initial temperatures at constant rotational speed for welding speeds of a) 40 mm/min and b) 100 mm/min. BW- beginning of weld; MW- middle of weld; EW- end of weld

**Process loads**

The analysis of the process loads during the plunging phase show that the level of axial force is relative constant for welds made at 22 °C (figure 5.60 a). The values vary between 9100 and 10200 N with an average force of 9400 N. In comparison the preheated joints vary between 8200 and 8700 N whereby an average value of 8540 N is calculated. As a result, the force level could be reduced by about 9 %. Regarding figure 5.60 (b), the influence of preheating on the torque is lower. The average torque for welds made under the condition of 22 °C is 10,8 Nm. Preheating enables only a diminish of 1,8 %. In both cases, the torque differs between 10 and 11,3 Nm.

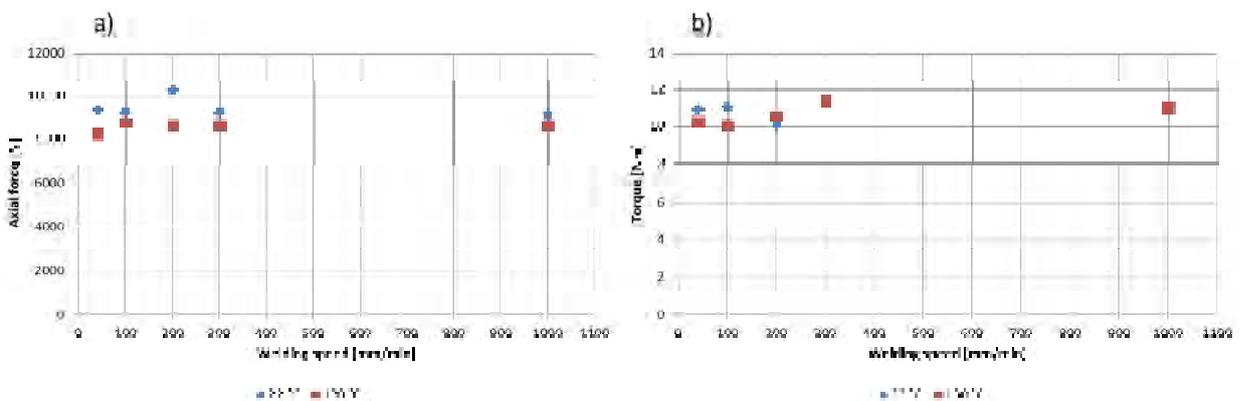


Figure 5.60: comparison of measured forces and torques for FSW of extruded AZ31/AW6016 at constant rotational speed: a) axial force as function of welding speed; b) torque as function of welding speed. (plunging phase)

The influence of preheating by the heating element on the loads during the welding phase is displayed in figure 5.61. The graph shows that the axial force (a) is reduced by 28,5; 7,5 and 6,7 % for 40; 200 and 300 mm/min. For  $f = 100$  and 1000 mm/min, the force elevate by 8,6 and 16,6 %, respectively. Concerning the welding torque in figure 5.61 (b), it is recognizable that the values decrease by 20,8; 10,1 and 3,7 % for welding speeds of 200; 300 and 1000 mm/min, respectively. The values for  $f = 100$  mm/min are equal, whereas the torque elevate by 26,9 % in case of 40 mm/min. Possible explanations are: Due to the fact, that all experimental settings are tested once, a general tendency could not be made. Moreover, the surface appearances show large differences for equal settings (rotational and welding speed) that indicate a high influence of the initial temperature on the material flow and thereby on the process loads.

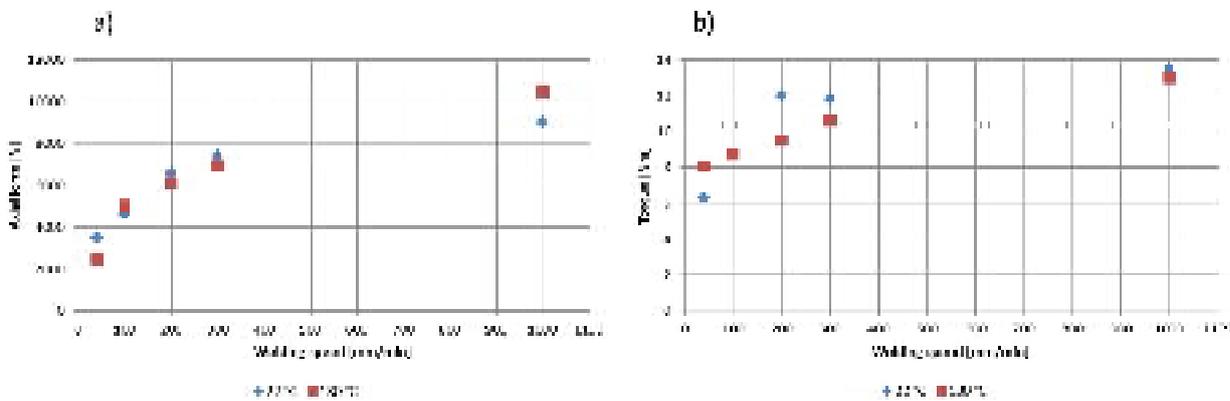


Figure 5.61: comparison of measured forces and torques for FSW of extruded AZ31/AW6016 at constant rotational speed: a) axial force as function of welding speed; b) torque as function of welding speed. (welding phase)

### Tensile tests

Figure 5.62 present the obtained tensile strength as function of the axial force and torque. As expected, the values of the joints made at 130 °C starting temperature are lower than those values of the conventional FSW process. The sole exception is represented by a welding speed of 40 mm/min. Under the given conditions, this joint exhibits the highest tensile strength with 115,8 N/mm<sup>2</sup> that corresponds about 55 % of the aluminum's tensile strength. The reason for the poor tensile strengths in case of preheated joints is the appearance of cracks during the process. In regard to figure 5.62, it is not possible to conclude a relation between force respective torque and tensile strength. Moreover, it can be seen that the values for one weld strongly vary. This observation was also made in the previous chapter. It indicates the instability of the process.

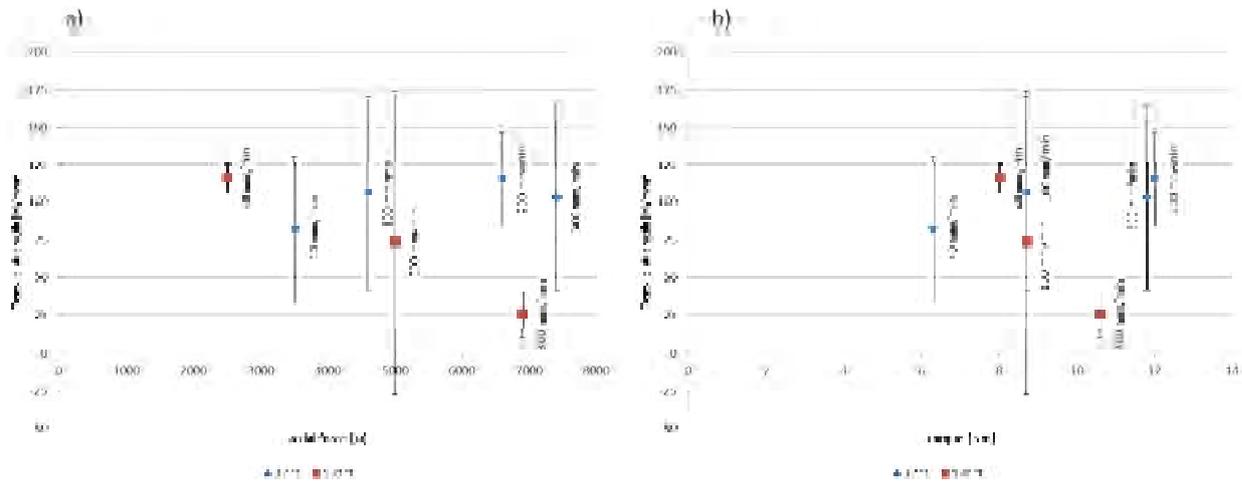


Figure 5.62: comparison of tensile strength for FSW of extruded AZ31/AW6016 for different welding speeds and initial temperatures at constant rotational speed subject to a) axial force; b) torque.

Considering the tensile strength as function of weld pitch, the graph (figure 5.63 a) exhibits no dependencies. A similar level of tensile strength is observable overall weld pitches. The results shown in figure 5.63 (b) indicate that the fracture length is also independent of the welding speed respective process loads. The highest fracture length with 2,4 mm (about 15,4 % of the aluminum's fracture length) is reached at a welding speed of 100 mm/min and a starting temperature of 22 °C.

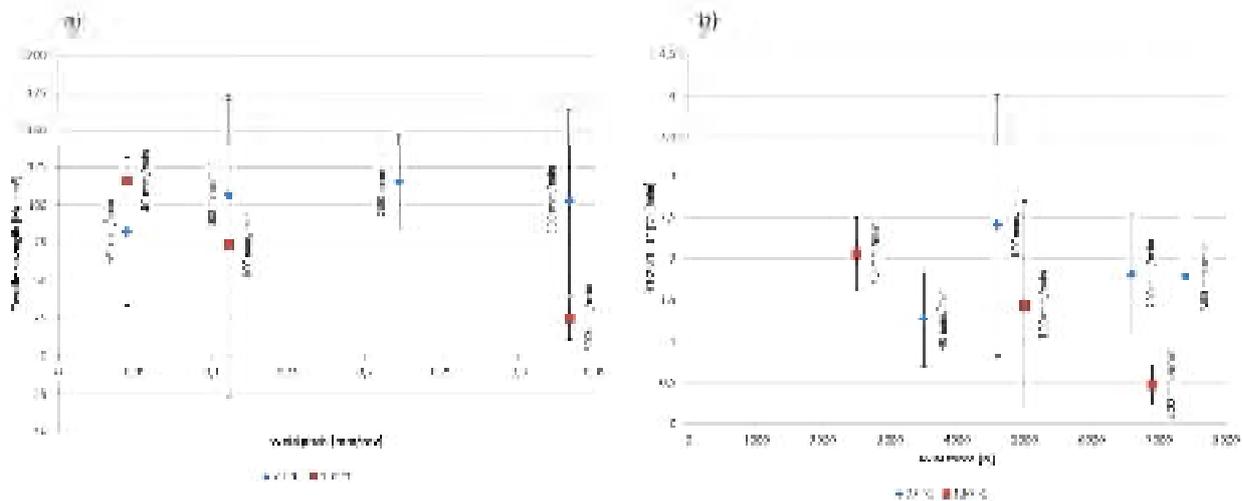


Figure 5.63: comparison of tensile properties for FSW of extruded AZ31/AW6016 for different welding speeds and initial temperatures at constant rotational: a) tensile strength as function of weld pitch; b) fracture length as function of axial force.

### Metallographic analysis

The micrographs for FSW of extruded AZ31/AW6016 dissimilar joints for a welding speed of 40 mm/min at the starting temperatures 22 °C and 130 °C are presented in figure 5.64 a) and b). It can be seen, that both cross-sections are defect free and the materials are well mixed. In case of the higher initial temperature, the plunging depth is recognizable deeper (figure 5.64 b). As a result, the pressure on the material increase, this enables an improved material flow which results in a larger flow arm (material is pushed more on the respective other side). As a result, the tensile properties are superior.

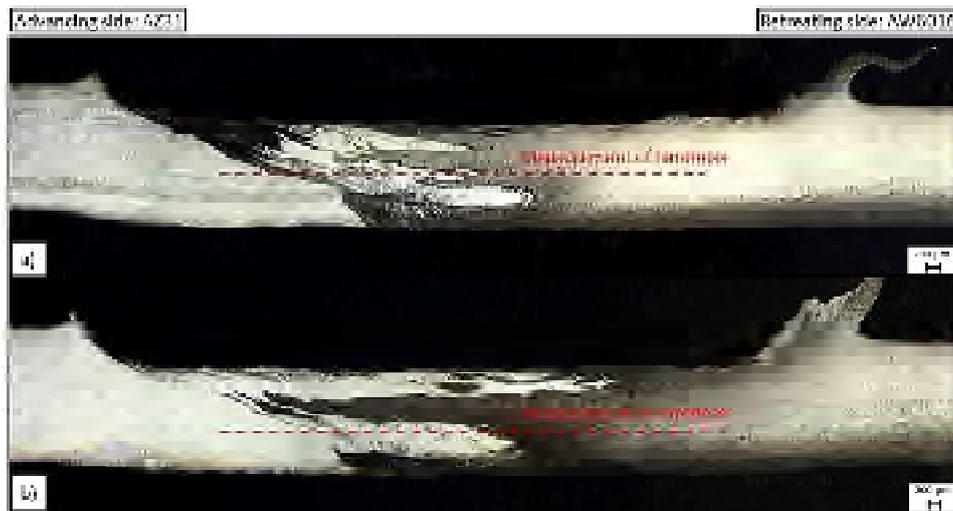


Figure 5.64: micrographs for FSW of extruded AZ31/AW6016 at constant rotational speed for 40 mm/min and a) 22 °C and b) 130 °C.



Figure 5.65: micrographs for FSW of extruded AZ31/AW6016 at constant rotational speed for 300 mm/min and a) 22 °C and b) 130 °C.

In comparison to the material flow at  $f = 40$  mm/min, figure 5.65 a) illustrate that the mixing is worse in case of a welding speed of 300 mm/min. The probable reason is insufficient heat generation. This results in a lack of penetration at the weld bottom and subsequently to poor tensile properties.

The effect of preheating at a welding speed of 300 mm/min is shown in figure 5.65 b). The cross-section exhibits large wormhole defect on the advancing side and a weak bond between the materials. Besides, the poor mixing is obviously, which results in inferior tensile properties.

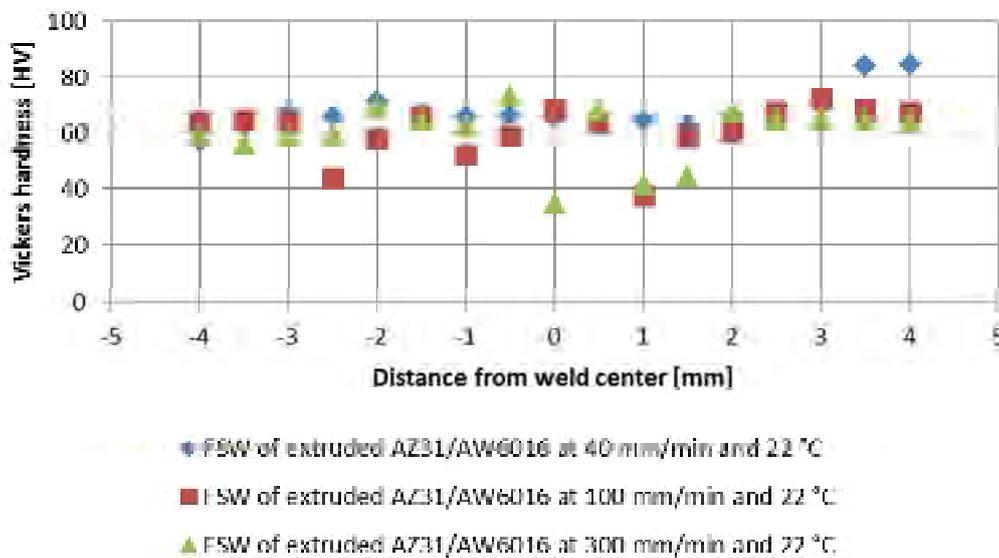


Figure 5.66: comparison of hardness profile for FSW of extruded AZ31/AW6016 at different welding speeds at constant rotational speed and initial temperature.

A comparison of hardness profiles for different welding speeds at an initial temperature of 22 °C is presented in figure 5.66. The measurements were carried out corresponding to the plotted lines in figure 5.64 and 5.65. The average measured hardness of the base metals are 55,8 HV for magnesium and 80,9 HV for aluminum. In general, the analysis of hardness is an indicator for the formation of intermetallic compounds. These brittle phases cause an erratic increase in hardness. However, none of the displayed profiles possess this behavior. All investigated joints exhibit a similar level of hardness.

For a welding speed of 40 mm/min, the profile shows a relative constant hardness level with to peak values on the retreating side because of the base material's hardness. Slight valleys are observable on both sides of the weld center. In case of 100 mm/min, the values scatter more. A peak hardness value is reached in the weld center with remarkable valleys on the

advancing and retreating side. The measurement for  $f = 300$  mm/min shows considerably differences of hardness on the advancing side compared to the retreating side.

The comparison of hardness profile for a welding speed of 40 mm/min at different initial temperatures (figure 5.67) shows remarkable differences. As mentioned before, the progression of hardness values is relative constant for the joint made at 22 °C. In contrast, the profile for 130 °C exhibit strong variations. The minimum value is obtained for the weld center. Towards advancing side, the hardness values are lower than on the retreating side. The peak values on the retreating side represent the behavior of the aluminum. In contrast, the high hardness on advancing side could be an indication for hardening.

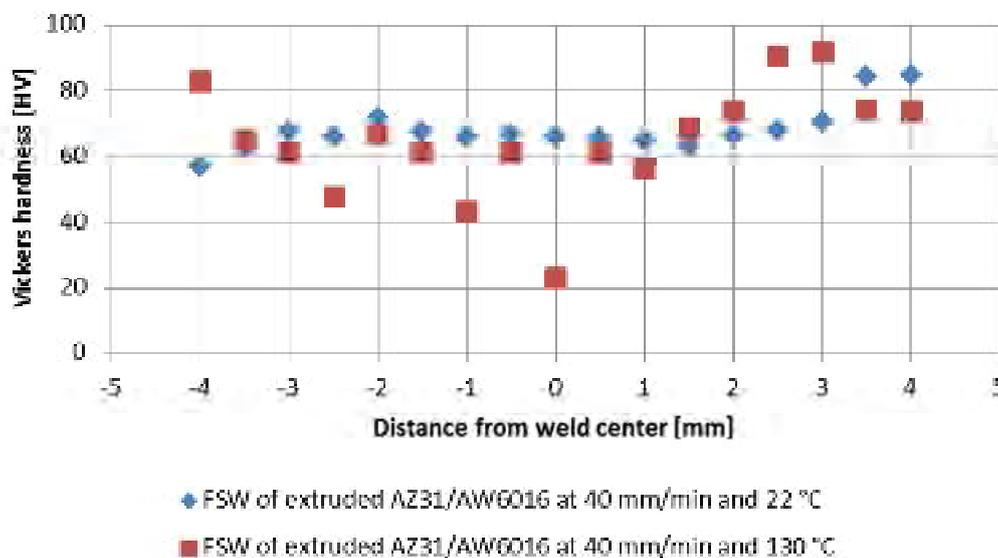


Figure 5.67: comparison of hardness profile for FSW of extruded AZ31/AW6016 at different initial temperatures for 40 mm/min at constant rotational speed.

The presented results show that the process forces as well as the tensile properties can be affected positive as well as negative by the initial temperature. In case of a welding speed of 40 mm/min, the axial force could be decreased. However, the torque increased. In this case the higher temperature results in an improved material flow and mixing, which cause higher tensile properties. A contrary effect is observable for higher welding speeds. Apparently, a starting temperature of 130 °C leads to the formation of defects during the process. A possible explanation is the difference in the thermal conductivities of the materials. This results in a high temperature gradient during the consolidation after welding. As a result cracks occur in the weld.

## 6. Summary and outlook

In the context of this thesis, the influence of the material's initial temperature on the process loads during FSW was regarded. The scientific background is provided by the material-specific yield stress and their dependency on temperature. This stress is required to deform a material plastically. By increase the temperature, the yield stress decline and consequently the required force to deform the material.

The investigation was focused on FSW of the magnesium alloy AZ31 with a thickness of 2,2 mm. To review the transferability to workpieces with a different thickness, the study included tests concerning 1,8 mm thick AZ31 sheets. Due to the industrial importance of dissimilar joints, the effect of higher starting temperatures was also investigated for FSW of dissimilar AZ31/AW6016 joints.

Concerning the 2,2 mm thick AZ31, different ways of preheating were compared. One beneficial way of preheating the joining members is applied by the LAFSW. At first, it was important to determine appropriate settings for laser power for different welding speeds. These were used in the LAFSW process. The results exhibit a remarkable reduction of axial force and torque by 16 and 25,9 %, respectively. This indicates the possibility to increase the welding speed without elevated process loads, whereby the efficiency of the welding process is improved. In addition, the local heating by laser results in an improvement of the joint surface at welding speeds of 1000 and 1400 mm/min. Indeed, the laser interaction seems to abet the formation of defects for a welding speed of 200 mm/min. As a result the tensile properties are deteriorated.

The other used method to change the initial temperature of the workpieces is preheating by a heating element. This enabled the approximately homogenous temperature distribution in the material. For this method, a beneficial effect of higher initial temperatures on process loads and surface appearance could be observed. Compared to LAFSW, the force could be decreased by a similar level (16 %). However, the torque during welding phase was declined by only 9,9 %. The influence on the loads during plunging phase was low (2,1 % less force, 1 % less torque). The increased defect formation could also be observed, which results in inferior tensile properties.

Similar observations are made for the investigation on AZ31 with a thickness of 1,8 mm. The axial force and torque (during welding phase) could be successfully reduced by 23,8 respective 16,9 %. In case of the plunging phase, the force was declined by 4,3 % and the torque by



5,2 %. In concern to welding speeds of 20 and 200 mm/min, the results showed poorer tensile properties. The reason was a deeper plunge depth because of the remarkable higher initial temperature.

A general statement about the relation between starting temperature of the materials and load generation during FSW of dissimilar AZ31/AW6016 cannot be made due to the amount of experiments for each parameter setting. In several cases, the additional temperature resulted in higher process loads. For welding speeds above 40 mm/min, the tensile properties of joints made at higher initial temperatures were significant lower. The reason is the formation of cracks along the weld line, probably caused by different physical properties of the joining members.

Additional studies should be made regarding the influence of preheating on the process loads during FSW of dissimilar joints to obtain reproducible results. Moreover, the relation between initial temperature and defect formation represent a crucial aspect that should be considered in detail. If defects could be avoided, the tensile properties would increase.

**Literature**

- /Ab 06/ Abbasi Gharacheh, M.; Kokabi, A.H.; Daneshi, G.H.; Shalchi, B.; Sarrafi, R.: The influence of the ratio of “rotational speed/traverse speed” ( $o/v$ ) on mechanical properties of AZ31 friction stir welds: In: International Journal of Machine Tools & Manufacture 46(2006), p. 1983–1987
- /Arb13/ Arbegast, William J.: Week 6 - Friction Stir Joining: Characteristic Defects. <[http://ampcenter.sdsmt.edu/2000/presentation\\_files/10%20MET%20492%20Week%206%20-%20Defects%20Characteriations11032009.pdf](http://ampcenter.sdsmt.edu/2000/presentation_files/10%20MET%20492%20Week%206%20-%20Defects%20Characteriations11032009.pdf)> (status 2008-10-08; access 2013-01-15)
- /Ath09/ Atharifar, Hosein; Lin, D.; Kovacevic, R.: Numerical and Experimental Investigations on the Loads Carried by the Tool During Friction Stir Welding. In: Journal of Materials Engineering and Performance 18 (2009), p. 339-350
- /Bac00/ Bachhofer, Andreas: Schneiden und Schweißen von Aluminiumwerkstoffen mit Festkörperlasern für den Karosseriebau. München: Herbert Utz Verlag, 2000
- /Bar08/ Bargel, Hans-Jürgen; Schulze, G.(Hrsg.): Werkstoffkunde. 10. edit. Berlin: Springer, 2008
- /Cao10/ Cao, Xinjin; Jahazi, M.: Friction Stir Welding of Dissimilar AA 2024-T3 to AZ31B-H24 Alloys. In: Materials Science Forum 638-642(2010), p. 3661-3666
- /Cha03/ Chao, Yuh J.; Qi, X.; Tang, W.: Heat Transfer in Friction Stir Welding - Experimental and Numerical Studies. In: Journal of Manufacturing Science and Engineering 125(2003), p. 135-145
- /Cha11/ Chang, Woong-Seong; Rajesh, S.R.; Chun C.-K.; Kim H.-J.: Microstructure and Mechanical Properties of Hybrid Laser-Friction Stir Welding between AA6061-T6 Al Alloy and AZ31 Mg Alloy. In: Journal of Materials Science and Technology 27(2011), Nr. 3, p.199-204

- /Che09/ Chen, Z.W.; Cui, S.: Strain and strain rate during friction stir welding/ processing of Al-7Si-0.3Mg alloy. In: IOP Conf. Series: Materials Science and Engineering 4 (2009), p. 1-5
- /Cho11/ Choi, Don-Hyun; Ahn, B.-W.; Lee, C.-Y. Yeon, Y.-M., Song, K. Jung, S.-B.: Formation of intermetallic compounds in Al and Mg alloy interface during friction stir spot welding. In: Intermetallics 19 (2011), p. 125-130
- /Col99/ Colligan, K.: Material Flow Behavior during Friction Stir Welding of Aluminum. In: Welding Journal 78(1999-07), p. 229-237
- /Cra06/ Crawford, Reginald; Strauss, A.M.; Cook, G. E.: A Mechanistic Study of the Friction Stir Welding Process. Online Article <  
<http://arc.aiaa.org/doi/abs/10.2514/6.IAC-06-C2.8.12>> (status 2006, access 2013-01-14)
- /Daf09/ Daftardar, Shivani: Laser assisted Friction Stir Welding: Finite Volume Method and Metaheuristic optimization. Louisiana State University and Agricultural and Mechanical College, Faculty of Industrial Engineering, Masterarbeit, 2009
- /Doe07/ Doege, Eckart; Behrens, B.-A.: Handbuch Umformtechnik. Berlin: Springer, 2007
- /Fir09/ Firouzdor, Vahid; Kou, S: Al-to-Mg Friction Stir Welding: Effect of Positions of Al and Mg with Respect to the Welding Tool. In: Welding Journal 88(2009-11), p. 213-224
- /Fuj08/ Fujii, Hidetoshi; Tatsuno, T.; Tsumura,.; Tanaka, M.; Nakata, K.: Hybrid Friction Stir Welding of Carbon Steel. In: Materials Science Forum 580 – 582 (2008-06), p. 393-396
- /Fro13/ Fronius International GmbH (Hrsg.): WIG Schweißen.  
[https://www.fronius.com/cps/rde/xchg/SID-AFFE441F-C113D959/fronius\\_international/hs.xsl/79\\_819\\_DEU\\_HTML.htm](https://www.fronius.com/cps/rde/xchg/SID-AFFE441F-C113D959/fronius_international/hs.xsl/79_819_DEU_HTML.htm) (status 2013; access 2013-02-10)
- /Gob06/ Gobrecht, Jürgen: Werkstofftechnik- Metalle. 2., überarbeitete Auflage. München: Oldenbourg, 2006

- /Gup11/ Gupta, Manoj; Sharon, Nai Mui Ling: Magnesium, Magnesium Alloys, and Magnesium Composites. Hoboken: Wiley, 2011
- /Her86/ Hermle: Maschinenhandbuch Hermle UWF 1000. 1986
- /IWB10/ IWB (Hrsg.): Erarbeitung von Konzepten zur Bewertung der Eignung von Anlagen für das Rührreibschweißen sowie zur Übertragbarkeit von Schweißparametern: Abschlussbericht. 2010
- /Jan13/ Janaki Ramulu, P.; Ganesh Narayanan, R.; V. Kailas, S.; Reddy, J.: Internal defect and process parameter analysis during friction stir welding of Al 6061 sheets. In: International Journal of Advanced Manufacturing Technology 65(2013), p. 1515-1528
- /Joh03/ Johnson, Richard; Threadgill, P.: Friction Stir Welding of Magnesium Alloys. In: Magnesium Technology (2003), p. 147-152
- /Käl05/ Källgren, Therese: Friction Stir Welding of Copper Canisters for Nuclear Waste. Stockholm, Royall Institute of Technology, Department of Materials Science and Engineering, Dissertation, 2005
- /Kam95/ Kammer, Catrin: Aluminium Taschenbuch, Bd. 1: Grundlagen und Werkstoffe. 15. Aufl. Düsseldorf: Alu Media, 1995
- /Kam00/ Kammer, Catrin: Magnesium-Taschenbuch. 1. edit. Düsseldorf: ALU Media, 2000
- /Ke04/ Ke, Liming; Xing, L.; Indacochea, J.E.: Material Flow Patterns and Cavity Model in Friction-Stir Welding of Aluminum Alloys. In: Metallurgical and Materials Transactions B 35B(2004-02), p. 153-160
- /Kew11/ Kewell Schweißtechnik GmbH (Hrsg.): Edelstahl-WIG-Schweißen. <http://kewell-schweisstechnik.de/wp-content/uploads/2011/10/Edelstahl-Wig-Schwei%C3%9Fen.pdf> (status 2011-10; access 2013-02-08)
- /Koh02/ Kohn, G.; Greenberg, Y.; Makover, I.; Munitz, A.: Laser-Assisted Friction Stir Welding. In: Welding Journal 81(2002), Online Article <<http://www.aws.org/wj/feb02/feature2.html>> (access:2013-02-17)

- /Kos09/ Kostka, A.; Coelho, R.S.; dos Santos, J.; Pyzalla, A.R.: Microstructure of friction stir welding of aluminium alloy to magnesium alloy. In: Scripta Materialia 60(2009-06), p. 953-956
- /Kou03/ Kou, Sindo: Welding Metallurgy. 2. edit. Hoboken: Wiley, 2003
- /Kum12/ Kumar; R.; Singh, K.; Pandey S.: Process forces and heat input as function of process parameters in AA5083 friction stir welds. In: Trans. Nonferrous Met. Soc. China 22(2012), p. 288-298
- /Lan08/ Lange, Kurt; Kammerer, M.; Pöhlandt, K.; Schöck, J.: Fließpressen - Wirtschaftliche Fertigung metallischer Präzisionswerkstücke. Berlin: Springer, 2008
- /Lea03/ McLean, A. A.; Powell, G. L. F.; Brown, I. H.; Linton, V. M.: Friction stir welding of magnesium alloy AZ31B to aluminum alloy 5083. In: Science and Technology of Welding and Joining Vol.8 N0. 6 (2003), p. 462-464
- /Lea08/ Leal, R.M.; Leitão, C.; Loureiro, A.; Rodrigues, D.M.; Vilaça, P.: Material flow in heterogeneous friction stir welding of thin aluminium sheets: Effect of shoulder geometry. In: Materials Science and Engineering A 498(2008), p. 384-391
- /Lie12/ Liebmann, Danny: Diffusion.  
<[http://yourliebmann.de/download/20080425\\_Diffusion.pdf](http://yourliebmann.de/download/20080425_Diffusion.pdf)> (status 2008-04-25; access 2012-12-09)
- /Loh10/ Lohwasser, Daniela; Chen, Z. (Hrsg.): Friction stir welding: From basics to applications. Oxford: Woodhead Publishing Ltd., 2010
- /Mes04/ Messler Jr., Robert W.: What's next for hybrid welding? In: Welding Journal 83(2004-03), p. 30-34
- /Mis05/ Mishra, R.S.; Ma Z.Y.: Friction stir welding and processing. In: Materials Science and Engineering R 50 (2005), p. 1-78
- /Mis07/ Mishra, Rajiv S.; Mahoney, Murray W.: Friction Stir Welding and Processing. ASM International, 2007

- /Mor05/ Mordike, Barry L.; Wiesner, P.: Fügen von Magnesiumwerkstoffen. Düsseldorf: DVS Media, 2005 (Fachbuchreihe Schweißtechnik Bd.147)
- /Müc05/ Mückelich, Silke: Beitrag zum flussmittelfreien Löten von Magnesiumwerkstoffen mit angepassten Lotwerkstoffen. Chemnitz: Eigenverlag TU Chemnitz, 2005 (Werkstoffe und Werkstofftechnische Anwendungen 21)
- /Mur82/ Murray, Joanne L.: The Al–Mg (Aluminum–Magnesium) system. In: Bulletin of Alloy Phase Diagrams 3 (1982-06), p. 60-74
- /Nan08/ Nandan, R.; DebRoy, T.; Bhadeshia, H. K. D. H.: Recent Advances in Friction Stir Welding – Process, Weldment Structure and Properties. Progress in Materials Science 53(2008), p. 980-1023
- /Nor04/ Norm DIN EN 573-1 2004. Aluminium und Aluminiumlegierungen – Chemische Zusammensetzung und Form von Halbzeugen - Teil 1
- /Nor10/ Norm DIN EN 1706 2010. Aluminium und Aluminiumlegierungen - Gußstücke - Chemische Zusammensetzung und mechanische Eigenschaften
- /Nor12/ Norm DIN EN ISO 25239-1 März 2012. Rührreißschweißen – Aluminium.
- /Nos03/ Noster, Ulf: Zum Verformungsverhalten der Magnesiumbasislegierungen AZ31 und AZ91 bei zyklischen und quasi-statischen Beanspruchungen im Temperaturbereich 20-300°C. Kassel, Univ. Kassel, Fachbereich Maschinenbau, Dissertation, 2003
- /Ost98/ Ostermann, Friedrich: Anwendungstechnologie Aluminium. Berlin: Springer, 1998
- /Pad09a/ Padmanaban, G.; Balasubramanian, V.: Selection of FSW tool pin profile, shoulder diameter and material for joining AZ31B magnesium alloy – An experimental approach. In: Materials and Design 30(2009-08), p. 2647-2656
- /Pad10/ Padmanaban, G.; Balasubramanian, V.: An experimental investigation on friction stir welding of AZ31B magnesium alloy. In: International Journal of Advanced Manufacturing Technology 49 (2010), p. 111-121
- /Pad10a/ Padmanaban, G.; Balasubramanian, V.; Sarin Sunda, J.K.: Influences of Welding Processes on Microstructure, Hardness, and Tensile Properties of AZ31B

- Magnesium Alloy. In: Journal of Materials Engineering and Performance 19(2010), Nr. 2, p. 155-165
- /Pat04/ Patent US 6,793,118B (2004-09-21). Palm, Frank. Pr.: De 10036170 2000-07-25
- /Pat06/ Patent US 7,078,647 B2 (2006-07-18). Kou, Sindo; Cao, Guoping. 2004-10-21
- /Pie07/ Pierron, Nicolas; Sallamand, P.; Matteï S.: Study of magnesium and aluminum alloys absorption coefficient during Nd: YAG laser interaction. In: Applied Surface Science 253(2007), p. 3208-3214
- /Raz11/ Razal Rose, A.; Manisekar, K.; Balasubramanian, V.: Effect of axial force on microstructure and tensile properties of friction stir welded AZ61A magnesium alloy. In: Trans. Nonferrous Met. Soc. China 21(2011), p. 974 – 984
- /Rod09/ Rodrigues, D.M. ; Loureiro, A.; Leitao, C.; Leal, R.M.; Chaparro, B.M.; Vilaça, P.: Influence of friction stir welding parameters on the microstructural and mechanical properties of AA 6016-T4 thin welds. In: Materials and Design 30(2009), p. 1913-1921
- /Ruh12/ Ruhstorfer, Markus F.: Rührreischweißen von Rohren. München, Techn. Univ., Fakultät für Maschinenwesen, Dissertation, 2012
- /Sat04/ Sato, Yutaka S.; Park, Seung Hwan C.; Michiuchi, Masato; Kokawa, Hiroyuki: Constitutional liquation during dissimilar friction stir welding of Al and Mg alloys. In: Scripta Materialia 50 (2004), p. 1233–1236
- /Sch03/ Schultz, L.; Freudenberg, J.: Physikalische Werkstoffeigenschaften <<http://www.ifw-dresden.de/de/institute/institute-for-metallic-materials/events/lectures/lecture-notes/physikalische-werkstoffeigenschaften/>> (status 2003/04; access 2013-03-02)
- /Sch04/ Schneider, J. A.; Nunes Jr., A.C.: Characterization of Plastic Flow and Resulting Microtextures in a Friction Stir Weld. In: Metallurgical and Materials Transactions B(2004-08), Nr. 35B, p. 777-783

- /Sch10/ Schulze, Günter: Die Metallurgie des Schweißens: Eisenwerkstoffe – Nichteisenmetallische Werkstoffe. 4. edit. Berlin: Springer, 2010
- /Sci07/ Scialpi, A.; De Filippis, L.A.C.; Cavaliere, P.: Influence of shoulder geometry on microstructure and mechanical properties of friction stir welded 6082 aluminium alloy. In: Materials and Design 28(2007), p. 1124-1129
- /Sep12/ Seperant, Florian: Interdiffusion des Aluminium-Magnesium-Systems - Quantitative Analyse und numerische Modellierung. Erlangen-Nürnberg, Universität, Naturwissenschaftliche Fakultät, Dissertation, 2012
- /Sin09/ Sinclair, Paul: Heated Friction Stir Welding: An Investigation into how pre-heating Aluminium 6061 affects process forces. Nashville, Vanderbilt University, Faculty of Industrial Engineering, Masterarbeit, 2009
- /Ska04/ Skar, Jan Ivar; Gjestland, H.; Djapic Oosterkamp, L.; Albright, D. L.: Friction Stir Welding of Magnesium Die Castings. In: Magnesium Technology (2004), p. 25-30
- /USD06/ U.S. Department of Energy (Hrsg.): New way to weld: ORNL team adds laser tech to expand the reach of a new welding technique. In: ORNL Reporter 84(2006), p. 1-10
- /Uym07/ Uyma, Falko: Untersuchungen auf dem Gebiet der Al-Mg-Si- und Al/Mg<sub>2</sub> Si-in-situ Legierungen. Freiberg, Techn. Univ., Fakultät für Werkstoffwissenschaft und Werkstofftechnologie, Dissertation, 2007
- /Völ09/ Völlner, Georg: Rührreibschweißen mit Schwerlast-Industrierobotern. München, Techn. Univ., Fakultät für Maschinenwesen, Dissertation, 2009
- /Wal06/ Wall, Edward; Sullivan, R.; Eberhardt, J.: High Strength Weight Reduction Materials: Annual Progress Report 2005. 2006. – Firmenschrift
- /Wei10/ Weißbach, Wolfgang; Dahms, M.: Werkstoffkunde: Strukturen, Eigenschaften, Prüfung. 17. edit. Wiesbaden: Vieweg +Teubner Verlag, 2010
- /Wil06/ Williams, S.W.; Colegrove, P.A., Shercliff, H.; Prangnell, P.; Robson, J.; Withers, P.; Richards D.; Sullivan, A.; Kamp, N.; Richards, D.; Lohwasser, D.; Poed, M.: Integrated Modelling of the Friction Stir Welding Process (Pro-



ceedings of the 6th International Symposium on Friction Stir Welding). Montreal, 2006

- /Yam09/ Yamamoto, Naotsugu; Liao J.; Watanabe, S.; Nakata, K.: Effect of Intermetallic Compound Layer on Tensile Strength of Dissimilar Friction-Stir Weld of a High Strength Mg Alloy and Al Alloy. In: Materials Transactions 50 (2009), Nr. 12, p. 2833-2838
- /Yan10/ Yan, Yong; Zhang, D.; Qiu, C.; Zhang, W.: Dissimilar friction stir welding between 5052 aluminum alloy and AZ31 magnesium alloy. In: Trans. Nonferrous Met. Soc. China 20(2010), p. 619-623
- /Zim10/ Zimmer, Sandra; Langlois, L.; Laye, J.; Bigo, R.: Experimental investigation of the influence of the FSW plunge processing parameters on the maximum generated force and torque. In: International Journal of Advanced Manufacturing Technology 47(2010), p. 201-215